Marginally Outer Trapped (Open) Surfaces in 4+1 Dimensional Spacetimes

by

© Sarah Mime MacDonald Muth

A thesis submitted to the School of Graduate Studies in partial fulfillment of the requirements for the degree of Master of Science.

Department of Mathematics and Statistics

Memorial University

October 2021

St. John's, Newfoundland and Labrador, Canada

Abstract

In binary black hole mergers and other highly dynamical spacetimes, the surface of most obvious interest, the event horizon, is often computationally difficult to locate. Instead, it is useful to use quasi-local characterizations of black hole boundaries, such as Marginally Outer Trapped Surfaces (MOTS), the outer-most of which is (often) the apparent horizon. Recent studies have shown that MOTS not only characterize boundaries, but may also be found in black hole interiors. This has been seen in 4D Schwarzschild and Reissner-Nordstrom, as well as in binary black hole mergers.

In this thesis, behaviours of MOTS—and their open generalization, Marginally Outer Trapped Open Surfaces (MOTOS)—in the interior of five-dimensional black holes are studied; both static (Schwarzschild), and rotating (Myers-Perry). Similar to four-dimensions, we find infinitely many self-intersecting MOTS in 5D Schwarzschild. We find finitely many self-intersecting MOTS in Myers-Perry, finding fewer as the rotation increases. However, we do find oscillations of the MOTOS, which is novel behaviour.

Keywords: black holes, binary black hole mergers, Myers-Perry, 5D black holes, MOTS, apparent horizons.

Dedicated to my grandfather.

Lay summary

Black holes are one of the most striking predictions of Einstein's theory of General Relativity, as they give us unique insight into the nature of space and time, and their existence in the universe as real, astrophysical objects is now accepted. In 2015, the first direct experimental evidence of gravitational waves was detected at LIGO; the waves their detectors found were produced by a binary black hole merger: an event wherein two black holes merge into one. The subject of this thesis deals with understanding the nature of a kind of surface, called Marginally Outer Trapped Surfaces (MOTS), which are used as proxies for finding black holes in spacetimes that change dramatically with time—like binary black hole mergers. These surfaces are used because, if initial data is specified at a given time, then they can be readily found and analyzed. This is in contrast to the usual surface that defines a black hole, called the event horizon.

In this thesis, Marginally Outer Trapped Surfaces are studied for two types of five-dimensional black holes: one which does not change with time (called Schwarzschild), and one which rotates (called Myers-Perry). Interesting looping behaviour is seen in these MOTS, as was seen before when they were studied for a four-dimensional black hole in [11]. We also see oscillating behaviour in surfaces which are like the MOTS, called Marginally Outer Trapped Open Surfaces (MOTOS).

Acknowledgements

The author acknowledges that, as is always the case, this work was made possible only with the help of those wiser and cleverer than she. Her gratitude goes out to her supervisors, Dr. Ivan Booth and Dr. Hari Kunduri, for their excellent pedagogy and patience throughout the writing of this thesis, and the entirety of her degree. It is not lost on her that her background is somewhat non-traditional, and she would like to thank them for taking a chance on her.

She is also grateful for the extensive edits, proofreading, advice, and puns, given to her by her collaborator, Dr. Robie Hennigar. She advises him in return to adopt a cat—sooner rather than later.

Many thanks to Carolin Sachgau, for enduring support and friendship. Move out of Germany, Carolin. No fish brains were harmed in the making of this thesis.

She also thanks Lu Buller, without whom the author would not have finished her undergraduate degree.

Finally, of course, the author would like to thank her family: her mother, father, step-father, and grandfather. She was a challenging child, and is an equally challenging adult; she appreciates their faith in her.

And she thanks Tyler, for choosing her.

Statement of contributions

All figures/plots included in chapters 5 and 6 were produced by the author, Sarah Muth. Figures in chapters 1 and 2 were taken from [20] and [30], and the previous work by the author's collaborators, [11]. There are references to the original source in the captions for all figures not produced by the author. Initial ideas and techniques for finding the MOTSodesic equations were provided by Dr. Ivan Booth and Dr. Robie Hennigar, and derivations of these in the 5-dimensional spacetimes was done collaboratively by Dr. Hari Kunduri, and the author, Sarah Muth.

Table of contents

List of figures

Chapter 1

Introduction

We study black holes because they are able to give us unique insight into the nature of space and time in our Universe: they are arguably the most dramatic and counter-intuitive prediction of Einstein's theory of General Relativity, and yet we now can be certain they are real, astrophysical objects. While the first observational evidence of a black hole was found in 1964, this field is more at the forefront now than it has ever been, since the detection of gravitational waves in 2015 [8]. Even before this, many potential candidates for black holes had been detected through a variety of methods—some found in X-ray binary systems, some found in galactic nuclei [26]. Now, gravitational wave detector experiments like LIGO and VIRGO collect data every day, and have the capacity to locate black holes previously invisible to us.

These gravitational waves were determined to have come from a binary black hole merger: two in-spiralling black holes, which finally merged into one. Understanding such a complex and dynamical spacetime requires numerical methods and simulations, as well as a notion of a black hole boundary [35, 33, 7, 5].

This thesis focuses on the novel behaviour we have seen in one such characterization of a boundary: the *marginally outer trapped surface*; first seen in [30] for binary black hole mergers, and later studied by my collaborators in 4D Schwarzschild spacetime [11], MOTS were found not only to characterize a black hole boundary, but also to produce complex self-intersecting behaviour inside the black hole. The purpose of this work is to show the generality of this behaviour through establishing its existence in multiple 5-dimensional spacetimes.

1.1 Event Horizons

In the study of black holes, the most obvious surface of interest is the event horizon—the surface beyond which light cannot escape, and thus from inside of which signals sent cannot be received by observers outside. That is, the event horizon is the surface which separates the interior and exterior of the black hole spacetime [28], and thus is something of a defining feature of any given black hole.

More precisely, the event horizon is the outermost surface traced out by a congruence of null geodesics which never escape to future null infinity. This surface is inherently global in its definition: one specifies boundary conditions that the geodesics have at future infinity (never escaping), and then traces the ones that satisfy this condition back in time, to find the location of the event horizon at the previous time. That is, the event horizon is a surface defined by boundary condition in the asymptotic future. It is, therefore, a surface defined for all time, and requires complete knowledge of the future to properly locate [9, 20, 37].

For a black hole like the Schwarzschild solution [34], for which the line element is

$$ds^2 = -\left(1 - \frac{2M}{r}\right) dt^2 + \left(1 - \frac{2M}{r}\right)^{-1} dr^2 + r^2 d\Omega^2, \tag{1.1}$$

the event horizon is at $r = 2M$—where there exists a coordinate singularity. But for a more complicated black hole spacetime, the location of the event horizon is not so obvious. A good example of this is the (in-going) Vaidya spacetime [36], where one considers a (locally) Schwarzschild black hole of some mass M_1, which then is irradiated by null rays until it is of mass $M_2 > M_1$. After the irradiation stops, the spacetime is once again (locally) that of Schwarzschild, but with the new larger mass. The line element for this spacetime during the irradiation is, taken from [28],

$$ds^2 = -f dv^2 + 2dvdr + r^2 d\Omega^2 \qquad \text{where} \qquad f(v) = 1 - \frac{2m(v)}{r}, \tag{1.2}$$

and these are in-going Eddington-Finkelstein -type coordinates [14][18], meaning that surfaces of constant v-coordinate are null and in-falling.

Before the irradiation, the Vaidya spacetime is simply Schwarzschild with mass $M_1 = m(v_1)$, and after, it is the same, but with mass $M_2 = m(v_2)$. v_1 is when the irradiation begins, and v_2 is when it stops.

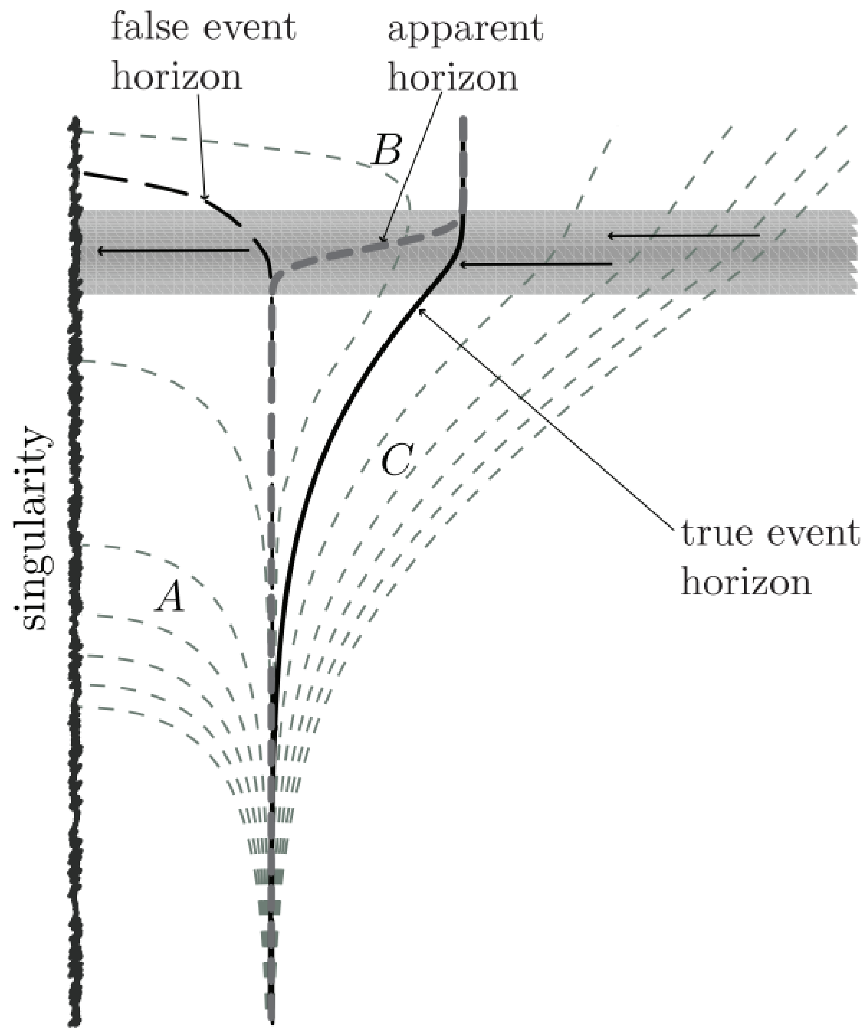

Figure 1.1: Taken from [13]; a diagram showing the difference between the location of the event horizon and the apparent horizon in Vaidya spacetime. The grey band indicates in-falling matter (irradiation), and the apparent horizon follows the mass function, being located at $r = 2m(v)$. The "false horizon" shown here is the path of null rays which begin at $r = 2m_1$ before the irradiation, and thus is inside the event horizon and intersects the singularity.

Where is the event horizon in such a spacetime? The following argument illustrates that the event horizon is defined for all time in the following way: if a congruence of null geodesics were to be just outside of $r = 2M_1$ when the irradiation occurs, then because the irradiation itself occurs instantaneously (in the frame of the horizon), this congruence will instantaneously be within the new horizon $r = 2M_2$. If they are within this horizon for a Schwarzschild black hole, we know that they cannot escape to future null infinity. Thus, the future of this congruence will be inside the horizon forever. But if we define the event horizon teleologically—as a surface which separates null rays that can never escape to future null infinity—then this $r = 2M_2$ surface must be the event horizon, after the irradiation occurs. Thus, to find the event horizon before the irradiation, one must trace back the null geodesics which end up at $r = 2M_2$, and wherever they originated, that is the event horizon at that point in time [28].

This example illustrates the global nature of the event horizon, and thus hopefully suggests to the reader why it might not always be practical computationally to use the event horizon to define a black hole: in numerical simulations, for example, surfaces which can be defined for an instant in time are much more widely used, as they are more convenient [21, 29, 4, 5, 33].

To this end, one defines the apparent horizon, which is more or less where we would naively expect the event horizon to be, at any instant in time. Unlike the event horizon, which, in a 4-dimensional spacetime, is a 2+1-dimensional surface (2 dimensions of space, 1 of time), the apparent horizon is defined on a constant timeslice of the spacetime, and so is only 2 dimensional. The 2+1-dimensional analogue of the event horizon for the apparent horizon is the tube that the AH traces out in time, called the dynamical horizon. For the previously described Vaidya spacetime, the apparent horizon, for some time before the irradiation, is indeed at $r = 2M_1$, after it is at $r = 2M_2$, and during the irradiation it follows the mass function $m(v)$, i.e., it is at $r(v) = 2m(v)$.

But then, what is the apparent horizon? The definition—to use the term loosely—given before, "where one would naively guess the event horizon would be, not knowing the future", is not very precise. We can make it more precise by first defining the expansion of a congruence of null geodesics, and from this, trapped surfaces and then marginally outer trapped surfaces (or MOTS), which are the subject of this work.

1.2 Expansions of Null Geodesics

A geodesic is a curve $\gamma = x^\alpha(s)$, which satisfies the geodesic equation

$$\ddot{x}^\alpha + \Gamma^\alpha_{\beta\gamma}\dot{x}^\beta\dot{x}^\gamma = \kappa(s)\dot{x}^\alpha \tag{1.3}$$

where $\kappa(s) = 0$ indicates affine parameterization. If one imagines a particle moving along the curve, where its location is indicated by the parameter, then relative to an affine parameterization, the particle has zero acceleration along its path. A null geodesic is one where the tangent vector to the path is null, that is, $\dot{x}^\alpha\dot{x}_\alpha = 0$.

A *congruence* of geodesics is a collection of such curves, which satisfies the condition that they do not cross anywhere—a point where they cross is called a *caustic* and is technically not part of the congruence. We label a congruence of geodesics according to the type of geodesics that form it; for example, a *null congruence* is one which is made up of null geodesics.

It is not, however, required for each of the curves of the congruence to be parallel to one another. Whether the geodesics in the congruence are converging or diverging can be expressed through the *expansion*, which is the rate of change in area for a surface element that all of the geodesics intersect once. A positive expansion indicates the geodesics of the congruence are diverging, and a negative expansion indicates they are converging.

If one considers some point P at which a light is turned on, then a congruence of null geodesics, that is, light rays, will be emitted from this point (note, however, the point itself is a caustic, so the congruence will be defined on points very near to it). The expansion of these geodesics at this point P indicates whether they are converging or diverging there; in the case of a light being turned on in flat space at P, the expansion will be positive, because the light rays will be diverging.

If one then were to consider some surface S, and a light turned on at every point of this surface, one will have to define two types of expansions: those associated with the light rays which are directed in toward the inside of the surface, and those associated with the light rays directed toward the outside of the surface.

More precisely, let $(\mathcal{M}, g_{\alpha\beta}, \nabla_\alpha)$ denote an $n+1$-dimensional spacetime. Then let a constant timeslice in this spacetime be denoted by $(\Sigma(t), h_{ij}, D_i)$. Now define a surface S in this constant timeslice. The normal to this surface, existing on the timeslice, will be $\hat{n} = n_i dx^i$, where x^i are the coordinates on the timeslice. This exists in the timeslice, but is defined only on the surface S.

One then takes the covariant derivative of this normal, $D_i n_j$, and pulling this back onto the surface gives its extrinsic curvature,

$$k_{AB} = e^i_A e^j_B D_i n_j, \tag{1.4}$$

where e^i_A are the pullback operators.

The timelike unit normal to the timeslice is $\hat{u} = u_\alpha dx^\alpha$ (future-directed), and will be proportional to $-dt$. The extrinsic curvature of the timeslice is the covariant derivative of this, $\nabla_\alpha u_\beta$, pulled back into the timeslice:

$$K_{ij} = \frac{\partial x^\alpha}{\partial x^i} \frac{\partial x^\beta}{\partial x^j} \nabla_\alpha u_\beta. \tag{1.5}$$

The operators $\partial x^i / \partial x^\alpha = e^\alpha_i$ are the pushforward/pullback operators.

An expansion is found from the extrinsic curvature by taking its trace. However, this is done with the metric on S, pushed forward into the timeslice; this is because the expansion is defined on S, and not in the whole timeslice. Letting quantities defined on S have upper case Latin indices (here and for the rest of this text), the inverse metric on S is denoted $\tilde{q}^{AB}$ and its pushed-forward analogue on the timeslice is $\tilde{q}^{ij}$. Then the expansion associated to each of $D_i n_j$ and K_{ij} are

$$\begin{gathered} \theta_u = \tilde{q}^{ij} K_{ij} = \tilde{q}^{ij} \left(\frac{\partial x^\alpha}{\partial x^i} \frac{\partial x^\beta}{\partial x^j} \nabla_\alpha u_\beta \right) \\ \theta_n = \tilde{q}^{ij} D_i n_j. \end{gathered} \tag{1.6}$$

From these two normals, you can see that one gets two expansions: one a timelike expansion (from the timelike normal $\hat{u}$), and one spacelike (from the spacelike normal $\hat{n}$). To get a null expansion, θ_ℓ, one requires a null normal, which is defined as a linear combination of these two normals [11]:

$$\hat{\ell}^+ = \hat{u} + \hat{n}, \quad \hat{\ell}^- = \frac{1}{2}(\hat{u} - \hat{n}) \tag{1.7}$$

Then, the null expansion can be found by finding the expansion of this null normal, that is, first taking its covariant derivative, and then contracting this with $\tilde{q}^{\alpha\beta}$, where here the metric will have to be pushed forward onto the full spacetime, as this is where $\hat{u}$ exists (so too will $\hat{n}$ in the above definition of $\ell^{\pm}$). However,

$$e^{\alpha}_{A}e^{\beta}_{B}\nabla_{\alpha}\ell^{+}_{\beta} = e^{\alpha}_{A}e^{\beta}_{B}\nabla_{\alpha}\left(u_{\beta}+n_{\beta}\right) = e^{i}_{A}e^{j}_{B}(e^{\alpha}_{i}e^{\beta}_{j}\nabla_{\alpha}u_{\beta}+D_{i}n_{j}) = e^{i}_{A}e^{j}_{B}(K_{ij}+D_{i}n_{j}) \tag{1.8}$$

which means that

$$\begin{aligned}\theta_{\ell} &= \tilde{q}^{\alpha\beta}\nabla_{\alpha}\ell^{+}_{\beta} = \tilde{q}^{AB}e^{\alpha}_{A}e^{\beta}_{B}\nabla_{\alpha}\ell^{+}_{\beta} = \tilde{q}^{AB}e^{i}_{A}e^{j}_{B}(K_{ij}+D_{i}n_{j}) \\ &= \tilde{q}^{ij}(K_{ij}+D_{i}n_{j}) = \theta_{u}+\theta_{n}\end{aligned} \tag{1.9}$$

That is to say, the timelike and spacelike expansions relate in the same way to the null expansion as the null normal does to the timelike and spacelike normals. So one may simply add the two expansions θ_u, θ_n to find the null expansion. (Of course, an analogous calculation holds for ℓ_{-}.)

One sees there are two choices of null normal, ℓ_{+} and ℓ_{-}. These correspond to what are calling the outward oriented null expansion, θ_{+}, and the inward oriented, θ_{-}. The outward (null) expansion is that associated to null rays which are directed from inside the surface toward the outside. This is found by defining the normal to the surface S in the usual convention (positive); the expansion calculated in 1.9 is an outward null expansion, $\theta_{\ell} = \theta_{+}$ (in this thesis, the notation θ_{ℓ} refers to this outward oriented expansion). The inward oriented null expansion is found by defining the spacelike normal in the negative direction (opposite to usual convection), and perhaps intuitively, this is associated to light rays which are directed from outside the surface toward the inside.

Now we may define trapped surfaces.

1.3 Trapped Surfaces

Before defining marginally outer trapped surfaces, which can be used to define the apparent horizon as mentioned previously, it will be useful to define trapped surfaces.

Considering again the example of a surface S, and on every point of it lights are turned on. Our every day experience is that of a surface which has positive outward null expansion, and negative inward: the null rays emitted from the surface which are directed outward from the surface are diverging, and those directed inward from the surface are converging (to a point at the centre, if, say, the surface is spherical).

The notion of a *trapped surface* was first introduced by Penrose in 1965 [27]. The intended purpose was to provide a quasi-local characterization of black holes, meaning a surface which could be located by an observer in order to detect whether a black hole exists [22, 21]. The trapped surface is defined as a spacelike surface, for which both the inward and outward directed null expansions are negative (converging). In the previous example, the inward oriented light rays behave the same, that is, they converge in toward the inside of the surface, but for the surface to be trapped, the outward directed light rays must also converge. In this sense, the light rays are "trapped" by the surface S. Intuition for such a surface can be developed through the classic example of Schwarzschild spacetime: every spherically symmetric surface inside the event horizon ($r = 2M$) of Schwarzschild is a trapped surface [22].

We may now define the apparent horizon, formally. Assuming a spacetime may be foliated by asymptotically flat slices of constant time, where any one of these is denoted Σ_t, then a point, p, in this timeslice is said to be *trapped* if it lies on a trapped surface existing on Σ_t. One then takes the union of all such trapped points $p \in \Sigma_t$, and the *apparent horizon* is then the boundary of this union [9, 20].

Under certain assumptions of smoothness, the apparent horizon will satisfy $\theta_\ell = 0$ [9], that is, it will have zero outward-oriented null expansion. This leads us to the definition of MOTS.

1.4 MOTS

MOTS stands for Marginally Outer Trapped Surface(s). These are spacelike surfaces for which the outward oriented null expansion is equal to zero, which are closed (in this case, "closed" means compact and without boundary), and for which one places no restriction on the inward oriented null expansion. So, one may have light rays directed inward that are diverging or converging. Outward-oriented light rays, however, are forced to have zero expansion, meaning they neither converge nor diverge at S: a unit area would have instantaneously parallel geodesics crossing it if a surface is a MOTS—that is, the shape produced by the light rays directed outward will stay the same size, rather than expanding out to infinity or converging in to the centre of S [9, 10].

In many spacetimes, the definition of the apparent horizon stated above coincides with it being the outermost MOTS in a timeslice [2]; separating the region of the timeslice wherein there are MOTS (or trapped surfaces), from the outer region (where there are not). While it is not always the case that these definitions coincide, for practical reasons, the apparent horizon is defined simply as this outermost MOTS—in numerical relativity, for example [9]. In this work, the two definitions coincide, but the latter is what will be relevant.

Unlike the event horizon, the apparent horizon—and all other MOTS—are defined for a constant time (since they are spacelike surfaces). This makes them useful, because they can be tracked throughout complex spacetimes like black hole mergers, while also behaving somewhat like the event horizon would. Indeed, for stationary spacetimes, constant-time slices of the event horizon coincide with the apparent horizon [9]. It is also true for general spacetimes that the apparent horizon occurs inside the event horizon [20], meaning the entirety of the region exterior to the black hole exists outside the apparent horizon. This means if only the solution outside the apparent horizon is computed, rather than outside the event horizon, no observable information will be lost (observable information being that which occurs outside the event horizon). Thus, apparent horizons (defined as being the outermost MOTS) are the standard boundaries tracked in numerical general relativity [19, 32, 31, 12].

There is one more condition that makes a surface a MOTS: a MOTS must be a closed surface. Closure of a surface is a global condition, and as such, one must know the topology of the whole timeslice to determine whether a surface is closed. This can lead to situations wherein two patches of surfaces that appear the same locally are such that one is a MOTS and one is not, because the former is closed but the latter is not in the entirety of the space. The issue with this, is it is not necessarily practical for understanding the local behaviour of black holes—if two surfaces appear the same locally, one should treat them as the same type of surface, in this case. For this reason, my collaborators considered a type of surface which they called a MOTOS: Marginally Outer Trapped Open Surface, which satisfies the condition of zero outward null expansion, but for which the condition of closure is relaxed [11].

1.5 MOTOS

A Marginally Outer Trapped Open Surface (MOTOS) was first defined in [11] as a surface such that the outward null expansion is equal to zero, and the surface itself is open. This is defined in a constant timeslice of the spacetime, as are the MOTS, and so not only is this definition local temporally, but also spatially—that is, unlike the MOTS, which are quasi-local objects, the MOTOS are purely local.

Soon we will see how the MOTOS and the MOTS are related, but for now, it can be said that MOTOS provide a useful way of locating MOTS, as well as of understanding their shape: one can follow a continuous series of MOTOS, and for a specific critical value, one of these MOTOS will close, and in this place, there will be a MOTS. In this way, the location and shape of MOTS are easily predictable, which is particularly valuable in the work my collaborators did (and are doing) [11, 32, 31, 12], and then the work on which this thesis focuses, because the MOTS in these cases are somewhat exotic.

Chapter 2

Motivation and Previous Work

2.1 Binary Black Hole Mergers

The behaviour of the event horizon in a binary black hole merger has been well-known for quite some time [20]: a conceptual diagram of it is often called a 'pair of pants' diagram, because it begins with the two black holes separated from one another, corresponding to the legs of the pants, and then once they merge, the mutual horizon which develops corresponds to the waist of the pants. Referring to figure 2.1, which is taken from Hawking and Ellis, one can see the event horizon labelled there.

However, event horizons cannot be defined locally in time [20] [37], and thus are not practical surfaces to follow throughout, say, a computational simulation of a merger. To this end, the apparent horizon is used, because it can be defined on a single time slice of the spacetime, and so lends itself to the methods used in such simulations [10] [9].

Now the behaviour of the apparent horizon is more complex (as can also be seen in the aforementioned figure 2.1) than the simple 'pair of pants' that describes the event horizon. At later times, once the black holes have merged—that is, inside the 'waist' of the event horizon—a new mutual apparent horizon develops, which sits outside the original two. Meanwhile, the original two continue to exist inside it.

Keeping in mind that the apparent horizon of a black hole is a MOTS, all of this gives some motivation to the search for MOTS in binary black hole merger spacetimes. In 2019, Pook-Kolb et. al. [30] followed the evolution of the MOTS involved such a

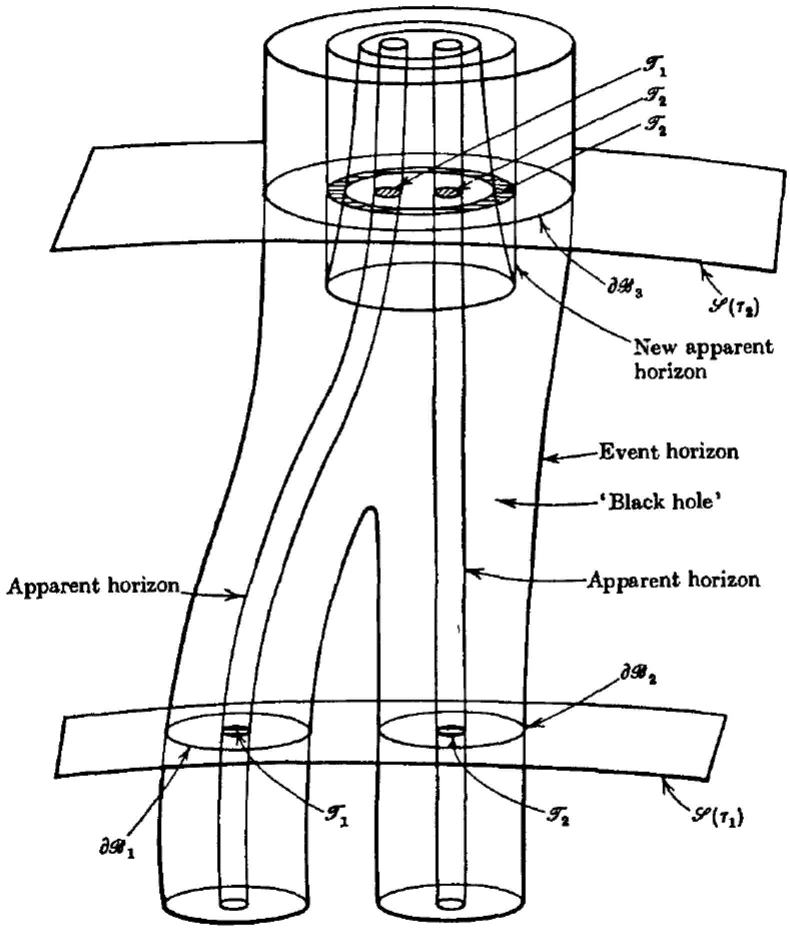

Figure 2.1: A "pair of pants" diagram from Hawking and Ellis [20].

merger, from a time before the two apparent horizons touched one another, to some time after the two black holes had merged and settled down into one new black hole. One can see a figure from this paper in figure 2.2, which is like the pair of pants diagram, but for MOTS.

The purple and red horizons visible at $t = 0$ are the apparent horizons of the two black holes, as represented by the innermost thin tubes in the figure 2.1. One sees that at a time $t_{\text{bifurcate}}$, the two apparent horizons get close enough that two mutual horizons develop around them; these are shown in blue and green in the figure. The outermost blue horizon behaves as the new apparent horizon, just as the second outermost horizon (labelled "new apparent horizon") in figure 2.1. Unlike the blue apparent horizon, the green MOTS hugs the purple and red apparent horizons of the two black holes throughout the merger. Why this is interesting is visible at the top

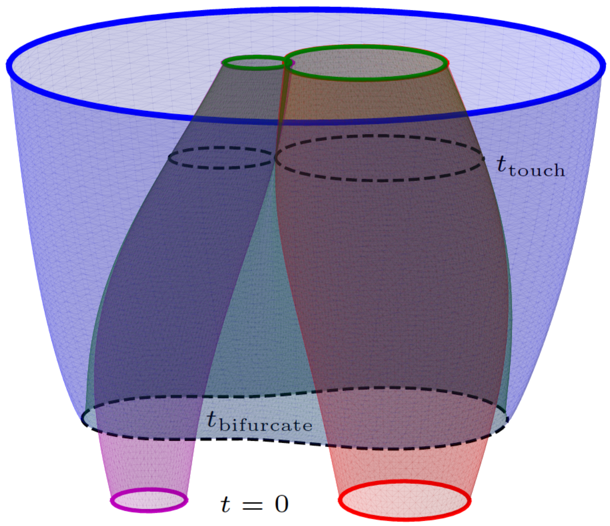

Figure 2.2: Figure taken from [30]; the analog of the pair of pants diagram, but for the MOTS followed in the simulation by Pook-Kolb et. al. in 2019 [30]

.

of figure 2.2, and made more obvious in the last panel of figure 2.3: the green MOTS produces a self-intersection as the red and purple horizons intersect one another.

The first panel of figure 2.3 shows all four of the MOTS, at some time after the bifurcation time when the two mutual (blue and green) horizons develop. Already here one can see the green horizon hugging the red and purple horizons, producing a peanut shape. The second panel is then at an instant before the time when the red and purple horizons touch one another; the cutout on the top right of this panel shows the 'waist' of the green horizon, visible when it was peanut shaped, narrowing so that it can hug the red and purple horizons more closely. Then the last panel and its cutout shows the green horizon producing two self-intersections, which one can see develop as the red and purple horizons move closer and intersect, and the green horizon continues to follow them.

The self-intersecting MOTS seen here were the first of such surfaces found. Of course, one can see that no such behaviour is present in the diagram of figure 2.1; that is, the self-intersections are a property only of MOTS, not of surfaces like the event horizon.

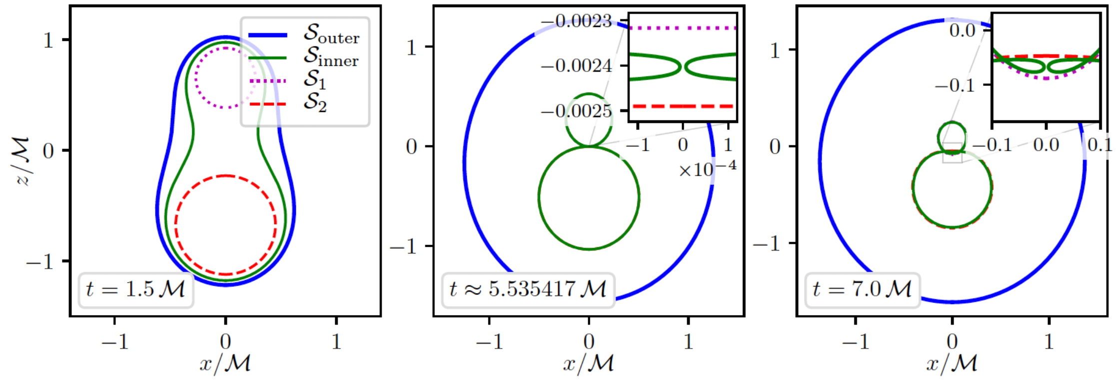

Figure 2.3: Figure taken from [30]; the same MOTS as in figure 2.2, but from a top-down perspective, where each panel represents an instant in time. One can see the green horizon hugging the red and purple for the first two panels, the second of which is an instant before the time when the horizons touch. Then, the cutout on the top right of the last panel shows the green horizon producing two self-intersections, which develop because it continues to hug the purple and red horizons after they intersect one another.

2.2 Self-intersections in 4D Schwarzschild MOTS

In 2020, motivated by the Pook-Kolb et. al. paper from the previous year, my collaborators published the paper [11], which searches for MOTOS (and through their closure, MOTS) in 4-dimensional Schwarzschild spacetime, using Painlevé-Gullstrand coordinates. Given how complicated the binary black hole merger spacetime is, they wondered whether the self-intersecting behaviour seen in [30] was a product of this complexity, or instead a more general phenomenon. To this end, they chose to search for self-intersecting MOTS in the simplest possible black hole spacetime; figuring if they could find it there, they could conclude the existence of such surfaces independent of the complexity of the spacetime.

However, a more direct motivation lies in the work of [15], where it was shown that for an extreme mass ratio merger, that is, a binary black hole merger where the mass of one of the black holes is much larger than the mass of the other, the spacetime near the smaller black hole (assuming it is non-rotating) can be approximated by Schwarzschild. This means that studying the MOTOS (and by extension, MOTS) of a Schwarzschild black hole directly leads to information about the structure of the MOTS involved in an extreme mass ratio merger [11].

2.2.1 Method

The method used in [11] is direct. One begins with the 4D Schwarzschild metric in Painlevé-Gullstrand coordinates (which will be discussed in some more detail in chapter 3),

$$g_{\alpha\beta}dx^\alpha dx^\beta = -\left(1-\frac{2m}{r}\right)d\tau^2 + 2\sqrt{\frac{2m}{r}}d\tau dr + dr^2 + r^2 d\Omega^2, \tag{2.1}$$

and takes slices of constant time, $\Sigma_t = \Sigma$, which are intrinsically flat, and (of course) spacelike. They then have metric

$$h_{ij}dx^i dx^j = dr^2 + r^2 d\Omega^2 \tag{2.2}$$

showing that they are flat. One finds their extrinsic curvature by taking the trace (as described in section 1.2) of the timelike normal to each of these Σ, which is

$$\hat{u} = \frac{\partial}{\partial\tau} - \sqrt{\frac{2m}{r}}\frac{\partial}{\partial r}, \tag{2.3}$$

from which the extrinsic curvature is found to be

$$K_{ij}dx^i dx^j = \sqrt{\frac{m}{2r^3}}dr^2 - \sqrt{2mr}d\Omega^2. \tag{2.4}$$

This is the extrinsic curvature pulled-back onto the time slice, hence it has the Latin indices. As in chaper 1 and for the rest of this text, Greek indices indicate something which exists in the full (4-dimensional here, but 5 later) spacetime, while lower Latin indices indicate something which exists on the (3-dimensional here) time slice, and upper case Latin indices are for objects which exist on the (2-dimensional here) hypersurface on the slice.

They then defined a general rotationally symmetric hypersurface in this timeslice, parameterized by (λ, ϕ) as

$$(\tau_0, r, \theta, \phi) = (T_0, R(\lambda), \Theta(\lambda), \phi), \tag{2.5}$$

where of course τ_0 is set to whichever leaf of the time foliation one is working on.

The tangent vector to this surface is

$$\frac{d}{d\lambda} = \dot{R}\frac{\partial}{\partial r} + \dot{\Theta}\frac{\partial}{\partial \theta}, \tag{2.6}$$

where the dots indicate differentiation with respect to the surface parameter λ (of course, ∂_ϕ is also tangent).

The metric on the hypersurface, denoted $\tilde{q}_{AB}$ as in chapter 1, is

$$\tilde{q}_{AB} dx^A dx^B = (\dot{R} + R^2\dot{\Theta}^2)d\lambda^2 + R^2 \sin^2 \Theta d\phi^2. \tag{2.7}$$

The spacelike normal to the hypersurface is

$$\hat{n} = \frac{R}{\sqrt{\dot{R}^2 + R^2\dot{\Theta}^2}} \left(\dot{\Theta}\frac{\partial}{\partial r} - \frac{\dot{R}}{R^2}\frac{\partial}{\partial \theta} \right). \tag{2.8}$$

As before, the null normals to the surface are $\hat{\ell}_+ = \hat{u} + \hat{n}$ and $\hat{\ell}_- = \frac{1}{2}(\hat{u} - \hat{n})$, but one may simply calculate the spacelike and timelike expansions, and take their linear combination in the same way as the normal one is using. For the work which this derivation is taken from [11], a method of numerical integration was used which required switching between the two null normal directions, so as to maintain a consistent outward direction. You will see that the updated method, used in this thesis, does not require such switching.

Continuing to follow the derivation of [11], the spacelike and timelike expansions are (respectively)

$$\theta_n = \frac{1}{\sqrt{\dot{R} + R^2\dot{\Theta}^2}} \left(\frac{R(\dot{R}\ddot{\Theta} - \dot{\Theta}\ddot{R}) + \dot{\Theta}\dot{R}^2}{\dot{R}^2 + R^2\dot{\Theta}^2} - \frac{\dot{R}\cot\Theta}{R} + 2\dot{\Theta} \right) \tag{2.9}$$

$$\theta_u = -\frac{\sqrt{2m}}{2R^{3/2}} \left(\frac{\dot{R}^2 + 4R^2\dot{\Theta}^2}{\dot{R}^2 + R^2\dot{\Theta}^2} \right). \tag{2.10}$$

They then set the null expansions equal to zero, which in this case means one of the following equations hold:

$$\theta^+ = 0 = \theta_u + \theta_n \tag{2.11}$$

$$\theta^- = 0 = \theta_u - \theta_n. \tag{2.12}$$

Which of these equations should be used is determined in [11] by which is outward-oriented; as said, they switched between them to maintain this outward orientation.

2.2.2 Solving for MOTOS

In [11], they chose to parameterize the hypersurface S with coordinate parameterizations, that is, $\lambda = r$ and $\lambda = \theta$. This provided them with 4 equations to solve to find MOTOS:

$$R^{Eq}_{\pm} : R_{\theta\theta} - \frac{3R_\theta^2}{R} + \frac{R_\theta \cot\theta}{R^2}(R_\theta^2 + R^2) - 2R \pm \sqrt{\frac{m}{2}}\frac{\sqrt{R_\theta^2 + R^2}(R_\theta^2 + 4R^2)}{R^{5/2}} = 0 \quad (2.13)$$

$$\Theta^{Eq}_{\pm} : \Theta_{rr} + \frac{3\Theta_r}{r} - \frac{\cot\Theta}{r^2}(1 + r^2\Theta_r^2) + 2\Theta_r^3 \mp \sqrt{\frac{m}{2}}\frac{\sqrt{1 + r^2\Theta_r^2}(1 + 4r^2\Theta_r^2)}{r^{5/2}} = 0 \quad (2.14)$$

where in the first equation the normal is in the direction

$$\hat{n} = \frac{R}{\sqrt{R_\theta^2 + R^2}}\left(\frac{\partial}{\partial r} - \frac{R_\theta}{R}\frac{\partial}{\partial\theta}\right) \quad (2.15)$$

and for the second equation, it is

$$\hat{n} = \frac{r}{\sqrt{1 + r^2\Theta_r^2}}\left(\Theta_r\frac{\partial}{\partial r} - \frac{1}{r^2}\frac{\partial}{\partial\theta}\right). \quad (2.16)$$

To find MOTS, the normal must be consistently outward directed, and thus if one were solving, say, (2.13), one would need to alternative between R^{Eq}_{+} and R^{Eq}_{-} so as to maintain the outward direction of $\hat{n}$ [11].

The issue they encounter in attempting to solve the above equations (2.13) and (2.14) numerically in [11] is the coordinate singularities, that is, $dR/d\theta \to 0 \iff d\Theta/dr \to \infty$ and $d\Theta/dr \to 0 \iff dR/d\theta \to \infty$.

Their solution to the issue is to switch between solving for $R(\theta)$ and $\Theta(r)$; when one of the derivatives blows up, they switch to solving for the other coordinate, which will have its corresponding derivative go to zero there. There is overlap between the solutions for $R(\theta)$ and $\Theta(r)$, and so they are able to patch these solutions together continuously and, in this way, get the full MOTOS solution without any singularities. However, this switching is no longer necessary for the work in the succeeding chapters, as the new method circumvents the coordinate singularity issues.

2.2.3 4D Schwarzschild Results (MOTS and MOTOS)

Beginning with the less interesting results from [11], one sees in figure 2.4 the marginally outer trapped open surfaces for the 4-dimensional Schwarzschild spacetime, which leave the z-axis from $z < 0$ and have upward oriented null normals. Noting in the right plot of figure 2.4, it appears at $z = -2$ there are two surfaces which have the same $z(0)$ value, but are not the same—one being the apparent horizon, and one being a MOTOS. Of course, there is a uniqueness theorem which requires that if two consistently oriented MOTS have the same $z(0)$ value in this way, they will be the same [6][3][24]. But, looking more closely, one can see that the null normal to the apparent horizon points downward, whereas that of the MOTOS points upward, meaning these aren't consistently oriented. If one were to instead choose to plot a MOTS which started at $z(0) = -2$ and had a downward null normal, the semi-circle of the apparent horizon would be the plot found.

The MOTOS which leave the z-axis for $z > 0$ and have (initially) upward oriented null normals have much more interesting behaviour than those which leave from the negative z-axis: there are similar self intersections [11] as were observed in [30]. One can see from figure 2.5 that the MOTOS which leave the axis for positive z much larger than $z = 2M$ have similar behaviour to those which leave the axis for negative z, but as they approach $2M$, they begin to wrap around the apparent horizon.

Figure 2.6(a) shows the behaviour of these MOTOS (in grey) around the apparent horizon (in black) both for $z(0) \to 2M$, and for $z(0) < 2M$. One can see here that as $z(0)$ approaches $2M$, the MOTOS wrap increasingly tightly around the apparent horizon, with the inflection point moving closer and closer to the negative z-axis (toward $-z(0)$). The apparent horizon itself, then, can be interpreted as the MOTOS for which the inflection point exists exactly at $-z(0)$, and thus for which the surface closes. Hence, this MOTOS is in fact a MOTS, that is, the apparent horizon.

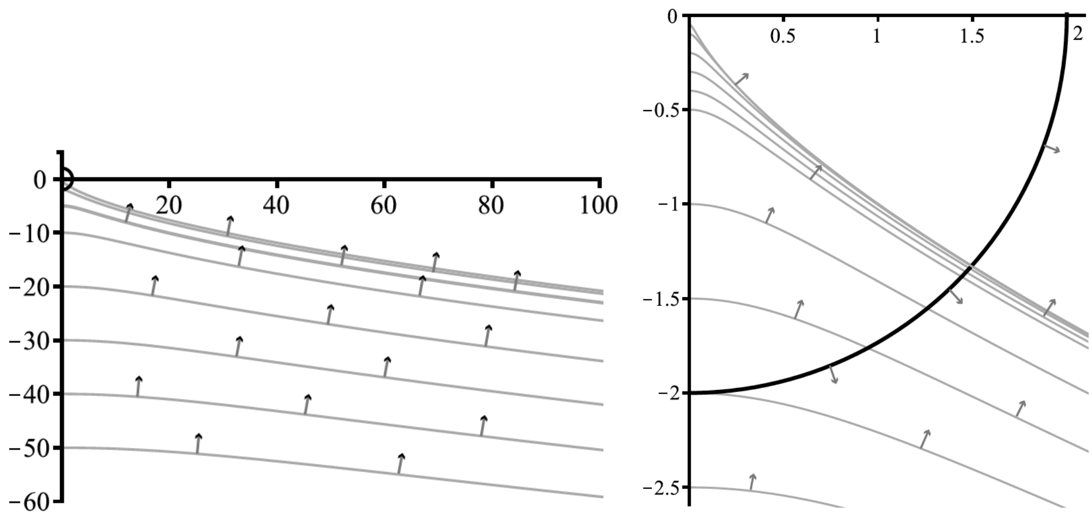

Figure 2.4: Figure taken from [11]; the left figure shows the apparent horizon at $r = 2M$ at a semicircle in black, and the MOTOS as lines in grey, which all leave the z-axis for values $z_0 < 0$. The arrows show the direction of the null normal. The right figure is a zoomed in version of the left, showing the MOTOS leaving the z-axis and crossing the apparent horizon. The vertical axis plots $R\sin(\Theta)$, the horizontal plots $R\cos(\Theta)$.

This behaviour—where a series of MOTOS close in to form a closed MOTS—occurs inside of $r = 2M$ as well. Observing figure 2.6(b), one sees grey MOTOS leaving the z-axis just outside of a black closed MOTS, which in this case has a self-intersection in it. Then the MOTOS which approach this MOTS from the inside all have two self-intersections—that is, two loops. The second loop moves down toward the z-axis, toward a specific z-value ($z(0) \approx 1.037M$ [11]), and narrows on itself as it does so. When it intersects the z-axis, it is at a single point, as the loop has narrowed to produce a cusp. This is how the closed MOTS is produced, analogously to how the apparent horizon can be seen as being produced by a series of the MOTOS.

Comparing figures 2.6(b) and 2.6(a), one can follow on 2.6(a) the series of MOTOS from just inside the apparent horizon, until the self-intersection is aligned with the horizontal axis. At this point, one can then look to 2.6(b) and find the outermost MOTOS in this figure to be the innermost in the former. In this way one sees a continuous series of them, which show the connection between the apparent horizon (a MOTS with zero loops) to the first self-intersecting MOTS.

And, in fact, they found that this same behaviour continues indefinitely [11], with

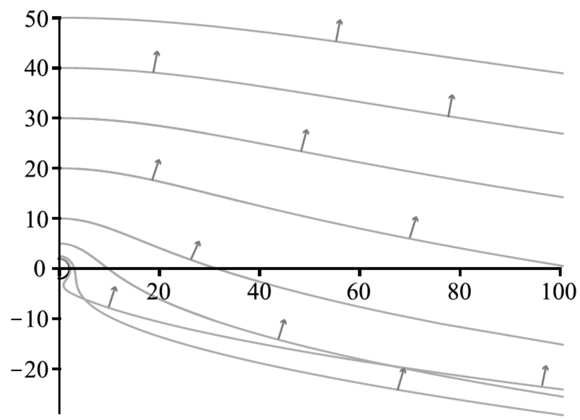

Figure 2.5: Figure taken from [11]; the analog of figure 2.4 (left) but for $z > 0$ leaving the axis. The null normals are initially upward pointing, and one can see they wrap around the apparent horizon as they get close to it. The vertical axis plots $R\sin(\Theta)$, the horizontal plots $R\cos(\Theta)$.

a MOTS having two loops existing inside the MOTS with one, one having three loops existing inside this, etc. Figure 2.7 shows the first 12 of these such MOTS, and the values of z from which they leave the axis. One can see the loops become smaller nearer to the horizontal axis, and the more loops there are, the more dramatic this appears.

In [11], they mention that they expect similar types of self-intersecting MOTS and MOTOS will exist in other spacetimes, which are axisymmetric. That they were able to find the self-intersections in the MOTS of the Schwarzschild spacetime, which is the simplest possible black hole solution, as motivated by their existence in the spacetime of a binary merger—substantially more complicated—suggests a level of generality. As well, one might expect that just as the solutions for Schwarzschild can be useful in understanding the extreme mass ratio mergers [15], it might be the case that finding these expected self-intersecting MOTS in other spacetimes would allow for an analogous application to mergers. This is further supported by [16], where the same authors followed a similar approach as in [15], but in this case the spacetime of the small black hole was that of Kerr, rather than Schwarzschild.

Motivated by this, the following work—which is the subject of this thesis—seeks to find self-intersecting MOTS in two different five-dimensional spacetimes: Schwarzschild, and Myers-Perry (a five dimensional analogue of Kerr).

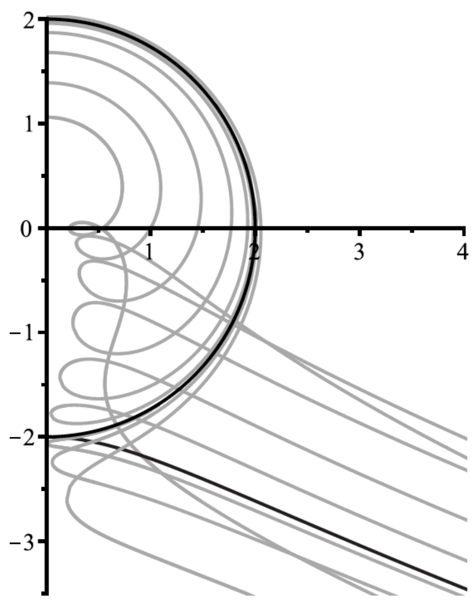

(a) The MOTOS with initially upward oriented null normals wrapping around the horizon $r = 2M$, as well as producing self-intersections for $z(0) < 2M$. Figure taken from [11].

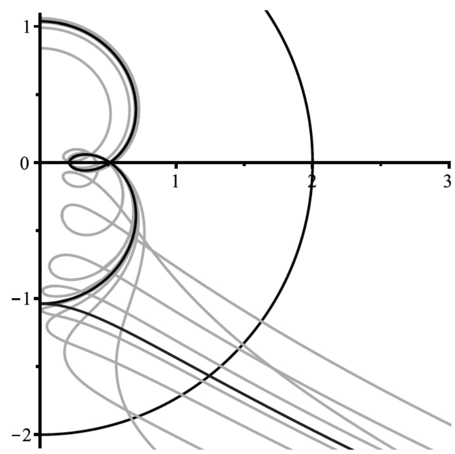

(b) The apparent horizon (which is a MOTS) is once again shown, but the first MOTS that exists inside $r = 2M$ is shown here as well (in black). This MOTS has a self-intersection not unlike those seen in [30]. The MOTOS around it behave analogously to those around the apparent horizon, except the ones inside it have two loops, and those outside have one.

Figure 2.6: The vertical axis plots $R \sin \Theta$, the horizontal plots $R \cos \Theta$.

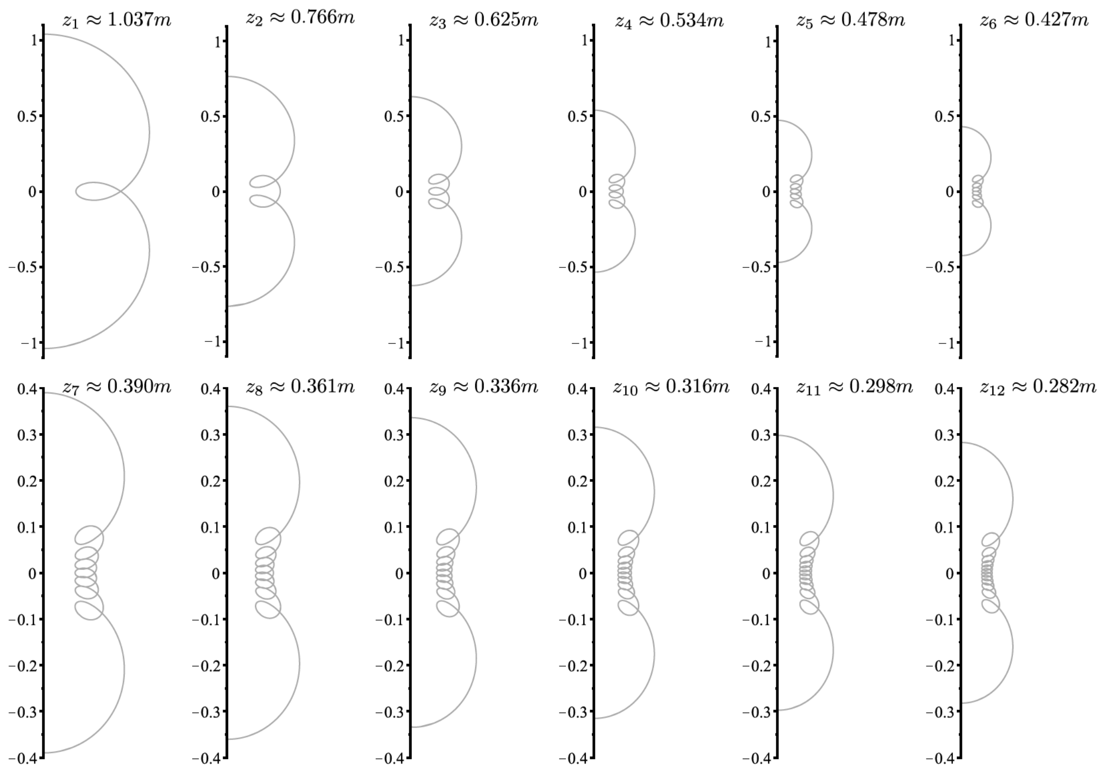

Figure 2.7: The first 12 closed self-intersecting MOTS for the 4D Schwarzschild spacetime; figure taken from [11].

Chapter 3

5-Dimensional Schwarzschild Spacetime

This section covers the generalization of Schwarzschild spacetime (in 3+1 dimensions) to $N + 1$ dimensions, hereafter referred to as $n + 3$ dimensions ($n \geq 1$), where this is the notation used in [15]. This general form is then used to define the 5-dimensional Schwarzschild metric in the usual Schwarzschild coordinates.

From here, the metric is converted into Painlevé-Gullstrand coordinates, in which the metric does not have a coordinate singularity at $r = r_0$, and therefore can be used to probe the inside of the black hole—as discussed in relation to the previous paper by my collaborators [11].

Finally, the second coordinates we choose, Weyl coordinates—which are a 4 dimensional analog of cylindrical coordinates—are motivated and explained, and the metric used for the succeeding work is given.

3.1 Motivation for Working in 5D

We choose to look for the self-intersecting MOTS in 5-dimensional spacetime for two reasons: the first being that the generalization of 4D Schwarzschild to 5D is not difficult, and thus one may easily see how adding a dimension to the spacetime affects the existence and behaviour of the MOTS. This, in turn, allows for one to make further conclusions about the generality of these self-intersecting surfaces. It is also the case, as will be seen in chapter 5, that 5-dimensional Myers-Perry spacetime, under certain assumptions about asymptotic flatness and all rotation parameters being equal, is simpler than its 4-dimensional analogue (Kerr). Thus choosing to work in 5 dimensions, in this case, is a good intermediate step to finding the looping MOTS in the Kerr spacetime.

The second reason involves binary black hole mergers more directly. As briefly mentioned before, in 2016, Emparan and Martinez [15] produced a model of an extreme mass ratio merger that involves approximating the large black hole as a congruence of null geodesics passing through a Schwarzschild spacetime of a black hole with mass m (that of the smaller of the two involved in the merger). In this paper, they followed the event horizon as $r \to \infty$ and found that

$$t_q(r \to \infty) = r + r_0 \ln\left(r/r_0\right) + O(1/r), \tag{3.1}$$

when the dimension of the spacetime was 4. Here, q is the impact parameter of each geodesic at infinity, that is, it will pass by the small black hole, and in Cartesian coordinates will have $x(r \to \infty) = q$. In this way one may choose a geodesic in the congruence through choice of its impact parameter. Then t_q is the Killing time of the geodesic which has impact parameter q.

However, they also in this paper considered the case of the event horizon for $D \geq 5$, and found here that

$$t_q(r \to \infty) = r + O(1/r^n), \tag{3.2}$$

meaning that for 5 dimensions specifically, $t_q(r \to \infty) = r + O(1/r^2)$. One notices immediately that the asymptotic behaviour of the event horizon when $D = 5$ does not have the logarithmic term that it has for $D = 4$.

This is relevant because it was hypothesized by my collaborators that the apparent horizon for this spacetime, which is a MOTOS in this case because it is open when the larger of the two black holes is approximated as a sheet congruence, should coincide with the event horizon when $r \to \infty$. Thus in [11] they also looked at these asymptotic expansions for MOTOS in the 4 dimensional Schwarzschild spacetime, but were not able to find a simple series involving powers of r and $\ln(r)$.

It is the existence of this logarithmic term which poses the problem. Since the asymptotic expansions of the event horizon for $D = 5$ are linear in r without any logarithmic terms, it is reasonable to expect that perhaps matching the asymptotic expansions of the apparent horizon for 5D Schwarzschild to that of the event horizon for $D = 5$ in [15] would be easier than for the four dimensional case. While this task is not the topic of this thesis, it suggests producing a complete and consistent picture of how MOT(O)S fit into the model introduced in [15] could be a tenable task when working in five dimensions.

3.2 The Schwarzschild Solution

The four-dimensional Schwarzschild metric was the first non-trivial solution found to Einstein's field equations, and is also arguably the most well-known:

$$ds^2 = -\left(1 - \frac{r_0}{r}\right) dt^2 + \left(1 - \frac{r_0}{r}\right)^{-1} dr^2 + r^2(d\theta^2 + \sin^2(\theta)d\phi^2). \tag{3.3}$$

Here $r_0 = 2M$ is the radius of the apparent horizon of the Schwarzschild black hole, and is notation used to be consistent with [15].

One can generalize this solution to an n+3-dimensional version [15],

$$ds^2 = -\left(1 - \frac{r_0^n}{r^n}\right) dt^2 + \left(1 - \frac{r_0^n}{r^n}\right)^{-1} dr^2 + r^2 d\Omega^2_{(n+1)}. \tag{3.4}$$

Mass is defined for 4+1 dimensions as having units of length squared, and thus the above $r_0^2 \propto M$ (where M is the mass parameter), rather than $\propto M^2$ as one might expect (when comparing to 4 dimensions). Indeed, the ADM mass of the black hole is $m_{ADM} = 3\pi r_0^2/8$.

3.3 Painlevé-Gullstrand and Toroidal Coordinates

Painlevé-Gullstrand coordinates were chosen in [11] for a few reasons. Firstly, they are horizon-penetrating, meaning that they have no coordinate singularity across $r = r_0$ and so one can see inside the apparent horizon with them. As well, the surfaces of constant time in Painlevé-Gullstrand are not static, and as such, there is a non-zero extrinsic curvature on these slices. This leads to the outward and inward oriented null expansions of these time slices to be independent of one another, as compared to

Schwarzschild coordinates, where if one vanishes, they both must [11]. This suggests Painlevé-Gullstrand coordinates are more general, in the sense relevant here, and thus a good choice.

As a brief review, to transform from the above four-dimensional Schwarzschild coordinates into PG, one first defines a new time coordinate $\tau = t - a(r)$, and chooses the function $a(r)$ such that the Schwarzschild metric in PG coordinates is

$$ds^2 = -\left(1 - \frac{r_0}{r}\right) d\tau^2 + 2\sqrt{\frac{r_0}{r}} d\tau dr + dr^2 + r^2 d\Omega^2. \tag{3.5}$$

Beginning with the $5D$ Schwarzschild metric in regular Schwarzschild coordinates,

$$ds^2 = -\left(1 - \frac{r_0^2}{r^2}\right) dt^2 + \left(1 - \frac{r_0^2}{r^2}\right)^{-1} dr^2 + r^2 d\Omega^2, \tag{3.6}$$

we make the same transformation $\tau = t - a(r)$. Setting $g_{rr} = 1$ specifies that

$$a' = \frac{r r_0}{r_0^2 - r^2} \Rightarrow a(r) = -\frac{1}{2} r_0 \ln(r_0^2 - r^2) + C \tag{3.7}$$

and the metric in Painlevé-Gullstrand coordinates will then be

$$ds^2 = -\left(1 - \frac{r_0^2}{r^2}\right) d\tau^2 + \frac{2r_0}{r} d\tau dr + dr^2 + r^2 d\Omega^2 \tag{3.8}$$

This is easily checked to be a solution of the vacuum Einstein equations. In this coordinate system, ∂_r is null.

3.3.1 Toroidal Foliation of the 3-sphere

Explicitly, the spherical part of the metric of (3.8) is

$$r^2 d\Omega^2 = r^2 \left(d\theta^2 + \sin^2\theta d\phi^2 + \sin^2\theta \sin^2\phi d\psi^2\right), \tag{3.9}$$

that is, regular 5-dimensional spherical coordinates. (Here $\theta \in (0, \pi]$, $\phi \in (0, \pi]$, and $\psi \in (0, 2\pi]$.) The problem exists in the last term of the metric, because it is dependent not only on θ but also on ϕ. This means that ϕ is not a Killing vector for this spacetime, which means that the assumptions one requires for the method (which will be described in chapter 4) do not hold. Thus, one must choose a different foliation of the 3-sphere, which allows for two of the angular coordinates to be Killing vectors. Choosing toroidal coordinates ϕ_1, ϕ_2 satisfies this, and in these coordinates the angular part of (3.8) is then

$$d\Omega_3^2 = d\theta^2 + \sin^2(\theta)d\phi_1^2 + \cos^2(\theta)d\phi_2^2, \tag{3.10}$$

where $\theta \in [0, \pi/2)$, and ϕ_1, ϕ_2 are periodic with period 2π (this ensures the whole of S^3 is covered). So the metric is

$$ds^2 = -\left(1 - \frac{r_0^2}{r^2}\right) d\tau^2 + \frac{2r_0}{r} d\tau dr + dr^2 + r^2 \left(d\theta^2 + \sin^2(\theta)d\phi_1^2 + \cos^2(\theta)d\phi_2^2\right). \tag{3.11}$$

Of course, the metric is then only dependent on r, θ, and the method which will be outlined in chapter 4 can be applied.

3.4 Weyl Coordinates

While one may solve for the MOTS in the above spherical/toroidal coordinates (and later some such solutions are included), we chose to solve for the MOTS also in an analog of cylindrical coordinates, called Weyl coordinates. This is because it allows for easier comparison to current work in progress on the 4-dimensional case, which employs the method outlined in chapter 2.

In 3 dimensional cylindrical coordinates (ρ, x, ϕ), the Killing field $\frac{\partial}{\partial \phi}$ vanishes on $\rho = 0$, the z-axis. One can define cylindrical coordinates using a general Killing field, m^a, and the symmetry about an axis that this generates. One defines

$$\rho = \sqrt{g_{ab} m^a m^b}. \tag{3.12}$$

For example, starting from spherical coordinates $ds^2 = dr^2 + r^2 d\theta^2 + r^2 \sin^2(\theta) d\phi^2$, for flat space if the Killing field is ∂_ϕ, then

$$\rho = \sqrt{g_{\phi\phi}} = r \sin(\theta), \tag{3.13}$$

which of course agrees with the usual definition of ρ in terms of spherical coordinates.

Weyl coordinates are then a generalization of this, where there exist two Killing fields, ∂_{ϕ_1} and ∂_{ϕ_2}, which each vanish on half of the $\rho = 0$ axis [1]. The ϕ_1, ϕ_2 are from the toroidal foliation of the 3-sphere.

To formulate Weyl coordinates, one first considers 4-dimensional flat space as $\mathbb{R}^2 \times \mathbb{R}^2$, with metric in the form

$$ds^2 = dr_1^2 + r_1^2 d\phi_1^2 + dr_2^2 + r_2^2 d\phi_2^2 \tag{3.14}$$

Comparing this with the metric in Cartesian coordinates, one can immediately see that $r_1 = \sqrt{x_1^2 + x_2^2}$, $r_2 = \sqrt{x_3^2 + x_4^2}$, and $\arctan(x_2/x_3) = \phi_1$, $\arctan(x_4/x_3) = \phi_2$.

If one then considers only the Killing field part of the metric (2.8), then one may define ρ via the determinant of this metric $g_K = r_1^2 d\phi_1^2 + r_2^2 d\phi_2^2$:

$$\rho = \sqrt{\det g_K} = \sqrt{r_1^2 r_2^2} = r_1 r_2. \tag{3.15}$$

One may then find z in terms of r_1, r_2 by finding the harmonic conjugate to $\rho = \sqrt{r_1^2 r_2^2}$.

Taking $\rho(r_1, r_2)$ to be a function on a connected open subset of $\mathbb{R}^2$, $z(r_1, r_2)$ is the harmonic conjugate of ρ if and only if the two functions together satisfy the Cauchy-Riemann equations (on the connected open subset). So, one requires that

$$\frac{\partial \rho}{\partial r_1} = r_2 = \frac{\partial z}{\partial r_2} \qquad\qquad \frac{\partial \rho}{\partial r_2} = r_1 = -\frac{\partial z}{\partial r_1}, \tag{3.16}$$

from which one gets $z = \frac{1}{2}(r_2^2 - r_1^2)$.

Spherical to Weyl Coordinate Transform

The transform from the metric of (3.11) to Weyl coordinates is

$$\begin{aligned} R &= \sqrt{2}(\rho^2 + z^2)^{1/4} \\ \theta &= \arctan\sqrt{\frac{\sqrt{\rho^2 + z^2} - z}{\sqrt{\rho^2 + z^2} + z}}, \end{aligned} \tag{3.17}$$

and of course the toroidal angular coordinates are the same.

The flat metric of $\mathbb{R}^4$ in the Weyl+toroidal coordinates is written

$$ds^2 = \frac{d\rho^2 + dz^2}{2\sqrt{\rho^2 + z^2}} + (\sqrt{\rho^2 + z^2} - z)d\phi_1^2 + (\sqrt{\rho^2 + z^2} + z)d\phi_2^2, \tag{3.18}$$

and $\rho \geq 0$, $-\infty < z < \infty$ will cover all of $\mathbb{R}^4$.

3.4.1 Metric in PG+Weyl

Finally, the metric for 5-dimensional Schwarzschild in Painlevé-Gullstrand Weyl coordinates is

$$\begin{aligned} ds^2 = -\left(1 - \frac{r_0^2}{2\sqrt{\rho^2 + z^2}}\right) d\tau^2 + \frac{r_0}{\rho^2 + z^2}(\rho d\rho + z dz)d\tau + \frac{d\rho^2 + dz^2}{2\sqrt{\rho^2 + z^2}} \\ +(\sqrt{\rho^2 + z^2} - z)d\phi_1^2 + (\sqrt{\rho^2 + z^2} + z)d\phi_2^2. \end{aligned} \tag{3.19}$$

From here, one may proceed in finding the marginally outer trapped surfaces in this spacetime.

Chapter 4

Finding the MOTSodesic Equations

There are two equivalent methods for finding the equations of motion, which define the MOTS (hereafter referred to as the *MOTSodesic* equations (a term coined in [31])): both of which concern taking first a time foliaton of the five-dimensional spacetime, and then defining a general rotationally-symmetric hypersurface on one of these spacelike "leaves".

The first method outlined employs directly (perhaps naively) the definitions from section 1.2; it requires one to find the timelike and spacelike expansions of the timeslice and the hypersurface (respectively), and then simply add them to get a null expansion. This method differs from that of [11] in that it employs an arclength parameterization of the hypersurface, which provides a relation that allows for the final equation to be separated into two coupled ODEs, each of which are second order in only one of the functions being solved for. This allows for the use of numerical solving techniques: in fact, it no longer requires the switching method as described in chapter 2 and employed in [11].

The second method is more conceptually illuminating, as it derives more general analogues to the geodesic equations for MOTS. Hence, calling the EOMS "MOTSodesic" equations. This method requires the assumption that both of the angular coordinates (which aren't functions of the parameter λ) be Killing vectors, and hence is the reason we employ the toroidal coordinates.

I will begin with the more direct, computational approach, and then having developed some intuition for the method, I will describe the more conceptually illuminating approach. The derivation is done explicitly for metric (3.19), however results will be included in succeeding chapters also for (3.8).

4.1 Preliminary Definitions

Begin with the spacetime $(\mathcal{M}, g_{\alpha\beta}, \nabla_\alpha)$, which is the 5-dimensional Schwarzschild spacetime. Here, ∇_α is the covariant derivative on the full spacetime and $g_{\alpha\beta}$ is the metric. Lowercase Greek indices represent objects existing in the full (5D) spacetime, lowercase Latin indices represent those which exist in the (4D) timeslice, and uppercase Latin indices represent the objects which exist on the (3D) hypersurface in this timeslice. D_i, D_A are covariant derivatives on the timeslice and hypersurface, respectively.

4.1.1 Defining the Time-Foliation

First take a timeslice in the 5-dimensional spacetime: setting $\tau = \text{const} \Rightarrow d\tau = 0$ in the metric of equation (3.19) to get spacelike leaves, each with metric

$$h_{ij}dx^i dx^j = \frac{d\rho^2 + dz^2}{2\sqrt{\rho^2 + z^2}} + (\sqrt{\rho^2 + z^2} - z)d\phi_1^2 + (\sqrt{\rho^2 + z^2} + z)d\phi_2^2. \tag{4.1}$$

This is the flat metric on $\mathbb{R}^4$ in these Weyl coordinates. Recall: $\rho > 0$, $z \in \mathbb{R}$, and ϕ_1, ϕ_2 are 2π-periodic angles.

4.1.2 Defining Rotationally-Symmetric Hypersurface

One then defines a rotationally-symmetric (spacelike) hypersurface in the timeslice. This is done by letting ρ and z be functions of the parameter λ: $\rho = R(\lambda)$, $z = Z(\lambda)$. Then the coordinates on the hypersurface are $(\lambda, \phi_1, \phi_2)$ and the metric on it is

$$\tilde{q}_{AB}dx^A dx^B = \frac{\dot{R}^2 + \dot{Z}^2}{2\sqrt{R^2 + Z^2}}d\lambda^2 + (\sqrt{R^2 + Z^2} - Z)d\phi_1^2 + (\sqrt{R^2 + Z^2} + Z)d\phi_2^2 \tag{4.2}$$

where the dot over either of the R or Z functions denotes derivative with respect to λ.

Arclength Parameterization

An arclength parameterization is then chosen, meaning that the norm of the tangent vector $\partial/\partial\lambda$ is set to one. This means that the coefficient of $d\lambda$ in the metric on the hypersurface is equal to one, and thus

$$\frac{\dot{R}^2 + \dot{Z}^2}{2\sqrt{R^2 + Z^2}} = 1, \tag{4.3}$$

which will be referred to as the the "arclength condition". This will be used explicitly in the computational method to switch from a single differential equation second order in both R and Z, into two coupled ODEs which are individually second order in either R or Z. These are substantially easier to solve numerically.

The metric on the hypersurface with the arclength condition imposed is then, of course,

$$\tilde{q}_{AB} dx^A dx^B = d\lambda^2 + (\sqrt{R^2 + Z^2} - Z) d\phi_1^2 + (\sqrt{R^2 + Z^2} + Z) d\phi_2^2. \tag{4.4}$$

It is readily seen that the hypersurface is flat (remembering that $\sqrt{R^2 + Z^2} \mp Z = r_1^2, r_2^2$ respectively).

4.2 Computational Method

4.2.1 Overview

The more computational method is conceptually more direct and thus simpler, but computationally more complicated—and it also lacks the obvious interpretation of the final ODEs as analogous to geodesic equations. As a review from section 1.2:

One defines the 5-dimensional timelike unit normal to the timeslice, u_α, and from this gets the covariant derivative of it, $\nabla_\alpha u_\beta$. This is pulled back to the timeslice (to get the extrinsic curvature $K_{ij} = e_i^\alpha e_j^\beta \nabla_\alpha u_\beta$), and then contracted using the pushed-forward inverse hypersurface metric, $\tilde{q}^{ij}$; this is of course the timelike expansion, $\theta_u = \tilde{q}^{ij} K_{ij}$.

One then finds the spacelike expansion analogously, taking the covariant derivative of the spacelike unit normal to the hypersurface, $D_i n_j$ and contracting it with the pushed-forward inverse hypersurface metric as well; $\theta_n = \tilde{q}^{ij} D_i n_j$.

Finally, these two expansions are added together to produce the null expansion, θ, and the resulting equation is set equal to zero, in accordance with the definition of a MOTS.

The last step is to use the arclength condition to separate the final DE into two, each of which are only second-order in each of the two coordinates. This eliminates the need for the switching in [11], and so makes the final ODEs much easier to solve numerically.

4.2.2 Timelike Expansion

The (future-pointing) normal to the timeslice is $-dT$, and this is already of unit length: $g^{\alpha\beta} dT_\alpha dT_\beta = -1$. Taking its covariant derivative, one gets the 5-dimensional extrinsic curvature to be

$$K_{\alpha\beta} = \begin{bmatrix} \frac{r_0^3}{4(z^2+\rho^2)} & \frac{r_0^2\rho}{4(z^2+\rho^2)^{3/2}} & \frac{r_0^2 z}{4(r^2+\rho^2)^{3/2}} & 0 & 0 \\ \frac{r_0^2\rho}{4(r^2+\rho^2)^{3/2}} & \frac{r_0(\rho^2-z^2)}{4(z^2+\rho^2)^2} & \frac{r_0 z\rho}{2(z^2+\rho^2)^2} & 0 & 0 \\ \frac{r_0^2 z}{4(r^2+\rho^2)^{3/2}} & \frac{r_0 z\rho}{2(z^2+\rho^2)^2} & \frac{r_0(z^2-\rho^2)}{4(z^2+\rho^2)^2} & 0 & 0 \\ 0 & 0 & 0 & \frac{r_0(z\sqrt{z^2+\rho^2}-(z^2+\rho^2))}{2(z^2+\rho^2)} & 0 \\ 0 & 0 & 0 & 0 & -\frac{r_0(z\sqrt{z^2+\rho^2}+(z^2+\rho^2))}{2(z^2+\rho^2)}. \end{bmatrix} \tag{4.5}$$

This is pulled back into the timeslice very obviously, because it is a coordinate hypersurface, and one has

$$K_{ij} = \begin{bmatrix} \frac{r_0(\rho^2-z^2)}{4(z^2+\rho^2)^2} & \frac{r_0 z\rho}{2(z^2+\rho^2)^2} & 0 & 0 \\ \frac{r_0 z\rho}{2(z^2+\rho^2)^2} & \frac{r_0(z^2-\rho^2)}{4(z^2+\rho^2)^2} & 0 & 0 \\ 0 & 0 & \frac{r_0(z\sqrt{z^2+\rho^2}-(z^2+\rho^2))}{2(z^2+\rho^2)} & 0 \\ 0 & 0 & 0 & -\frac{r_0(z\sqrt{z^2+\rho^2}+(z^2+\rho^2))}{2(z^2+\rho^2)} \end{bmatrix} \tag{4.6}$$

defined on the 4-dimensional spacelike slice.

The timelike expansion is found by contracting this with the pushed-forward inverse hypersurface metric, $\tilde{q}^{ij}$. It is pushed-forward using the operators $\hat{e}^i_A = \partial x^i / \partial x^A$; that is,

$$\tilde{q}^{ij} = q^{AB} \hat{e}^i_A \hat{e}^j_B = q^{AB} \frac{\partial x^i}{\partial x^A} \frac{\partial x^j}{\partial x^B}, \tag{4.7}$$

so that

$$\tilde{q}^{ij} = \begin{bmatrix} \dot{R}^2 & \dot{R}\dot{Z} & 0 & 0 \\ \dot{R}\dot{Z} & \dot{Z}^2 & 0 & 0 \\ 0 & 0 & \frac{1}{(\sqrt{Z^2+R^2}-Z)} & 0 \\ 0 & 0 & 0 & \frac{1}{(\sqrt{Z^2+R^2}+Z)} \end{bmatrix}. \tag{4.8}$$

So, finally, one gets

$$\theta_u = \tilde{q}^{ij} K_{ij} = -\frac{r_0}{\sqrt{R^2+Z^2}} + \frac{r_0(\dot{R}R + \dot{Z}Z)^2}{4(R^2+Z^2)^2} - \frac{r_0(\dot{R}Z - \dot{Z}R)^2}{4(R^2+Z^2)^2} \tag{4.9}$$

for the timelike expansion. Here, $\rho = R(\lambda)$, $z = Z(\lambda)$ are set in the extrinsic curvature.

4.2.3 Spacelike Expansion

Finding Spacelike Normal

We require a unit normal to the hypersurface in the $\partial_\rho, \partial_z$ direction. This can be found easily by making the assumption that it will be of the form

$$\hat{N} = n_1 d\rho + n_2 dz \tag{4.10}$$

for some n_1, n_2. The tangent to the hypersurface is of course

$$\hat{T} = \frac{\partial}{\partial \lambda} = \frac{\partial \rho}{\partial \lambda}\frac{\partial}{\partial \rho} + \frac{\partial z}{\partial \lambda}\frac{\partial}{\partial z} = \dot{R}\frac{\partial}{\partial \rho} + \dot{Z}\frac{\partial}{\partial z}, \tag{4.11}$$

and so enforcing that these are normal to one another gives

$$N_i T^i = 0 = \dot{R} n_1 + \dot{Z} n_2 \Rightarrow n_1 = -\frac{\dot{Z} n_2}{\dot{R}}. \tag{4.12}$$

The second equation is found because it is a unit vector. That is,

$$N_i N^i = 1 = 2\sqrt{Z^2 + R^2}(n_1^2 + n_2^2). \tag{4.13}$$

Notice that $n_1 = \mp\dot{Z}/(\dot{R}^2 + \dot{Z}^2)$, $n_2 = \pm\dot{R}/(\dot{R}^2 + \dot{Z}^2)$ satisfy both conditions (making use of the arclength condition that $\dot{R}^2 + \dot{Z}^2 = 2\sqrt{R^2 + Z^2}$).

So the unit normal to the hypersurface is then

$$N_i dx^i = \pm\left(\frac{\dot{Z}}{\dot{R}^2 + \dot{Z}^2}d\rho - \frac{\dot{R}}{\dot{R}^2 + \dot{Z}^2}dz\right). \tag{4.14}$$

The outward pointing normal is N_+, that is, the normal that points in the direction of positive $d\rho$. This is chosen so as to get MOTS.

Spacelike Expansion

Similarly to how we proceed for the timelike expansion, an analog to the extrinsic curvature is defined for the hypersurface, using this normal. That is, one must find

$$\theta_N = \tilde{q}^{ij} D_i N_j \tag{4.15}$$

where $D_i N_j$ is like the extrinsic curvature, but for the hypersurface, and $\tilde{q}^{ij}$ is the (inverse) hypersurface metric, pushed forward into the timeslice.

However, $\tilde{q}^{ij}$ may be written

$$\tilde{q}^{ij} = \frac{\partial x^i}{\partial\lambda}\frac{\partial x^j}{\partial\lambda} + \hat{\phi}_1^i\hat{\phi}_1^j + \hat{\phi}_2^i\hat{\phi}_2^j, \tag{4.16}$$

where

$$\hat{\phi}_1 = (\sqrt{Z^2 + R^2} - Z)^{-1/2}\frac{\partial}{\partial\phi_1} \tag{4.17}$$

$$\hat{\phi}_2 = (\sqrt{Z^2 + R^2} + Z)^{-1/2}\frac{\partial}{\partial\phi_2}. \tag{4.18}$$

Then writing the expansion out in full,

$$\begin{aligned}\theta_N &= \left(\frac{\partial x^i}{\partial\lambda}\frac{\partial x^j}{\partial\lambda} + \hat{\phi}_1^i\hat{\phi}_1^j + \hat{\phi}_2^i\hat{\phi}_2^j\right)\left(\frac{\partial N_i}{\partial x^j} - \Gamma^k_{ij}N_k\right)\\ &= \frac{\partial x^i}{\partial\lambda}\frac{\partial N_i}{\partial\lambda} - \frac{\partial x^i}{\partial\lambda}\frac{\partial x^j}{\partial\lambda}\Gamma^k_{ij}N_k - (\sqrt{R^2+Z^2}-Z)^{-1}\Gamma^k_{\phi_1\phi_1}N_k\\ &- (\sqrt{R^2+Z^2}+Z)^{-1}\Gamma^k_{\phi_2\phi_2}N_k,\end{aligned} \tag{4.19}$$

which in turn simplifies to

$$\theta_N = \frac{\ddot{Z}\dot{R} - \ddot{R}\dot{Z}}{\dot{R}^2 + \dot{Z}^2} + \frac{Z\dot{R} - R\dot{Z}}{2(Z^2+R^2)} + \frac{\dot{Z}}{R}. \tag{4.20}$$

4.2.4 Equations of Motion

The null expansion, which is then set to zero as the condition for a MOTS, is found by adding the timelike and spacelike expansions together. This provides a single ordinary differential equation, second order in both R and Z:

$$\begin{aligned}\theta_\ell &= 0 = \theta_u + \theta_N\\ &= \frac{r_0}{\sqrt{R^2+Z^2}}\left(-1 + \frac{(\dot{R}R + \dot{Z}Z)^2}{4(R^2+Z^2)^{3/2}} - \frac{(\dot{R}Z - \dot{Z}R)^2}{4(R^2+Z^2)^{3/2}}\right)\\ &+ \frac{\ddot{Z}\dot{R} - \ddot{R}\dot{Z}}{\dot{R}^2 + \dot{Z}^2} + \frac{Z\dot{R} - R\dot{Z}}{2(Z^2+R^2)} + \frac{\dot{Z}}{R}\end{aligned} \tag{4.21}$$

Separation into Coupled ODEs

For ease of numerical solving, one then utilizes the arclength condition to separate this ODE into two coupled ODEs.

First, the arclength condition is differentiated, thereby obtaining an expression for the second derivative of either R or Z in terms of the other, and their first derivatives:

$$\begin{aligned}\dot{R}^2 + \dot{Z}^2 &= 2\sqrt{R^2+Z^2}\\ \Rightarrow \ddot{R} &= \frac{R\dot{R} + Z\dot{Z}}{\dot{R}\sqrt{R^2+Z^2}} - \frac{\dot{Z}\ddot{Z}}{\dot{R}}\\ \Rightarrow \ddot{Z} &= \frac{R\dot{R} + Z\dot{Z}}{\dot{Z}\sqrt{R^2+Z^2}} - \frac{\ddot{R}\dot{R}}{\dot{Z}}.\end{aligned} \tag{4.22}$$

These can each be substituted into equation (3.17)to obtain the aforementioned coupled ODEs,

$$\ddot{R} = \frac{R}{\sqrt{R^2+Z^2}} + \frac{\dot{Z}Z(\dot{Z}Z+\dot{R}R)}{R(R^2+Z^2)} - r_0\dot{Z}\left(\frac{1}{\sqrt{R^2+Z^2}} - \frac{(\dot{R}R+\dot{Z}Z)^2-(\dot{R}Z-\dot{Z}R)^2}{4(R^2+Z^2)^2}\right)$$
$$\ddot{Z} = \frac{Z}{\sqrt{R^2+Z^2}} - \frac{\dot{R}Z(\dot{Z}Z+\dot{R}R)}{R(R^2+Z^2)} + r_0\dot{R}\left(\frac{1}{\sqrt{R^2+Z^2}} - \frac{(\dot{R}R+\dot{Z}Z)^2-(\dot{R}Z-\dot{Z}R)^2}{4(R^2+Z^2)^2}\right). \tag{4.23}$$

Note that, of course, the RHS of each of these contains only first derivatives of Z and R (and the functions themselves), but also that it is only the last term which has the coefficient r_0 (the mass term). That is, the mass comes in only with the timelike expansion, given that there is no r_0 dependency for the metric on the time slice (4.1).

4.3 MOTSodesic Method

This section will describe the more conceptual, "MOTSodesic" method for finding the equations of motion. It will begin with a general explanation of the method, and then this will be specialized to this particular metric.

4.3.1 General MOTSodesic Method

Begin with a spacetime $(\mathcal{M}, g_{\alpha\beta}, \nabla_\alpha)$, and on this define a time foliation, where each leaf of the foliation is some $\Sigma_t = \Sigma(t)$. For the case of both 5D Schwarzschild and Myers-Perry, $\Sigma_t = \Sigma$, i.e. there will be no time dependence in the metrics on these leaves. Any single time slice has (Σ_t, h_{ij}, D_i), where D_i is the covariant derivative on the slice, and h_{ij} is the metric.

One defines coordinates (t, x^A, ϕ^a), where x^A refer to the coordinates which will parameterize the curves that will be the MOTS, and the ϕ^a refers to the symmetry coordinates—these must be Killing vectors of the spacetime. The assumption of being able to separate the coordinates in this way is why the toroidal angular coordinates are required for the 5D Schwarzschild metric.

Still working in the full spacetime $\mathcal{M}$, find the covariant derivative of the normal to one of these slices, $K_{\alpha\beta} = \nabla_\alpha u_\beta$, where u_β is the normal to Σ_t. This is then pulled back onto Σ_t using the operators $e_i^\alpha = \partial x^\alpha / \partial x^i$, to get $K_{ij} = e_i^\alpha e_j^\beta K_{\alpha\beta}$, which is the extrinsic curvature to the timeslice. All of this is, of course, the same as in the computational method.

Now the two methods begin to differ. One now may forget entirely about $\mathcal{M}$, and work only with the timeslice (Σ_t, h_{ij}, D_i), along with K_{ij}.

Define an axisymmetric surface S on Σ_t through the parametric equations

$$x^A = X^A(\lambda), \;\; \phi^a = \phi^a \tag{4.24}$$

where $A = \{1, 2\}$ here (not referring to the hypersurface uppercase Latin indices). The coordinates on S are then (λ, ϕ^a), but one may instead refer to the curves defined on Σ_t by $X^A(\lambda)$.

The unit tangent vector to S, in Σ_t, is

$$\hat{T} = \dot{X}^A \frac{\partial}{\partial x^A} \tag{4.25}$$

where here these are the first and second coordinates on Σ_t, x^A. The dot denotes derivatives with respect to the parameter λ. Of course, $X^A(\lambda) = (X^1(\lambda), X^2(\lambda))$, i.e. these will be curves in general, so $\hat{T}$ will only have 2 nonzero entries.

Then define the unit normal one form to S,

$$\hat{N} = F\dot{X}^2 dx^1 - F\dot{X}^1 dx^2 \tag{4.26}$$

where F is a normalization factor.

We then recognize that the metric h_{ij} on Σ_t can be written

$$h^{ij} = T^i T^j + N^i N^j + (\hat{\phi_a})^i (\hat{\phi^a})^j, \tag{4.27}$$

where here, $\hat{\phi^a} = \frac{1}{||\partial/\partial\phi^a||} \frac{\partial}{\partial\phi^a}$. This will be a unit vector in the direction $\partial/\partial\phi^a$, and so there will be however many of them as there are symmetry coordinates ϕ^a. Then, in the above decomposition of the metric, each of these must be included. It is worth noting that in the case there exists cross terms in these coordinates in the metric, the vectors will have entries in more directions than just the ϕ^a direction.

The (inverse) metric on S is called $\tilde{q}^{AB}$, and the push-forward of this onto Σ_t is the part of h_{ij} that is orthogonal to $\hat{N}$:

$$\tilde{q}^{ij} = T^i T^j + (\hat{\phi}_a)^i (\hat{\phi}^a)^j. \tag{4.28}$$

Taking the trace of the extrinsic curvature of S on Σ_t, one then observes

$$\begin{aligned} k_N = \theta_N = \tilde{q}^{ij} D_i N_j &= \left(T^i T^j + (\hat{\phi}_a)^i (\hat{\phi}^a)^j \right) D_i N_j \\ &= -N_j T^i D_i T^j - N_j (\hat{\phi}_a)^i D_i (\hat{\phi}^a)^j \\ &= -\kappa - N_j (\hat{\phi}_a)^i D_i (\hat{\phi}^a)^j. \end{aligned} \tag{4.29}$$

The first scalar on the RHS is called κ, and the second is something which is easy to calculate.

Of course, k_N is the spacelike expansion, and the timelike expansion is

$$k_u = \theta_u = \tilde{q}^{ij} K_{ij}, \tag{4.30}$$

which one calculates directly. But using the fact that we are looking for MOTS, a linear combination of these will be equal to zero. So,

$$\begin{aligned} \epsilon k_u + k_N &= 0 \\ \Rightarrow \epsilon k_u - \kappa - N_j (\hat{\phi}_a)^i D_i (\hat{\phi}^a)^j &= 0 \\ \Rightarrow \kappa = \epsilon k_u - N_j (\hat{\phi}_a)^i D_i (\hat{\phi}^a)^j&, \end{aligned} \tag{4.31}$$

where $\epsilon = \pm 1$ allows one to set the direction of the null normal. This allows us to avoid calculating κ explicitly—as is done in the computation approach from the previous section—since it is arduous.

Now, one works with the 2-dimensional curves defined by $(X^1(\lambda), X^2(\lambda))$. Let $\bar{D}_A$ be the covariant derivative defined on the 2D curves. Then $T^A \bar{D}_A T^B$ will be perpendicular to T_B. This means that

$$T^A D_A T^B = \tilde{\kappa} N^B \tag{4.32}$$

for some $\tilde{\kappa}$. But, in fact, $\tilde{\kappa} = \kappa$ from before, and so we have that

$$\begin{aligned}
\dot{X}^A \left(\frac{\partial \dot{X}^B}{\partial X^A} + \Gamma^A_{BC} \dot{X}^C \right) &= \kappa N^B \\
\frac{dX^A}{d\lambda} \frac{\dot{X}^B}{\partial X^A} + \Gamma^B_{AC} \dot{X}^C \dot{X}^A &= \kappa N^B \\
\frac{d^2 X^A}{d\lambda^2} + \Gamma^B_{AC} \dot{X}^A \dot{X}^C &= \kappa N^B.
\end{aligned} \tag{4.33}$$

This gives two coupled ODEs. One can see that this looks very much like the geodesic equation for a non-affinely parameterized geodesic, except the acceleration to the curve is proportional to the normal on the RHS. Hence, we call these the "MOTSodesic" equations.

4.3.2 MOTSodesic Method for 5D Schwarzschild

One starts with the spacetime $(\mathcal{M}, g_{\alpha\beta}, \nabla_\alpha)$, where here $g_{\alpha\beta}$ is the 5-dimensional metric of (3.19) in Painlevé-Gullstrand Weyl coordinates,

$$\begin{aligned}
ds^2 = -\left(1 - \frac{r_0^2}{2\sqrt{\rho^2 + z^2}}\right) d\tau^2 + \frac{r_0}{\rho^2 + z^2}(\rho d\rho + z dz) d\tau + \frac{d\rho^2 + dz^2}{2\sqrt{\rho^2 + z^2}} \\
+ (\sqrt{\rho^2 + z^2} - z) d\phi_1^2 + (\sqrt{\rho^2 + z^2} + z) d\phi_2^2.
\end{aligned} \tag{4.34}$$

The metric on each leaf of the time foliation is then

$$h_{ij} dx^i dx^j = \frac{d\rho^2 + dz^2}{2\sqrt{\rho^2 + z^2}} + (\sqrt{\rho^2 + z^2} - z) d\phi_1^2 + (\sqrt{\rho^2 + z^2} + z) d\phi_2^2 \tag{4.35}$$

Then we define a surface using the parametric equations $\rho = R(\lambda)$, $z = Z(\lambda)$, with coordinates on the surface being $(\lambda, \phi_1, \phi_2)$. In the case of this metric, the symmetry coordinates $\hat{\phi}^a$ in the previous section are $\hat{\phi}_1$ and $\hat{\phi}_2$, each unit vectors in the directions of $\partial/\partial\phi_1$ and $\partial/\partial\phi_2$, respectively. $X^1 = R(\lambda)$ and $X^2 = Z(\lambda)$.

The extrinsic curvature K_{ij} is as in (4.5), and of course the tangent vector $\hat{T}$ is

$\hat{T} = \dot{R}\frac{\partial}{\partial\rho} + \dot{Z}\frac{\partial}{\partial z}$, while the normal to S is

$$\hat{N} = \pm\left(-\frac{\dot{Z}}{\dot{R}^2+\dot{Z}^2}d\rho + \frac{\dot{R}}{\dot{R}^2+\dot{Z}^2}dz\right), \tag{4.36}$$

and one chooses the negative, in this case, so that the $d\rho$ term is positive.

Then $k_u = \tilde{q}^{ij}K_{ij}$ is also as in the previous section (timelike expansion),

$$k_u = -\frac{r_0}{\sqrt{R^2+Z^2}} + \frac{r_0(\dot{R}R+\dot{Z}Z)^2}{4(R^2+Z^2)^2} - \frac{r_0(\dot{R}Z-\dot{Z}R)^2}{4(R^2+Z^2)^2}. \tag{4.37}$$

Now define the toroidal angular unit vectors $\hat{\phi}_1$ and $\hat{\phi}_2$. These will be

$$\begin{aligned}\hat{\phi}_1 &= (\sqrt{R^2+Z^2}-Z)^{-1/2}\frac{\partial}{\partial\phi_1}\\ \hat{\phi}_2 &= (\sqrt{R^2+Z^2}+Z)^{-1/2}\frac{\partial}{\partial\phi_2},\end{aligned} \tag{4.38}$$

where they each only have a component in one direction (ϕ_1 and ϕ_2 tangent directions, respectively) because there do not exist cross terms of these in the metric (4.1).

The next step is to find the scalar κ, where here $\epsilon = 1$:

$$\begin{aligned}\kappa &= \epsilon k_u - N_j\hat{\phi}_1{}^i D_i\hat{\phi}_1{}^j - N_j\hat{\phi}_2{}^i D_j\hat{\phi}_2{}^j\\ \kappa &= k_u - N_j\Gamma^j_{\phi_1\phi_1}(\sqrt{R^2+Z^2}-Z)^{-1} - N_j\Gamma^j_{\phi_2\phi_2}(\sqrt{R^2+Z^2}+Z)^{-1}\end{aligned} \tag{4.39}$$

$$\kappa = \frac{r_0}{4}\left(\frac{Z^2(3\dot{R}^2+\dot{Z}^2)+R^2(3\dot{Z}^2+\dot{R}^2)-4R\dot{R}Z\dot{Z}}{(R^2+Z^2)^2}\right) + \frac{\dot{Z}}{R} \tag{4.40}$$

Now using this, equations (4.33) are specified to this case to get the coupled ODEs

$$\begin{aligned}\ddot{R} + \Gamma^R_{RR}\dot{R}^2 + 2\Gamma^R_{RZ}\dot{R}\dot{Z} + \Gamma^R_{ZZ}\dot{Z}^2 &= \kappa N^R\\ \Rightarrow \ddot{R} = \kappa\dot{Z} &+ \frac{R(\dot{R}^2-\dot{Z}^2)+2Z\dot{R}\dot{Z}}{2(R^2+Z^2)}\end{aligned} \tag{4.41}$$

$$\begin{aligned}\ddot{Z} + \Gamma^Z_{RR}\dot{R}^2 + 2\Gamma^Z_{RZ}\dot{Z}\dot{R} + \Gamma^Z_{ZZ}\dot{Z}^2 &= \kappa N^Z\\ \Rightarrow \ddot{Z} = -\kappa\dot{R} &+ \frac{Z(\dot{Z}^2-\dot{R}^2)+2R\dot{Z}\dot{R}}{2(R^2+Z^2)}\end{aligned} \tag{4.42}$$

Throughout this calculation, the arclength condition is used to simplify the expressions.

4.3.3 Schwarzschild Event Horizon Solution

The Schwarzschild event horizon will exist at $r_0 = 2\sqrt{R^2+Z^2}$ in the coordinates chosen. An important consistency check on the MOTSodesic equations derived is whether this equation solves them.

The parametric equations for the event horizon at $r_0 = 2\sqrt{R^2+Z^2}$ are

$$\begin{aligned} R(\lambda) =& \frac{r_0^2}{2}\sin\left(\frac{2\lambda}{r_0}\right) \\ Z(\lambda) =& \frac{r_0^2}{2}\cos\left(\frac{2\lambda}{r_0}\right), \end{aligned} \tag{4.43}$$

where the parameterization $2\lambda/r_0$ is chosen so that the arclength condition, $\dot{R}^2+\dot{Z}^2 = 2\sqrt{R^2+Z^2}$, holds.

Substituting these into the solution for κ in the previous section, one gets

$$\kappa = \frac{1}{r_0}, \tag{4.44}$$

and then it is easy to see that the RHS of 4.41 is equal to $-2\sin(2\lambda/r_0) = R''(\lambda)$, and that of 4.42 is $-2\cos(2\lambda/r_0) = Z''(\lambda)$. So this is a solution, as required.

4.4 Series Expansions at $R = 0$

In the final MOTSodesic equations which we solve numerically, one sees the scalar κ diverges for $R = 0$ because of the $\dot{Z}/R$ term. In our numerical solver, we simply start the integrator slightly off the z-axis (with, say, $\lambda = 1/10000$ and $R(1/10000) = 1/10000$). However, to be sure this does not qualitatively affect the results we find, we must perform a series expansion about small λ for these solutions.

Find the series expansions by first setting

$$\begin{aligned} R(\lambda) &= R_0 + R_1\lambda + R_2\lambda^2 + R_3\lambda^3 + O(\lambda^4) \\ Z(\lambda) &= Z_0 + Z_1\lambda + Z_2\lambda^2 + Z_3\lambda^3 + O(\lambda^4) \end{aligned} \tag{4.45}$$

with as yet undetermined constants R_i, Z_i.

One first enforces the condition that for $\lambda = 0$, $R = 0$, meaning that $R_0 = 0$. Substituting (4.36) into the MOTSodesic equations, one immediately sees that $\dot{Z}(0) = 0$, as there exists a term in the expansion which is of order $1/\lambda$, for which the coefficient has $\dot{Z}$. This is consistent with what is expected, as it means that all closed MOTS must leave the z-axis perpendicularly: otherwise, there would be conical singularities in them, and they would not be smooth [11].

Setting each order coefficient to zero, one is able to determine that R_2 and Z_3 are also equal to zero. Z_2 and R_3 are found to be dependent on R_1 and Z_0. However, one must still enforce the arclength condition, which, when (4.36) are substituted into it, gives that

$$R_1 = \sqrt{2Z_0} \tag{4.46}$$

must be satisfied for it to hold.

Substituting this into the above-mentioned solutions for R_3 and Z_2,

$$\begin{aligned} R_3 &= \frac{-9r_0^2 + 4Z_0(1+3Z_0) - 3\sqrt{2Z_0}r_0(1+6Z_0)}{12\sqrt{2Z_0^3}(1+2Z_0)^2} \\ Z_2 &= -\frac{3\sqrt{2}r_0 + 4Z_0\sqrt{Z_0}}{4\sqrt{Z_0}(1+2Z_0)} \end{aligned} \tag{4.47}$$

and the series expansions for $Z(\lambda)$ and $R(\lambda)$ for small λ are then

$$\begin{aligned} R(\lambda) &= \sqrt{2Z_0} + \frac{-9r_0^2 + 4Z_0(1+3Z_0) - 3\sqrt{2Z_0}r_0(1+6Z_0)}{12\sqrt{2Z_0^3}(1+2Z_0)^2}\lambda^3 + O(\lambda^4) \\ Z(\lambda) &= Z_0 - \frac{3\sqrt{2}r_0 + 4Z_0\sqrt{Z_0}}{4\sqrt{Z_0}(1+2Z_0)}\lambda^2 + O(\lambda^4) \end{aligned} \tag{4.48}$$

These solutions hold to fourth order in λ, and the ODEs hold to second order. Z_0 is a free parameter as expected, given that the z-axis may be left from any value of z, as long as it is perpendicular to the z-axis (as discussed, $\dot{Z}(0) = Z_1 = 0$). The choosing of Z_0 sets which MOTOS (or MOTS, for specific values) the solutions (R, Z) describe.

Chapter 5

Results: 5D Schwarzschild MOTS

This chapter discusses the results found when numerically solving the MOTSodesic equations of (4.41) and (4.42), and will also include the results of following the method of section 4.3.2 starting from the metric (3.11), that is, 5D Schwarzschild in toroidal coordinates, but without the transform into Weyl coordinates. One may compare these more directly to the plots of [11] as shown in chapter 2, while the Weyl results may be compared directly to the previously discussed paper in process by the same authors.

We find qualitatively identical results for 5D Schwarzschild as in 4D; the majority of plots are able to be reproduced with qualitatively identical behaviour. Most notably, the infinite number of closed MOTS found in 4D are also found in 5D, and the connection between the MOTOS and the MOTS – that is, a series of MOTOS may be followed until a cusp meets the z-axis and here a MOTS will be found – exists in the same way.

Note: in this chapter, all plots of results in Weyl coordinates have $R(\lambda) = \rho$ (cylindrical-like radial coordinate) on the horizontal axis, and $Z(\lambda) = z$ on the vertical. All plots in the non-Weyl coordinates have been converted into Cartesian coordinates; that is, the horizontal axis is $x = R(\lambda)\cos(2\Theta(\lambda))$ and the vertical is $y = R(\lambda)\sin(2\Theta(\lambda))$. As well, for the entirety of this chapter, the parameter $r_0 = 1$; however, the values from which the MOTS leave the vertical axis simply scale as $r_0 Z(0)$ (or, for the non-Weyl coordinates, $r_0 R(0)$).

5.1 $Z(0) < 0$ MOTOS

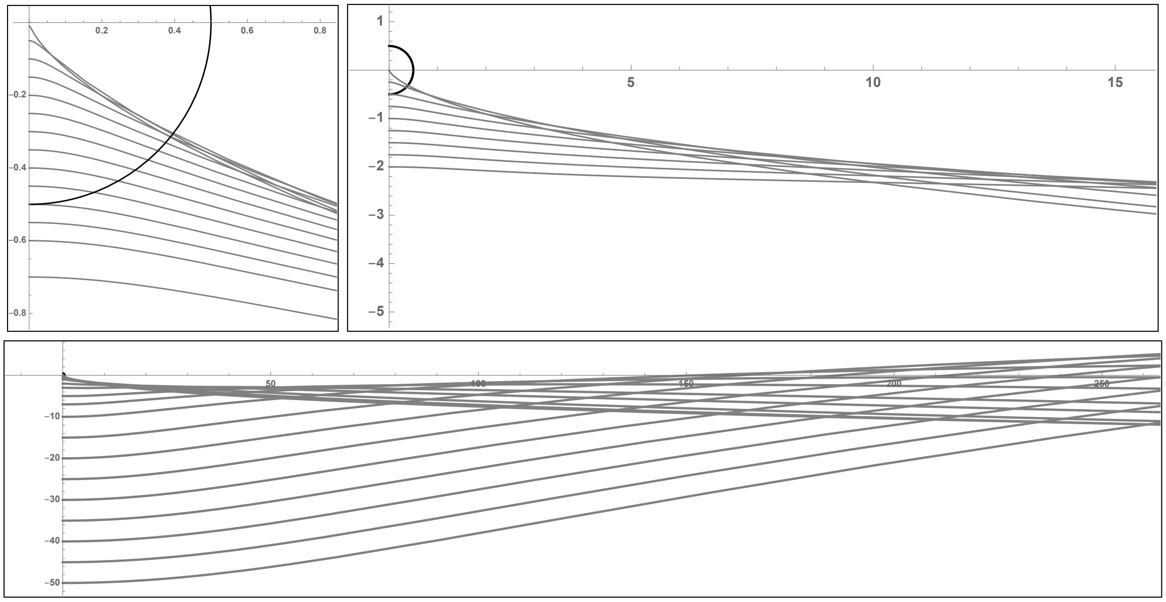

Figure 5.1: Analogous plots for 5D Schwarzschild in Weyl coordinates to figure 2.4. On the left is a more zoomed in plot, and on the right one can see that the MOTOS are curving up, but moving toward flatness as $R \to \infty$. These are plots of $(R(\lambda), Z(\lambda))$. Note that for all Weyl plots, the vertical axis is $Z(\lambda)$, and the horizontal is $R(\lambda)$.

We begin with the MOTOS that leave the z-axis at negative values. These are shown in figure 5.1. It is important to keep in mind, for this and the succeeding section: despite the metric being symmetric under $Z \mapsto -Z$, the MOTOS are not symmetric across the x-axis. This is because the null normal has an orientation (upward pointing in the case of these plots). If one were to instead choose a downward pointing null normal, the orientation of all plots here would reflect across the x-axis.

One can see a qualitative difference in these plots as compared to $4D$; one of the few that exist. There is a crossing that occurs of the MOTOS which have larger Z_0 and those which have Z_0 close to or inside the apparent horizon ($0 > Z_0 > -1/2$). The crossing begins around $r = 3$ and continues for arbitrarily large r. In 4 dimensions, none of this crossing behaviour was observed (see figure 2.4). However, it appears it may be the case that the crossing causes the ordering of the MOTOS to simply reverse; that is, it seems that the MOTOS visible in figures 5.1 and 5.2 take the opposite order from which they left the axis, with the MOTOS leaving closest to $Z = 0$ being at the bottom, and the MOTOS which left the axis for the most negative Z-value, being at the top (for $R \to \infty$). This is most clear from the bottom plot in figure 5.2. However, more detailed analysis is required to establish this.

Much like in $4D$, however, the MOTOS appear to flatten out for large r, that is, they seem to asymptote to a constant value of Z. This is consistent with what is observed from figure 2.4. The difference is that one must go to larger r-values to see flatness in the MOTOS, as compared to 4D—the warping effect seen near the apparent horizon has stronger and more far-reaching influence in 5 dimensions than it does in 4.

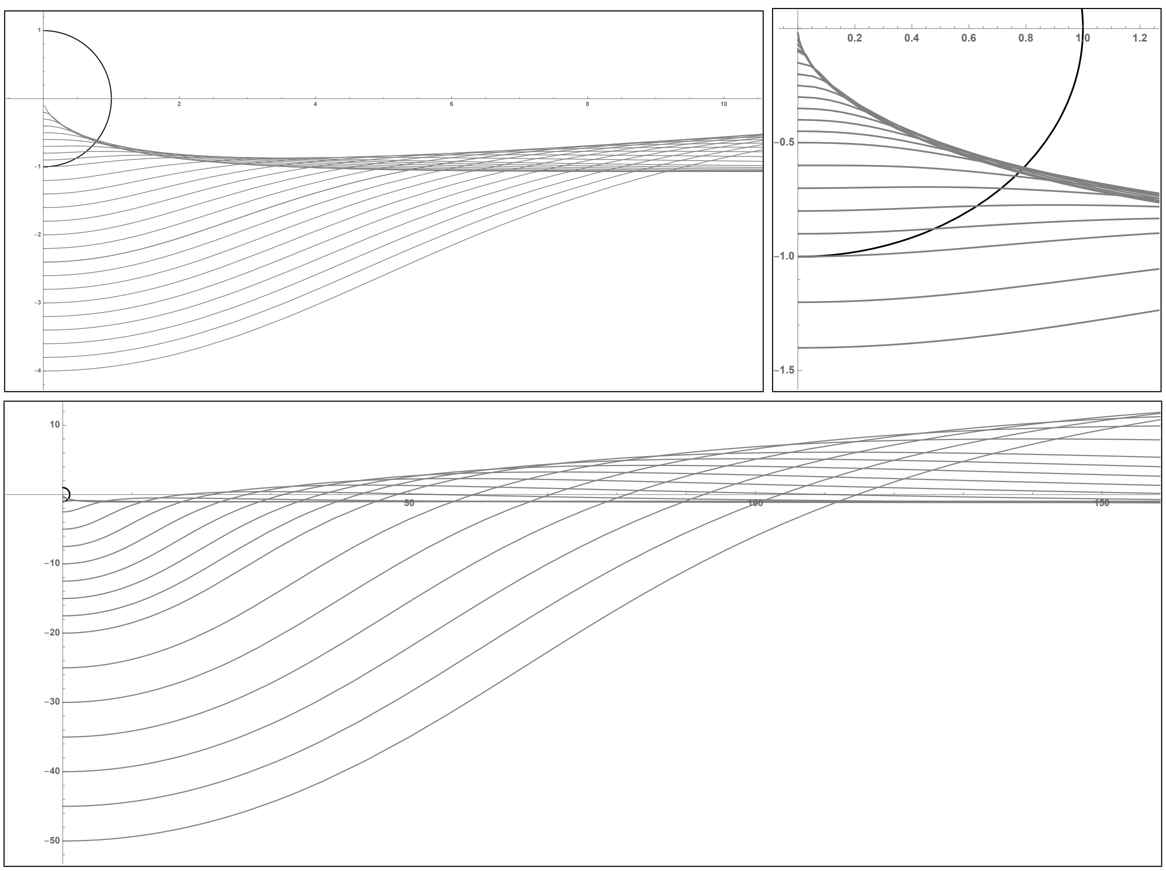

Figure 5.2: MOTOS that leave the z-axis for $0 > Z(0)$ with upward oriented null normals, from the MOTSodesics of metric (3.11). The vertical axis plots $R(\lambda)\sin(2\Theta(\lambda))$, and the horizontal plots $R(\lambda)\cos(2\Theta(\lambda))$.

Figure 5.2 is the same as 5.1, but for the MOTSodesics which are generated when starting with the metric (3.11); that is, without making the final transformation into the Weyl (cylindrical) coordinates. These are plots of Cartesian coordinates

$R(\lambda)\cos(2\Theta(\lambda))$ and $R(\lambda)\sin(2\Theta(\lambda))$, where of course the coordinates along the MOTOS are $R(\lambda)$ and $\Theta(\lambda)$. This figure plots twice the angles because the coordinate θ has range $0 < \theta < \pi/2$ (from the choice of toroidal angular coordinates, and thus existence of cosine in the metric), and we wish to have visually similar results to the other cases. Note also that the apparent horizon in these coordinates exists at $R = 1$.

The same crossing behaviour is seen here, with the MOTOS flattening out as $R \to \infty$. However, in these coordinates, the MOTOS which have $R(0) \gg 1$ (with $\Theta(0) = -\pi/2$, so that the range is now $-\pi/2 < \theta < 0$—that is, leave from the negative z-axis) begin to flatten for $\Theta > -\pi/4$.

5.2 $Z(0) > 1/2$ MOTOS

The apparent horizon, shown in figures 5.1 as a black semi-circle, leaves the z-axis for $Z(0) = 1/2$ in Weyl coordinates. The top left plot of figure 5.3 shows the MOTOS which leave the axis for values of $Z(0)$ very close to but $> 1/2$. These are MOTOS which are closely approaching closure, with the bottom half producing a sharpening curve, which gets progressively closer to the axis. The other plots of this figure show $Z(0) > 1/2$, and increasingly far away from the apparent horizon.

These plots resemble the analogous four-dimensional ones (figure 2.5) more closely than the negative-z plots; the same sort of crossing occurs for MOTOS very close to the apparent horizon, and we see the same sort of concavity in the MOTOS for $Z(0) \gg 1/2$. Of course, as for the MOTOS which have $Z(0) < 0$, the effect of the apparent horizon extends out further for 5 dimensions than for 4, with the MOTOS which have $Z(0) = 50$ still being noticeably concave downwards, despite the apparent horizon having half the radius (as compared to 4 dimensions).

The top left plot of figure 5.4 shows the MOTOS just outside of the apparent horizon for positive values of $R(0)$ in the Schwarzschild coordinates with the toroidal angular coordinates (that is, without the transformation into Weyl), while the other plots in this figure show the MOTOS for $R(0)$ increasingly large, and leaving from the positive axis. Qualitatively similar behaviour in seen both to the 5-dimensional case with the Weyl coordinates and to the 4-dimensional case, with the same sort of concavity and crossing existing in all three. As is true for the $Z(0) \ll 1/2$ or $R(0) \ll 1$ (in the case of these coordinates) MOTOS, the 5-dimensional apparent horizon has a

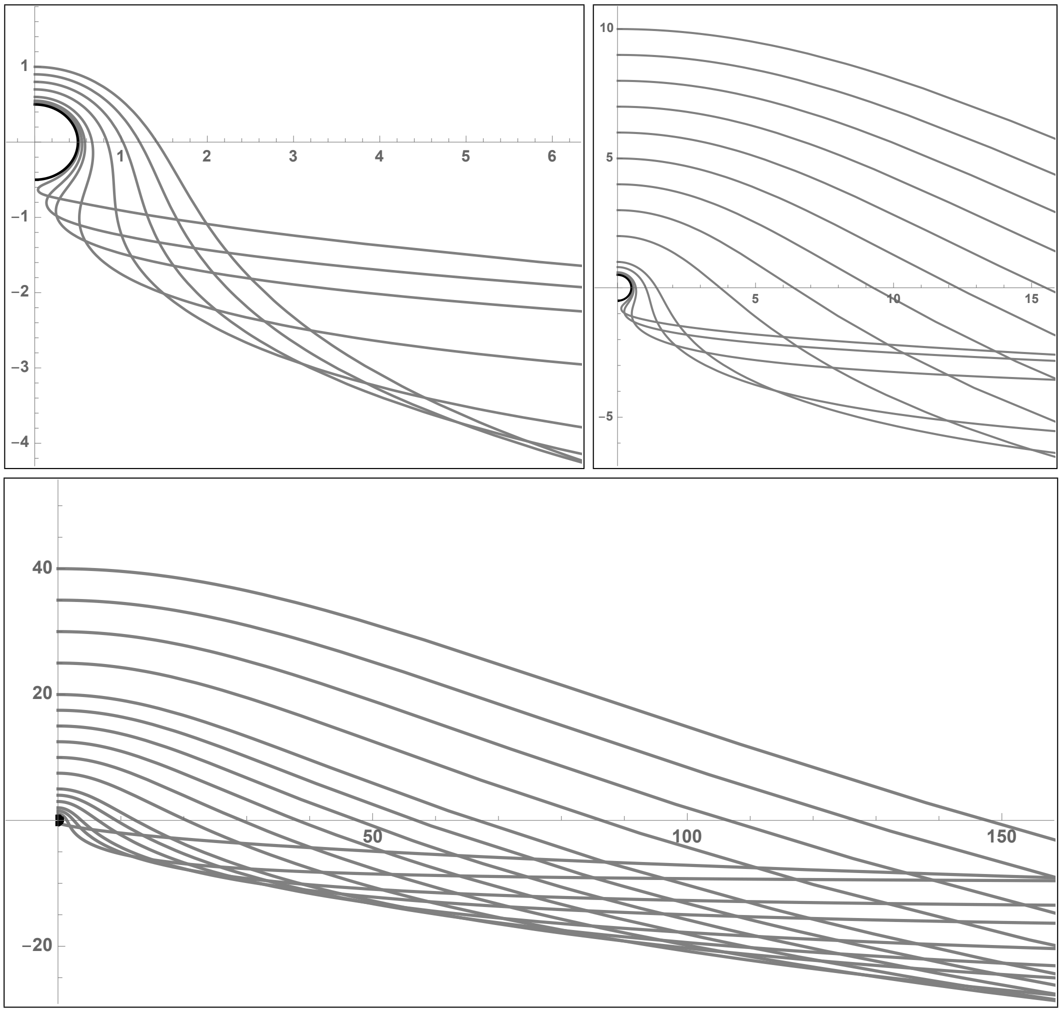

Figure 5.3: The MOTOS which leave the z-axis for positive Z_0, where $Z_0 > 1/2$, which is the location of the apparent horizon. From top left clockwise, the plots are increasingly zoomed out. This is for the metric in Weyl coordinates; vertical axis plots Z, horizontal plots R.

stronger effect than in 4-dimensions—the MOTOS out at $Z(0) = R(0) = 50$ are still noticeably wrapping around this MOTS, whereas in 4D they are nearly flat by this distance.

5.3 Self-Intersecting MOTOS

The most interesting behaviour of the MOTOS occurs for $1/2 < Z(0) < 0$ (alternatively, $0 < R(0) < 1$ in the non-Weyl coordinates). This is when we see the same

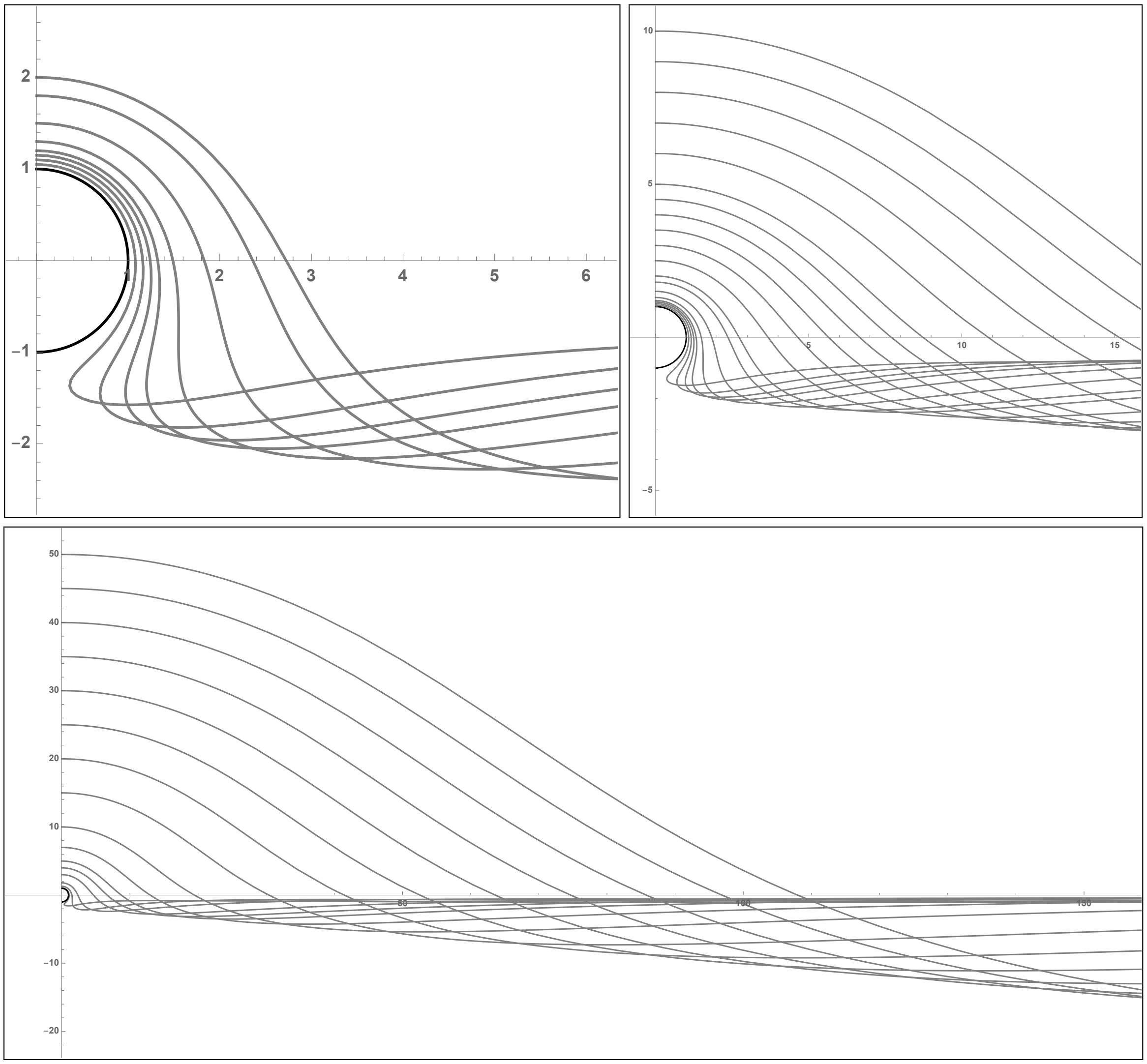

Figure 5.4: The MOTOS for $R_0 > 1$, and for $R_0 \gg 1$, in the Schwarzschild spacetime with the non-Weyl coordinates. Very similar qualitatively to the $4D$ case (2.5), except the apparent horizon at $R = 1$ has a larger influence out for further $R(\lambda)$. Vertical axis plots $R\sin(2\Theta)$, horizontal plots $R\cos(2\Theta)$.

sort of self-intersections as were first seen in [30], and subsequently seen in [11] for 4D Schwarzschild. To determine whether such self-intersections exist in the MOTOS (and thus in the MOTS) of this spacetime as they did in the others, is the main motivation for the work in this thesis.

The first such figure which shows the self-intersections is 5.5. Both plots show MOTOS near the apparent horizon in Weyl coordinates ($Z(0) = 1/2$). The left shows

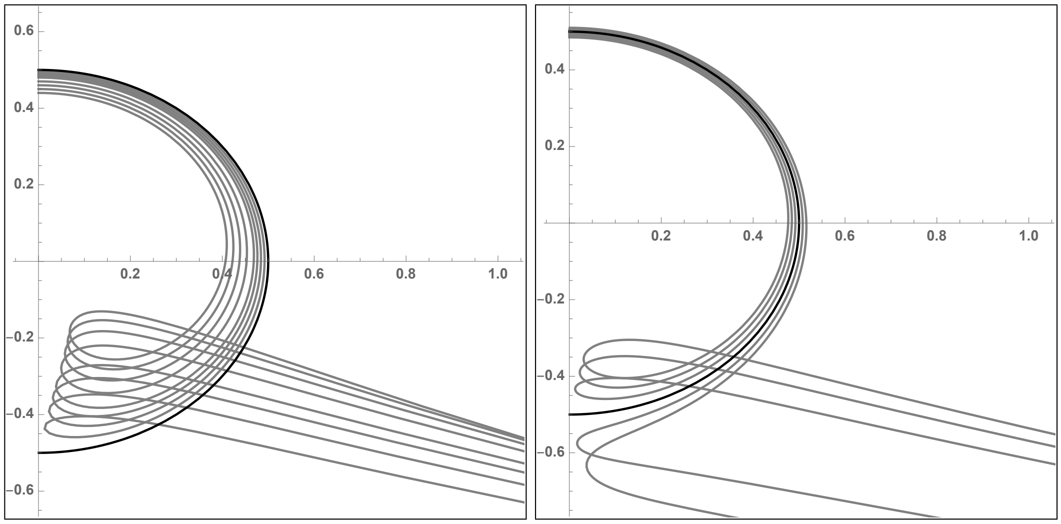

Figure 5.5: Two plots showing the MOTOS just inside and just outside the apparent horizon, which is a MOTS, in the Weyl coordinates. Vertical axis plots Z, horizontal plots R.

self-intersecting MOTOS which leave the z-axis just inside the horizon—all such self-intersecting MOTOS will satisfy $0 < Z(0) < 1/2$. Notice how the loop produced grows in size and moves toward the horizontal axis as it leaves the z-axis from smaller values of $Z(\lambda)$. When the loop narrows sufficiently to produce a cusp, this will instead be a MOTS (closed), rather than a MOTOS, because it intersects the z-axis at the point of the cusp. In this way, it is clear how a series of MOTOS may be followed to find the location and shape of the MOTS.

This process—where a MOTS is seen as special (closed) case in a continuous series of MOTOS—occurs precisely the same in $5D$ as it did in [11]. It is also observed for the self-intersecting MOTS; figure 5.7 shows for the Weyl coordinates (left) and the toroidal/spherical coordinates (right) the way the MOTOS which have a self-intersection approach the apparent horizon MOTS. The loop moves out, initially appearing to follow the path of the red MOTS itself, toward the negative z-axis, where it will then narrow and turn into a cusp, producing the apparent horizon. This occurs analogously for the MOTOS which one may trace from the two loop MOTS (blue in the figure). One also sees here another visual distinction between these two coordinate systems: the MOTS for the Weyl coordinates produce narrower loops, and the spherical/toroidal coordinates produce loops which flatten against the vertical axis. These are artefacts of the coordinates chosen, not physical differences.

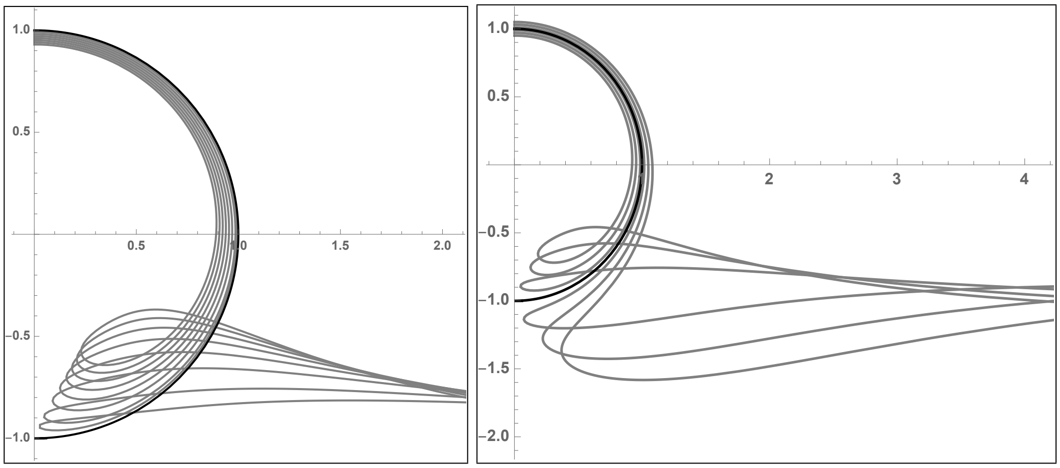

Figure 5.6: The MOTOS near the apparent horizon (show in black) for the non-Weyl coordinates of $5D$ Schwarzschild. Qualitatively identical behaviour as in figure 5.5, though one sees the same sort of bunching together of the MOTOS as R increases as was seen in figure 5.2.

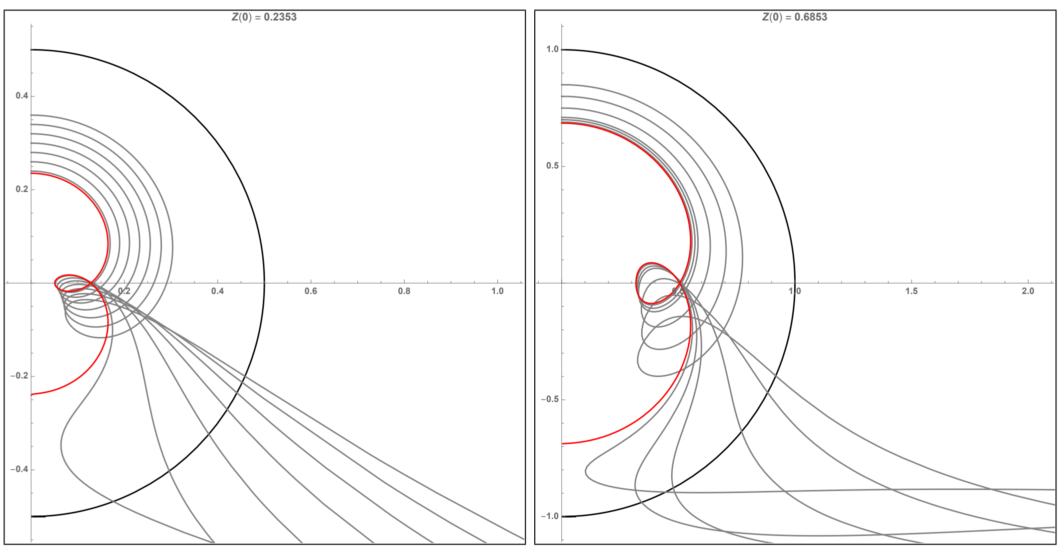

Figure 5.7: These show the way the MOTOS (grey) outside of the one-loop MOTS (red) approach the apparent horizon (zero loop MOTS). The left is for Weyl and the right is for the non-Weyl coordinates. The labels indicate the approximate value of $Z(0)$ for which the closed (red) MOTS occurs. Vertical axis plots $R\sin(2\Theta)$, horizontal plots $R\cos(2\Theta)$.

5.4 Self-Intersecting MOTS

Finally, we discuss the self-intersecting MOTS that are found. Two of these were shown in the previous section (in red and blue). As in [11], we find infinitely many in

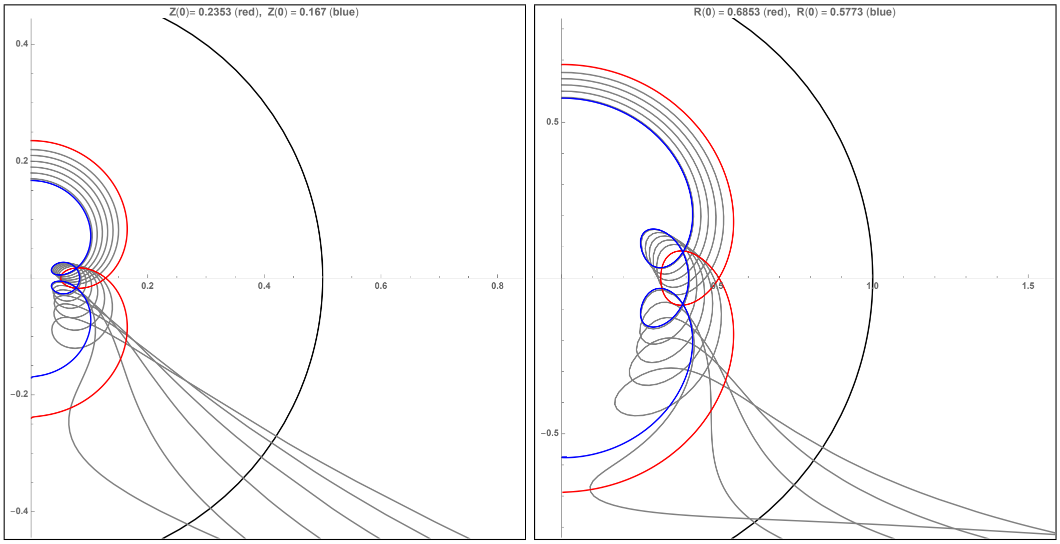

Figure 5.8: The two loop (blue) and one loop (red) MOTS inside the Weyl coordinate (left) and toroidal coordinate (right) 5D Schwarzschild black holes. The behaviour of the loops of the (grey) MOTOS is analogous to those which approach the AH from outside the one loop MOTS. **Left**: vertical axis plots Z, horizontal plots R. **Right**: vertical axis plots $R\sin 2\Theta$, horizontal plots $R\cos 2\Theta$.

the 5D Schwarzschild black hole (for both horizon-penetrating coordinate systems).

Figures 5.9, 5.10, and 5.11 show the first twelve self-intersecting MOTS for the Weyl coordinates and the non-Weyl coordinates (respectively). The shapes of the loops in the Weyl coordinates are much narrower along the horizontal axis, whereas in the non-Weyl coordinates, they are more circular; this is a coordinate effect. The timeslice metric in the Weyl coordinates is

$$ds^2 = \frac{d\rho^2 + dz^2}{2\sqrt{\rho^2 + z^2}} + (\sqrt{\rho^2 + z^2} - z)d\phi_1^2 + (\sqrt{\rho^2 + z^2} + z)d\phi_2^2, \tag{5.1}$$

and we plot on the (ρ, z) plane. This plane is conformally flat with conformal factor $1/(2\sqrt{\rho^2 + z^2})$, meaning the MOTS we see are distorted. Thus, while one cannot make statements about the relative size of the MOTS from figures 5.9 and 5.10, the shapes can be compared.

In the non-Weyl coordinates, the timeslice has metric

$$ds^2 = dr^2 + r^2 d\theta^2 + r^2(\sin^2(\theta)d\phi_1^2 + \cos^2(\theta)d\phi_2^2), \tag{5.2}$$

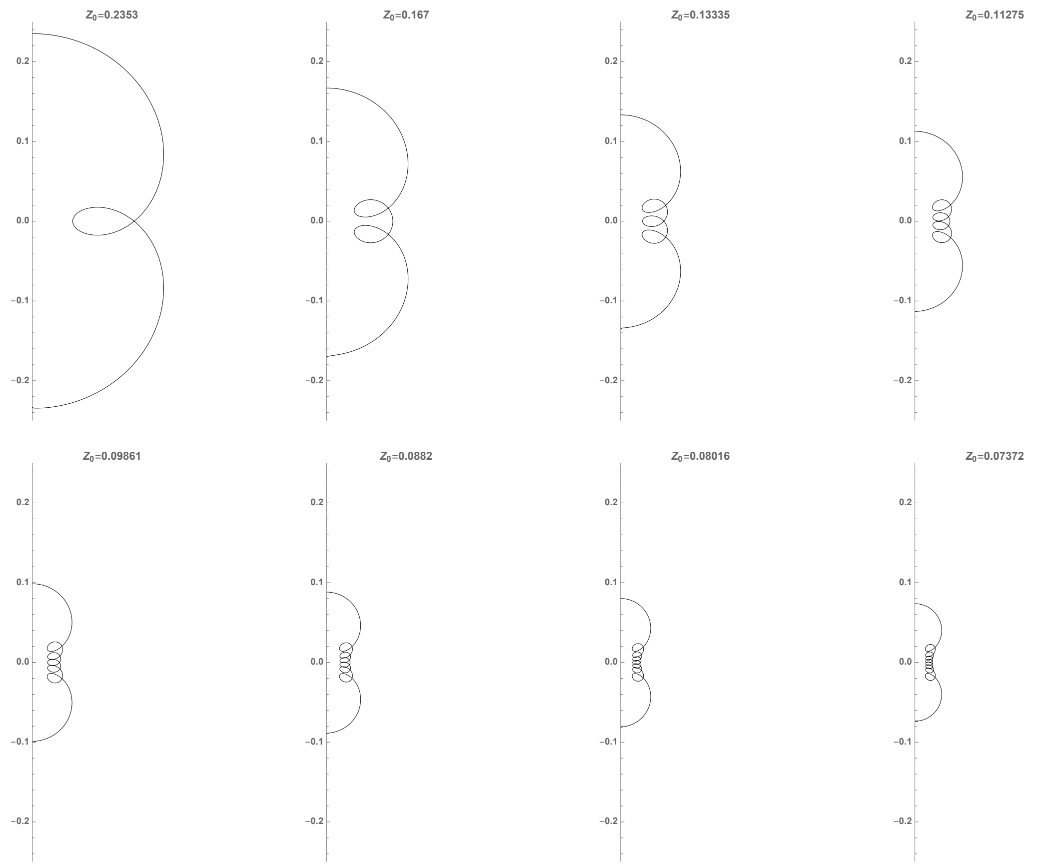

Figure 5.9: The first eight self-intersecting MOTS for the 5D Schwarzschild spacetime, in Weyl coordinates. The axis has the same scale for all plots, but does not have the same scale as compared to the figure 5.10. Plot of (R, Z).

and so the (r, θ) plane is flat. Then making the transformation $x = r\cos(2\theta)$, $y = r\sin(2\theta)$ will not affect this. So both the shapes and the relative sizes of the MOTS in figure 5.11 are not distorted.

From this figure, notice that the size of the MOTS decreases more slowly as they get smaller, with the most dramatic difference in relative size being between the single loop and double loop MOTS. It also appears to be the case that the loops themselves take an almost spherical shape in these coordinates, with the outermost two loops being larger more dramatically as compared to the Weyl coordinates.

Figure 5.13 shows the MOTS with seven to twelve self-intersections for the non-Weyl coordinates; one sees that the shapes of the MOTS differ qualitatively as compared to the 4D case, likely due to the toroidal rather than spherical angular coordinates. Whereas in 4D the MOTS seemed to hug in toward the vertical axis around

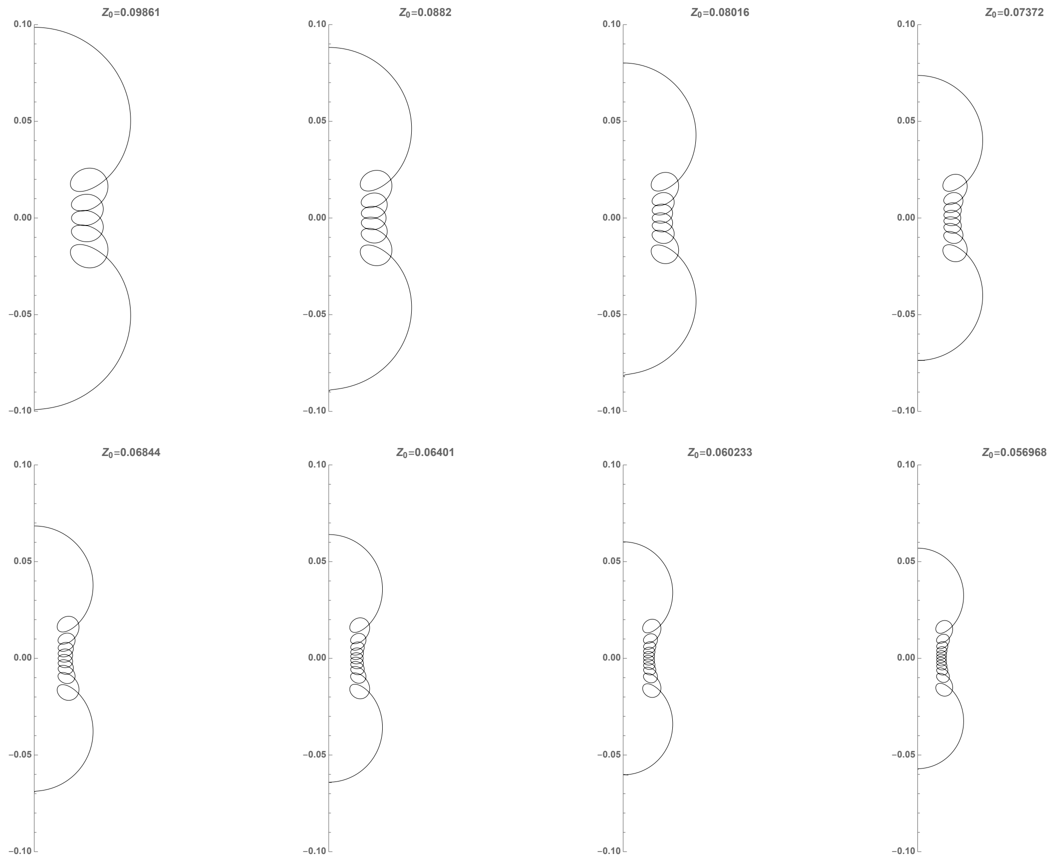

Figure 5.10: The MOTS with five to 12 loops, in the Weyl coordinates, for 5D Schwarzschild. The axis is zoomed in for these plots as compared to figure 5.9, but is the same scale for each plot in this figure. Plot of (R, Z).

the loops, in 5D they appear more or less parallel to it. One can see here that the more spherical shape the loops take in 5D was not a result of the scaling; this is still visible, and is not the case in 4D.

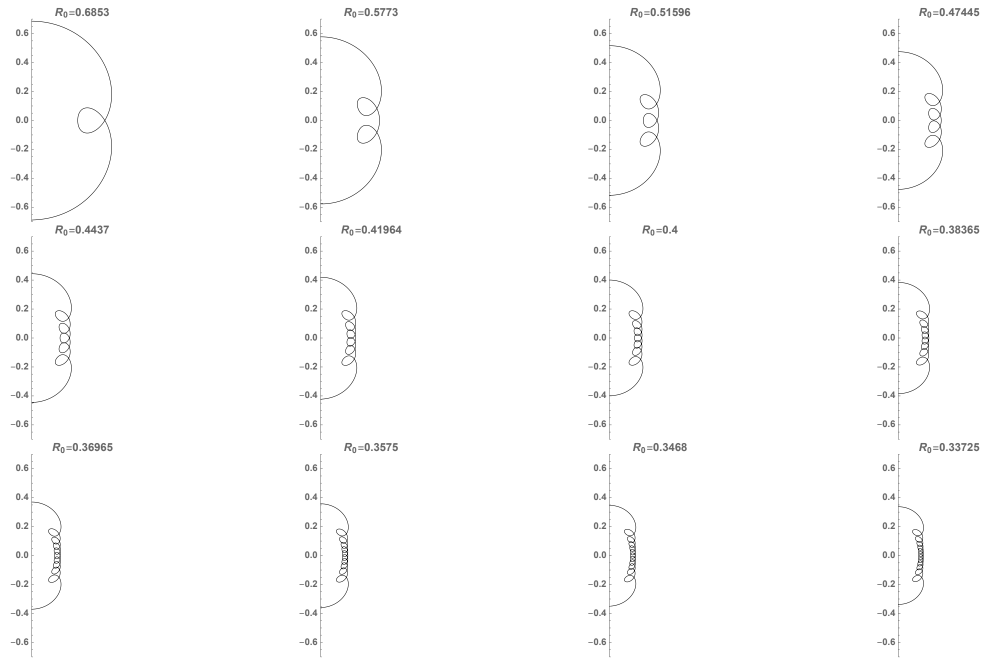

Figure 5.11: The first twelves self-intersecting MOTS in the toroidal (non-Weyl) coordinates. These are all shown on the same scale axis, because the loops remain visible for smaller MOTS. Note that the plane on which the MOTS are plotted—(r, θ)—is flat in these coordinates (not just conformally so as in the (ρ, z)-plane of the Weyl coordinates), so the size of one MOTS may be accurately compared to the next with these plots. The labels are multiples of r_0, the mass parameter in the metric. Plot of $(R\cos 2\Theta, R\sin 2\Theta)$.

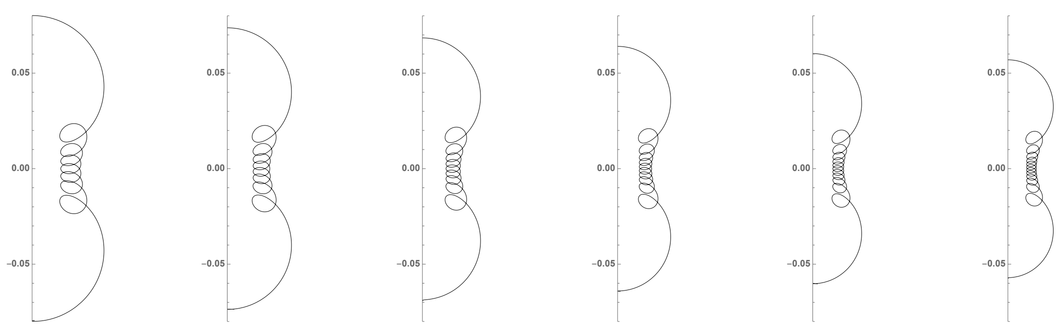

Figure 5.12: The many-looped self-intersecting MOTS for the $5D$ Schwarzschild spacetime in the Weyl coordinates, zoomed in for comparison to the $4D$ case. Note the axis values will not be the same, because $M = 1$ was chosen in [11], whereas in this work $r_0 = 1$ was chosen. One can see that the plots are very similar in shape to the $4D$ case. Plot of (R, Z).

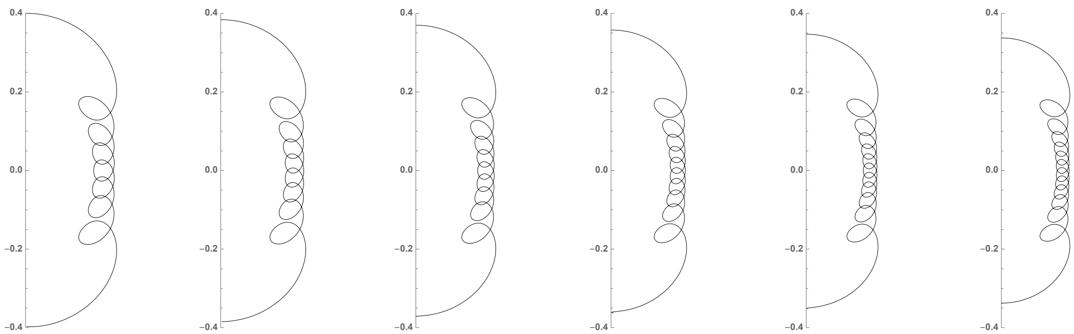

Figure 5.13: Many-looped MOTS for the non-Weyl coordinates, zoomed in. Plot of $(R\cos 2\Theta, R\sin 2\Theta)$.

5.5 Summary

The primary and most obvious takeaway from the MOTOS and MOTS discussed in this chapter is that adding a dimension to the spacetime largely does not affect the existence or behaviour of the self-intersections: there are still infinitely many self-intersecting closed MOTS in the $5D$ Schwarzschild spacetime, just as there were for 4-dimensions. The self-intersecting MOTOS also relate to the closed MOTS in the same way— one is able to follow a continuous sequence of them and find the shape and location of a MOTS as the occurrence of a closed surface in the sequence of open ones. This suggests that the choice in [11] to search for these open MOTOS (that is, to relax the closure condition in the search for vanishing null expansion surfaces) was a good one, as it is useful for two spacetimes which are distinct in a non-trivial way (that is, having differing dimension).

The qualitative differences between the 4- and 5-dimensional MOTS and MOTOS are far fewer than the similarities. A key one is the difference in shape for the MOTOS with large r and $r_{AH} < Z(0)$. This indicates that the effect of the apparent horizon in 5 dimensions extends out farther than it does in 4, warping MOTOS which are very far away. This is seen both for the Weyl and the spherical coordinates similarly, so it is at least somewhat coordinate invariant. We also see more intersections between MOTOS near to the apparent horizon, for $Z(0) < 0$. This is particularly relevant because a motivation for working in 5 dimensions was that the asymptotic behaviour of the MOTOS might be simpler than in $4D$, something suggested by the lack of logarithmic term in (3.2) from [15], as compared to (3.1). In [11], they expected the

MOTOS would take a clean ordered form for $r \to \infty$, but did not turn out to be true. Similarly it seems that this is once again not true for 5 dimensions, at least visually from the plots seen at the beginning of this chapter.

On one hand—if it is the case that the aymptotics are similarly poorly behaved in $5D$ as in $4D$—this shows that the $5D$ Schwarzschild black hole behaves analogously to the $4D$, which is consistent with the similarity in MOTS we see. On the other hand, it suggests that perhaps at least one of our motivations for adding a dimension to the spacetime did not yield the simplifications we had hoped. In fact, in 4-dimensions, while the MOTOS that left the positive z-axis did not remain cleanly ordered for large r, those which left the negative z-axis retained the order from which they left; in 5-dimensions, it is not as obvious whether there is any clean sort of ordering that occurs for the negative-z MOTOS. Thus the ordering of the MOTOS might be worse in five-dimensions than it was in four, but further study is required to establish whether this is the case. Hence, an important next step is to take expansions of the MOTOS in the large r limit.

Chapter 6

5D Rotating Black Hole Spacetime

Now that the methods have been described and applied to the simpler case of the $5D$ Schwarzschild metric, one can take the next step and apply them to a $5D$ rotating black hole. The steps are (mostly) the same, and we see the same self-intersecting MOTS. Here only the second ("MOTSodesic") method is followed, as it leaves less room for error.

6.1 5D Myers-Perry Metric

For the specific case of a Myers-Perry black hole [25] where all rotation parameters are equal and one enforces that the spacetime is asymptotically flat, one gets the metric as in [23] (where, compared to that work, $M = \mu$ and $\ell \to \infty$ which is the asymptotically flat condition):

$$ds^2 = -f^2 dt^2 + g^2 dr^2 + h^2(d\psi + \tilde{A}d\phi - \Omega dt)^2 + \frac{r^2}{4}(d\theta^2 + \sin^2(\theta)d\phi^2). \tag{6.1}$$

Here,

$$\begin{aligned} f^2 &= \frac{r^2}{g^2 h^2}, & g^2 &= (1 - \frac{2\mu}{r^2} + \frac{2\mu a^2}{r^4})^{-1}, \\ h^2 &= r^2(1 + \frac{2\mu a^2}{r^4}), & \tilde{A} &= \frac{\cos(\theta)}{2}, \\ \Omega &= \frac{2\mu a}{r^2 h^2}. \end{aligned} \tag{6.2}$$

For these coordinates, $\theta \in [0, \pi)$, ϕ and $\psi \in [0, 2\pi)$, $t \in \mathbb{R}$, and $r \in (r_+, \infty)$, where r_+ is the largest positive root of $1/g^2$.

The horizon at r_+ has S^3 topology, with metric

$$ds^2 = h(r_+)^2 \left(d\psi + \tilde{A}d\phi\right)^2 + \frac{r_+^2}{4}\left(d\theta^2 + \sin^2\theta d\phi^2\right). \tag{6.3}$$

6.1.1 PG-Like Coordinates

As in the static case, we require coordinates that are non-singular across the horizon. This occurs at $r_+ = \sqrt{\mu + \sqrt{\mu(\mu - 2a^2)}}$. This is the positive root of $1/g^2$, g^2 being the only coefficient in the metric which is singular for an $r \neq 0$.

To find Painlevé-Gullstrand-like coordinates for this metric, introduce the coordinates

$$T = t - A(r) \qquad \Psi = \psi - B(r). \tag{6.4}$$

Putting the metric into these new coordinates,

$$\begin{aligned} ds^2 = &- (f^2 - \Omega^2 h^2)dT^2 + 2\left(h^2\Omega(\Omega A' - B') - f^2 A'\right)dTdr \\ &+ (h^2(\Omega A' - B')^2 - f^2 A'^2 + g^2)dr^2 + h^2 d\Psi^2 - 2h^2(\Omega A' - B')d\Psi dr \\ &- 2h^2\Omega d\Psi dT + 2\tilde{A}d\Psi d\phi - 2h^2\tilde{A}(\Omega A' - B')d\phi dr + h^2\tilde{A}^2 d\phi^2 - 2h^2\tilde{A}\Omega d\phi dT \\ &+ \frac{r^2}{4}(d\theta^2 + \sin^2(\theta)d\phi^2), \end{aligned} \tag{6.5}$$

one can then see that the choice $\Omega A' = B'$ should be made, as this sets three different coefficients to zero, and thereby simplifies the equation. This gives

$$\begin{aligned} ds^2 = &- (f^2 - \Omega^2 h^2)dT^2 - 2f^2 A' dT dr + (g^2 - f^2 A'^2)dr^2 \\ &+ h^2\left(d\Psi^2 - 2\Omega d\Psi dT + 2\tilde{A}d\Psi d\phi - 2\tilde{A}\Omega d\phi dT + \tilde{A}d\phi^2\right) + \frac{r^2}{4}(d\theta^2 + \sin^2(\theta)d\phi^2). \end{aligned} \tag{6.6}$$

A second equation is required to determine B and A uniquely, so for convenience the choice $g^2 - f^2 A'^2 = 1$ is made to set the coefficient of dr^2 to unity. This means that

$$f^2 A' = \pm\sqrt{f^2(g^2-1)} = \pm\frac{\sqrt{2\mu(r^2-a^2)}}{\sqrt{h^2 r^2}} \tag{6.7}$$

and the metric is then

$$\begin{aligned} ds^2 =& -f^2 dT^2 + 2\frac{\sqrt{2\mu(r^2-a^2)}}{\sqrt{h^2r^2}} dT dr + dr^2 + h^2\left(d\Psi + \tilde{A} d\phi - \Omega dT\right)^2 \\ &+ \frac{r^2}{4}(d\theta^2 + \sin^2(\theta) d\phi^2). \end{aligned} \tag{6.8}$$

The final coordinate transform that is made is

$$\begin{aligned} T &= t \mp \sqrt{2}\int^r \frac{\sqrt{(r^2-a^2)\mu}\sqrt{r^4+2a^2\mu}}{r^4+2\mu(a^2-r^2)} dr \\ \Psi &= \psi \mp 2\sqrt{2}a\mu \int^r \frac{\sqrt{(r^2-a^2)\mu}}{\sqrt{r^4+2a^2\mu}(r^4+2\mu(a^2-r^2))} dr. \end{aligned} \tag{6.9}$$

where when $a = 0$, this reduces to the Schwarzschild metric in Painlevé-Gullstrand coordinates as in 3.8.

Immediately noticeable is that this coordinate system fails when $r = a$. Though it is true that this surface always exists inside the inner horizon of this spacetime (the inner horizon occurs at $r_- = \sqrt{\mu - \sqrt{\mu(\mu - 2a^2)}}$), this will still become relevant (and will limit) our analysis of the MOT(O)S of the spacetime. A short discussion of how—as next steps—it may be remedied is included at the end of this chapter.

6.2 Derivation of MOTSodesics

6.2.1 Hypersurface, Extrinsic Curvature

As before, we define a foliation of the spacetime in constant-time slices, which each have metric

$$h_{ij} dx^i dx^j = dr^2 + h^2\left(d\Psi + \tilde{A} d\phi\right)^2 + \frac{r^2}{4}(d\theta^2 + \sin^2(\theta) d\phi^2). \tag{6.10}$$

If $a = 0$, this metric is flat and $h^2 = r^2$.

One then defines again a rotationally symmetric hypersurface via the parametric equations $\gamma(\lambda, \Psi, \phi) = (R(\lambda), \Theta(\lambda), \Psi, \phi)$, and the coordinates on this hypersurface are the parameters of the γ. Then the metric on the hypersurface is

$$q_{ab}dx^a dx^b = d\lambda^2 + h^2 d\Psi^2 + 2h^2 \tilde{A} d\Psi d\phi + \left(\frac{1}{4}R^2 \sin^2(\Theta) + h^2 \tilde{A}^2\right) d\phi^2 \tag{6.11}$$

where the coefficient of the $d\lambda$ term has been set to one, that is, an arclength parameterization has been chosen (as before). This corresponds to, in this case,

$$\dot{R}^2 + \frac{1}{4}R^2\dot{\Theta}^2 = 1. \tag{6.12}$$

We also require the extrinsic curvature of the timeslice, K_{ij}, which can be found from the normal

$$u_\alpha = -\frac{r}{h}dT, \tag{6.13}$$

to be

$$K_{ij} = \begin{bmatrix} \frac{\sqrt{2\mu}(r^4-2a^2(r^2+\mu))}{\sqrt{(r^2-a^2)r^3h^2}} & 0 & -\frac{4a\mu}{r^2h} & -\frac{2a\mu\cos\theta}{r^2h} \\ 0 & -\frac{\sqrt{\mu(r^2-a^2)}}{2\sqrt{2}r} & 0 & 0 \\ -\frac{4a\mu}{r^2h} & 0 & -\frac{\sqrt{2\mu(r^2-a^2)}(r^4-2a^2\mu)}{r^5} & -\frac{\sqrt{\mu(r^2-a^2)}(r^4-2a^2\mu)\cos\theta}{\sqrt{2}r^5} \\ -\frac{2a\mu\cos\theta}{r^2h} & 0 & -\frac{\sqrt{\mu(r^2-a^2)}(r^4-2a^2\mu)\cos\theta}{\sqrt{2}r^5} & -\frac{\sqrt{\mu(r^2-a^2)}(r^4-2a^2\mu\cos^2\theta)}{2\sqrt{2}r^5} \end{bmatrix}. \tag{6.14}$$

This is of course pulled back into the timeslice, $K_{ij} = e_i^\alpha e_j^\beta K_{\alpha\beta}$. Here $e_i^\alpha = \frac{\partial x^\alpha}{\partial x^i}$, where x^α are the coordinates on the full $5D$ spacetime, and x^i are the coordinates on the 4D timeslice—this is the same sort of pullback/push-forward operator as was seen in chapter 4.

6.2.2 Finding k_u

Just like the $5D$ Schwarzschild derivation, we find the timelike expansion k_u as the trace of the extrinsic curvature

$$k_u = \tilde{q}^{ij}K_{ij}, \tag{6.15}$$

where in this case, the pushed-forward hypersurface metric is

$$\tilde{q}^{ij} = \begin{bmatrix} \dot{R}^2 & \dot{R}\dot{\Theta} & 0 & 0 \\ \dot{R}\dot{\Theta} & \dot{\Theta}^2 & 0 & 0 \\ 0 & 0 & \frac{R^2+h^2\cot^2\Theta}{R^2h^2} & \frac{-2\cot\Theta\csc\Theta}{R^2} \\ 0 & 0 & \frac{-2\cot\Theta\csc\Theta}{R^2} & \frac{4\csc^2\Theta}{R^2} \end{bmatrix}. \tag{6.16}$$

So then

$$k_u = \frac{\sqrt{2}\mu\left((a^2-R^2)(2a^2\mu+3R^4)+\dot{R}^2(2R^6-2a^4\mu-3a^2R^4)\right)}{R^3\sqrt{\mu(R^2-a^2)}(2a^2\mu+R^4)}, \tag{6.17}$$

where here the $\dot{\Theta}$ terms have been replaced with $4(1-\dot{R}^2)/R^2$ (from the arclength condition) to simplify the expression.

6.2.3 Angular Vectors

Remember that the metric on the time slice can be expressed as

$$h_{ij} = T_iT_j + N_iN_j + \hat{\psi}_i\hat{\psi}_j + \hat{\phi}_i\hat{\phi}_j, \tag{6.18}$$

where here the normal to the hypersurface is

$$N = \frac{R\dot{\Theta}}{2}dr - \frac{R\dot{R}}{2}d\theta, \tag{6.19}$$

and so the (inverse) pushed-forward hypersurface metric is then

$$\tilde{q}^{ij} = T^iT^j + \hat{\psi}^i\hat{\psi}^j + \hat{\phi}^i\hat{\phi}^j. \tag{6.20}$$

That is, the part that is orthogonal to the normal part of 6.18. Therefore, to find the vectors $\hat{\Psi}$ and $\hat{\phi}$, enforce the following:

$$\begin{aligned} \tilde{q}^{\psi\psi} &= (\hat{\psi}^\psi)^2 + (\hat{\phi}^\psi)^2 = \frac{R^2+h^2\cot^2\Theta}{R^2h^2} \\ \tilde{q}^{\psi\phi} &= \hat{\psi}^\psi\hat{\psi}^\phi + \hat{\phi}^\psi\hat{\phi}^\phi = -\frac{2\cot\Theta\csc\Theta}{R^2} \\ \tilde{q}^{\phi\phi} &= (\hat{\psi}^\phi)^2 + (\hat{\phi}^\phi)^2 = \frac{4\csc^2\Theta}{R^2}. \end{aligned} \tag{6.21}$$

Choosing $\hat{\psi}^{\phi} = 0$, this will then set

$$\begin{aligned} \hat{\psi} &= \frac{1}{h}\frac{\partial}{\partial \psi} \\ \hat{\phi} &= -\frac{\cot\Theta}{R}\frac{\partial}{\partial \psi} + \frac{2\csc\Theta}{R}\frac{\partial}{\partial \phi}. \end{aligned} \tag{6.22}$$

One can check that these vectors have unit norm and are orthogonal, as required.

6.2.4 Finding κ

As before, the scalar κ that appears in the MOTSodesic equations is found via

$$\kappa = k_u - N_i \hat{\Psi}^j D_j \hat{\Psi}^i - N_i \hat{\phi}^j D_j \hat{\phi}^i. \tag{6.23}$$

The second and third terms are the accelerations in the Ψ and ϕ directions, respectively. The former is

$$K_\Psi = N_i \hat{\Psi}^j D_j \hat{\Psi}^i = \frac{(2a^2\mu - R^4)\dot{\Theta}}{2R^2h^2}, \tag{6.24}$$

and the latter is

$$K_\phi = N_i \hat{\phi}^j D_j \hat{\phi}^i = \frac{2\cot\Theta \dot{R}}{R} - \frac{\dot{\Theta}}{2}, \tag{6.25}$$

so that

$$\begin{aligned} \kappa &= k_u - K_\Psi - K_\phi \\ &= \sqrt{2\mu}\frac{((a^2 - R^2)(2a^2\mu + 3R^4) + \dot{R}^2(2R^6 - 2a^4\mu - 3a^2R^4)}{R^5\sqrt{(R^2 - a^2)}h^2} + \frac{R^5\dot{\Theta} - 2\cot\Theta R^2h^2\dot{R}}{R^3h^2}. \end{aligned} \tag{6.26}$$

6.2.5 MOTSodesics

Finally, the MOTSodesics can be found using the scalar κ. In general, of course, the EOMs follow the formula

$$\frac{d^2X^A}{d\lambda^2} = -\Gamma^A_{BC}T^BT^C + \kappa N^A, \tag{6.27}$$

where here, again, $X^A = (R, \Theta)$, and the Christoffel symbols correspond to those on the curve with coordinates X^A. (Also, $N^A = (N^r, N^\theta)$, and $T^A = (\dot{R}, \dot{\Theta})$.)

Then the MOTSodesic equations for this spacetime are

$$\ddot{R} = -\Gamma^R_{\Theta\Theta}\dot{\Theta}^2 + \frac{1}{2}\kappa R\dot{\Theta} \Rightarrow \ddot{R} = \frac{R\dot{\Theta}}{2}\left(\frac{\dot{\Theta}}{2} + \kappa\right) \tag{6.28}$$

and

$$\ddot{\Theta} = -2\Gamma^\Theta_{\Theta R}\dot{R}\dot{\Theta} - 2\kappa\frac{\dot{R}}{R} \Rightarrow \ddot{\Theta} = -\frac{2\dot{R}}{R}\left(\dot{\Theta} + \kappa\right) \tag{6.29}$$

where a dot denotes derivative with respect to λ. One can see that, while κ is more complicated than in the $5D$ Schwarzschild case, the MOTSodesics as they appear here look simpler.

6.3 Series Expansions at $R = 0$

Similarly as was done for the Schwarzschild case, we complete series expansions for small λ, which are once again accurate to second order. This is done, of course, by setting

$$\begin{aligned} R(\lambda) &= R_0 + R_1\lambda + R_2\lambda^2 + R_3\lambda^3 + O(\lambda^4) \\ \Theta(\lambda) &= \Theta_0 + \Theta_1\lambda + \Theta_2\lambda^2 + \Theta_3\lambda^3 + O(\lambda^4), \end{aligned} \tag{6.30}$$

The MOTSodesic equations will hold to second order in λ.

In this case, it will not be true that $R_0 = 0$ when $\lambda = 0$, but rather that R_0 will play the role that Z_0 did in the series expansion for Schwarzschild. Thus, we will end up with R_0 a freely specifiable parameter at the end, which is used to choose which MOTOS is being described.

Substituting (6.30) into the equations (6.28) and (6.29), and also enforcing the arclength condition to get a relationship between R_0 and Θ_1, one gets

$$
\begin{aligned}
&\Theta_0 = 0,\;\; R_1 = 0,\;\; \Theta_2 = 0,\;\; R_3 = 0 \\
&\Theta_3 = \frac{(3R_0^4 + 2a^2\mu)(R_0^2 - \sqrt{2\mu(R_0^2 - a^2)})}{4R_0^3(R_0^4 + 2\mu a^2)} \\
&R_2 = \frac{3R_0^4 + 2a^2\mu}{12R_0^7(R_0^4 + 2a^2\mu)^2}\left(-5R_0^8 + 4a^4\mu^2 + \right. \\
&\quad 4a^2R_0^2\mu\left(2\sqrt{2\mu(R_0^2 - a^2)} - \mu\right) + 2R_0^6\left(-3\mu + 4\sqrt{2\mu(R_0^2 - a^2)}\right)\Big) \\
&\Theta_1 = 2/R_0
\end{aligned}
\tag{6.31}
$$

Using these coefficients in equations (6.30), this is a solution to second order in λ, for small values of this parameter. Specifically, it holds when $R \to 0$. However, as with the Schwarzschild case, we do not plot these solutions, as they give qualitatively indistinguishable results from those found by plotting the MOTSodesic equations from R small but non-zero, as one can choose arbitrarily small R at which to begin—hence they affect numerical details of the results, but not the qualitative behaviour.

6.4 Results

This section will discuss the MOTOS and MOTS for various values of the rotation parameter a, with the mass parameter, μ, set equal to 1. To scale these, simply multiply the value of R at which the MOT(O)S leave the z-axis by $\sqrt{\mu}$.

The $5D$ Schwarzschild case, which is what the Myers-Perry black hole reduces to when the rotation parameter is set to zero, is discussed first, and of course the results are the same as in the previous section—though these coordinates are once again slightly different from the two already introduced.

Then, the rotation parameter is varied from a very near zero, to $a = 0.5$; because the Painlevé-Gullstrand -like coordinates used here only hold for $r > a$, they are unable to probe inside this surface, and thus MOTS which exist inside it cannot be found. So, as this surface increases in size, the number of MOTS that exist between it and the apparent horizon reduces. For $a = 0.5$, no MOTS can be found between these two surfaces. Further discussion of the failure of the coordinates will follow the rest of the results.

Note that all (Myers-Perry) plots in this chapter have $x = R(\lambda)\cos(\Theta(\lambda))$ on the horizontal axis, and $y = R(\lambda)\sin(\Theta(\lambda))$ on the vertical. The (non-Weyl) Schwarzschild plots are the same as in the previous chapter, that is, $x = R\cos(2\Theta)$, $y = R\sin(2\Theta)$.

6.4.1 $a = 0$ (Schwarzschild)

Firstly, observe the figure that shows the first ten self-intersecting MOTS of Schwarzschild ($a = 0$) in the Myers-Perry coordinates, 6.1. Comparing this to 6.2, which is the first ten MOTS in the Schwarzschild spacetime in the non-Weyl coordinates, we see they are more or less indistinguishable (apart from differences in overall scale). This is as expected, given that the coordinates used for the Myers-Perry spacetime (as outlined in the previous section) are the spherical/toroidal type coordinates, rather than the cylindrical-type Weyl coordinates, and so the behaviour for this $a = 0$ case should be the same as in the analogous coordinates from the previous chapter.

Unlike in the previous chapter, the values of R_0 from which the MOTS leave the vertical axis must be multiplied by $\sqrt{\mu}$ to scale with the mass of the Myers-Perry black hole (whereas for the Schwarzschild black hole, it was multiplied by r_0).

6.4.2 MOTS for $a \neq 0$

Setting $a \neq 0$ introduces rotation to the spacetime. The already present appearance of the loops hugging a spherical surface, which is visible in the $a = 0$ MOTS, is more pronounced as this surface becomes non-zero in size. We also notice that the loops begin to intersect each other much sooner (when there are fewer loops), whereas in the static case, this doesn't occur until the MOTS with at least seven loops.

As discussed, the coordinates used fail across the surface $R = a$, and so the size of this surface constrains how many MOTS can be found in the spacetime. Figure 6.3 shows the first five closed MOTS for the $a = 0.1$ Myers-Perry black hole. We see here that the loops are warped around the surface $R = a$, which is shown in red. It is also noteworthy that the loops begin to intersect each other when the number of them is greater than two.

Figure 6.4(a) shows the last closed MOTS that can be found for $a = 0.1$. While

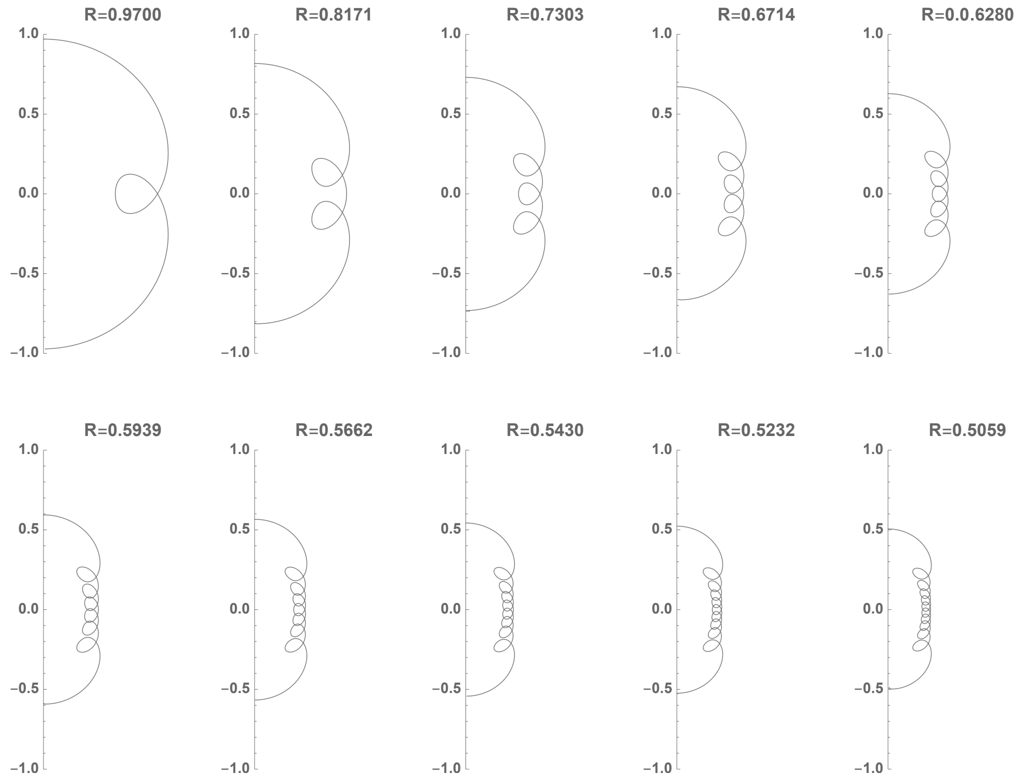

Figure 6.1: The first 10 self-intersecting MOTS in the $a = 0$ MP spacetime, which is of course simply Schwarzschild. The horizontal axis plots $R\cos\Theta$; the vertical plots $R\sin\Theta$.

there are more open MOTOS which may be found – that is, which do not cross the $R = a$ surface – any other closed MOTS will cross this surface, and thus cannot be probed using these coordinates.

As the rotation parameter increases, the number of MOTS which can be found reduces very quickly: figure 6.5 shows the MOTS which exist outside $R = a$ for $a = 0.3$, $a = 0.35$, and $a = 0.4$. By the latter, there is only one closed MOTS (aside from the apparent horizon), which is visible in these coordinates. Figure 6.4(b) shows what happens for $a = 0.5$, where one can find neither self-intersecting MOTS nor self-intersecting MOTOS: they begin to curve as though they are going to produce a self-intersection, but then they run into the $R = a$ surface, and thus can no longer be followed using these coordinates.

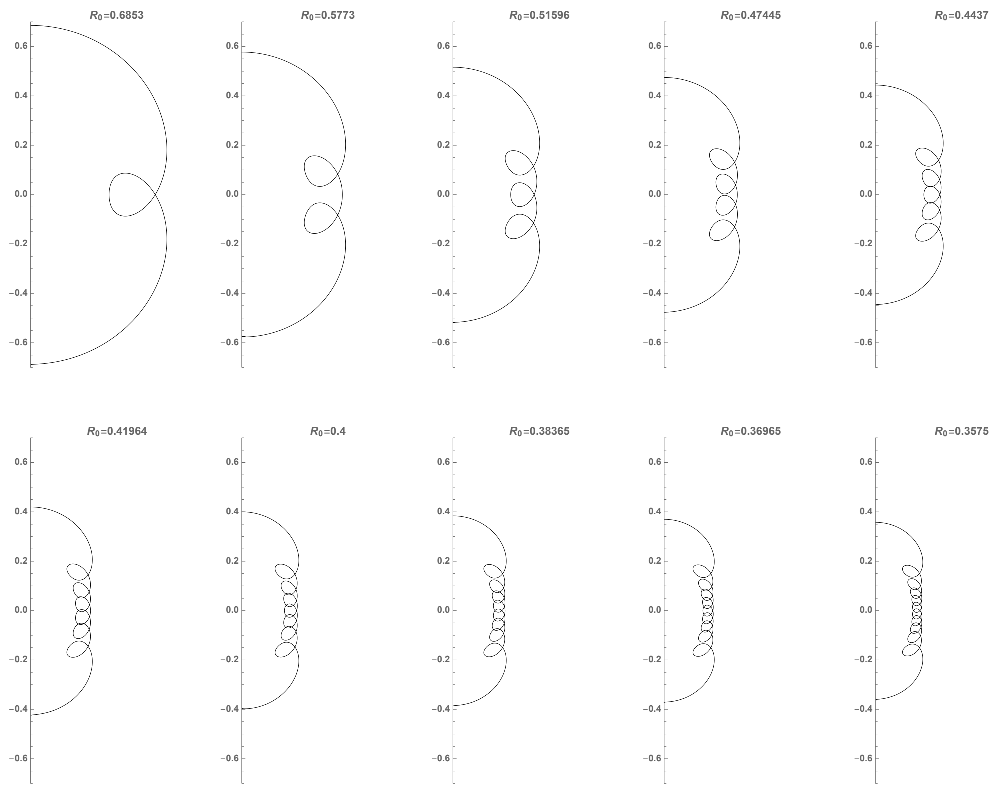

Figure 6.2: The first ten MOTS for the non-Weyl coordinates for 5D Schwarzschild, from chapter 5. One can see, aside from the scale of the coordinates, they are indistinguishable from the $a = 0$ Myers-Perry. The horizontal axis plots $R \cos 2\Theta$; the vertical plots $R \sin 2\Theta$.

6.4.3 $a \neq 0$ MOTOS

The open MOTOS that leave the vertical axis outside of the apparent horizon, that is, those which do not have self-intersections, behave very similarly for nonzero rotation as they do for the static case. They wrap around the apparent horizon, with its effect extending out to large R (see figure 6.6). They also flatten out parallel to the horizontal axis for large R, as in the static case. Comparing figure 6.7 to 6.6, we see that increasing the rotation does not affect these MOTOS very strongly, especially compared to how dramatically it affects the MOTS and MOTOS inside the apparent horizon (the difference between the number of looped MOTS being reflected by however many loops exist in figure 6.4(a) for $a = 0.1$, as compared to only one looped MOTS existing for $a = 0.4$).

The MOTOS that leave the positive vertical axis inside the apparent horizon also

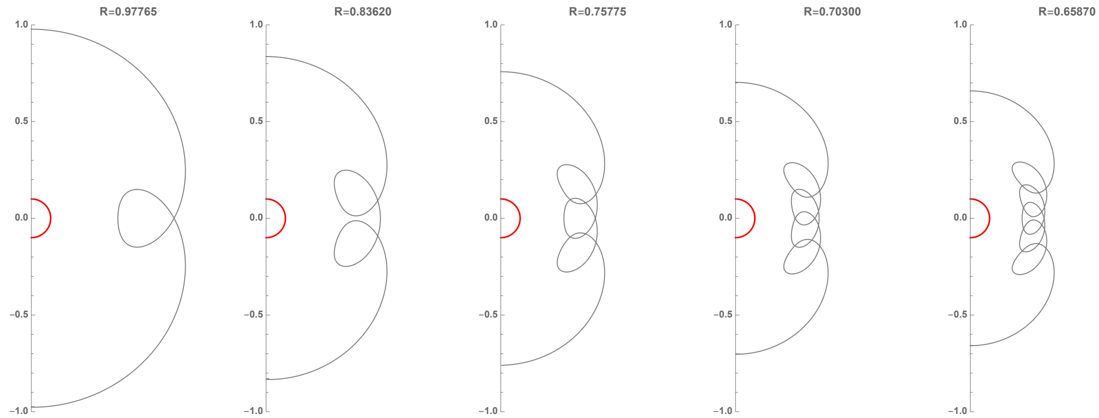

Figure 6.3: The first five MOTS for an $a = 0.1$ Myers-Perry black hole. The surface $R = a$ is shown in red. Plots $(R\cos\Theta, R\sin\Theta)$.

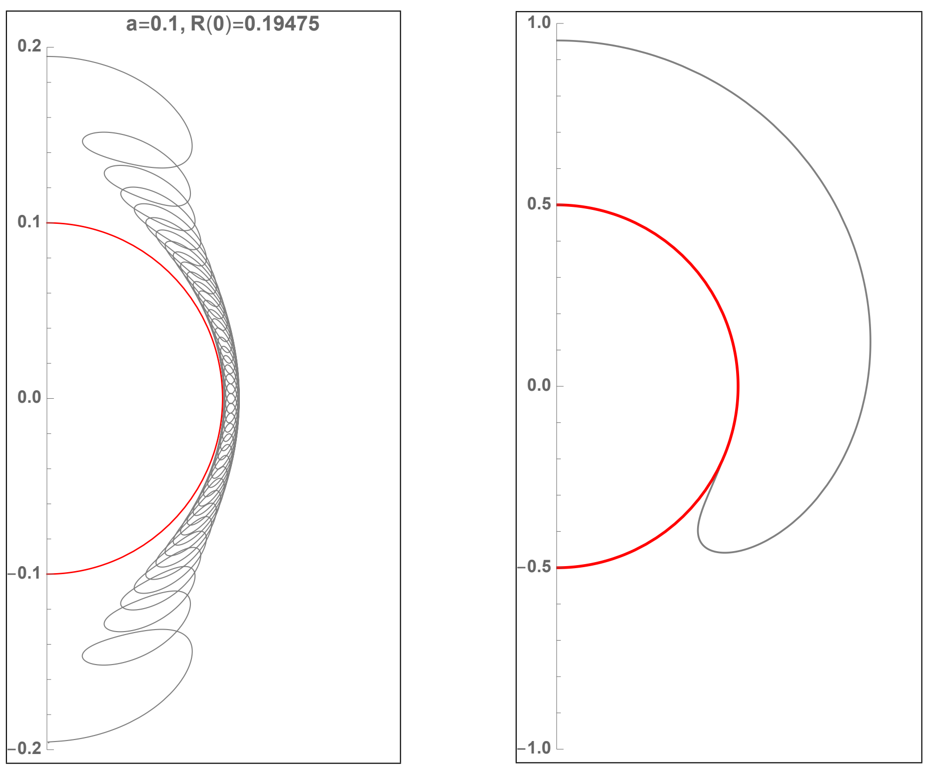

(a) Last closed MOTS for $a = 0.1$ which can be found outside $R = a$.

(b) MOTOS that intersects $R = a$, for $a = 0.5$; no closed MOTS can be found.

Figure 6.4: These plot $(R\cos\Theta, R\sin\Theta)$.

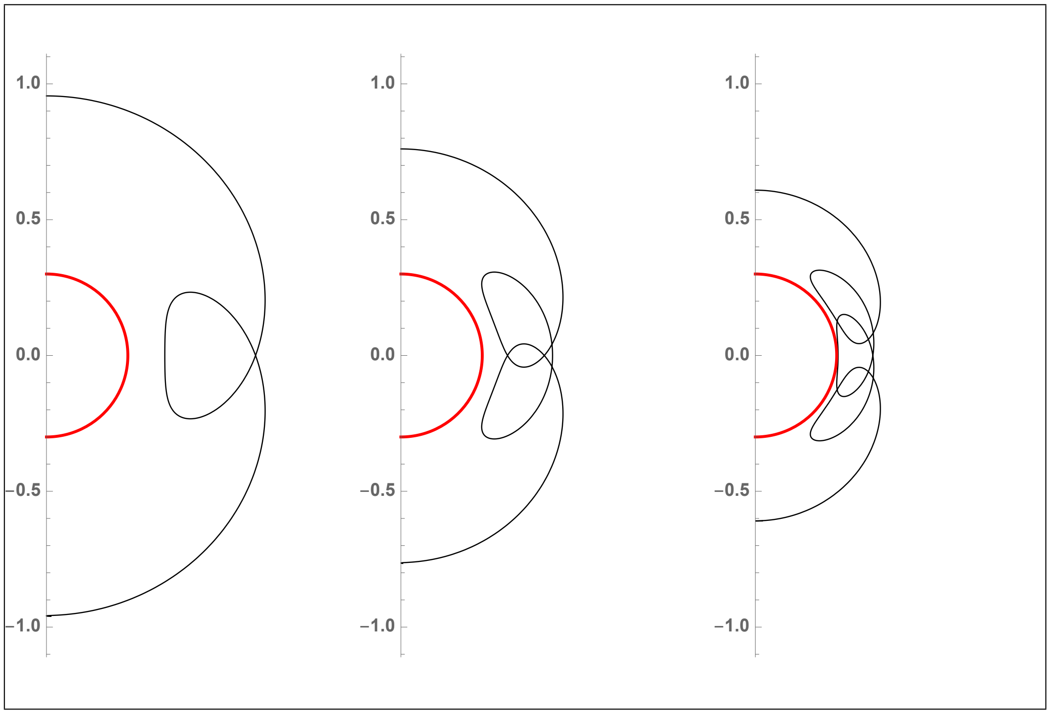

(a) $a = 0.3$

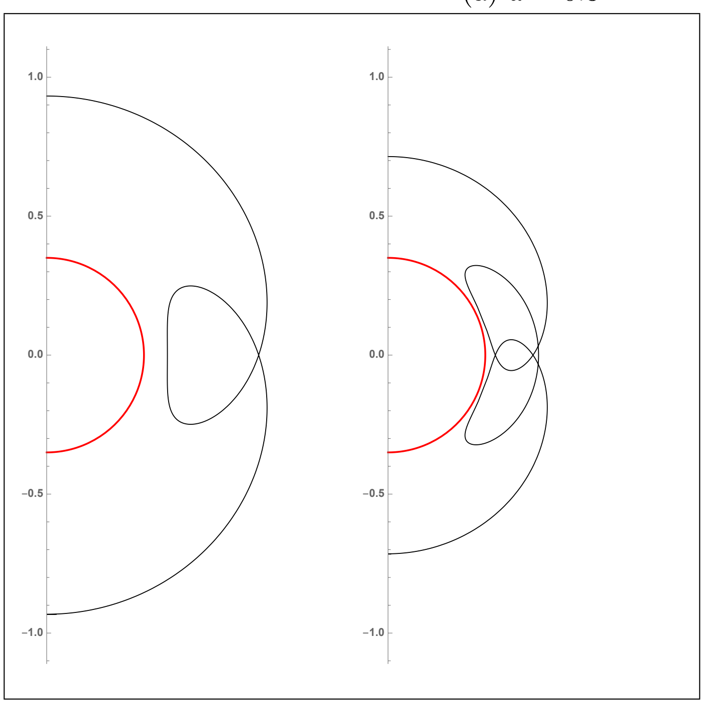

(b) $a = 0.35$

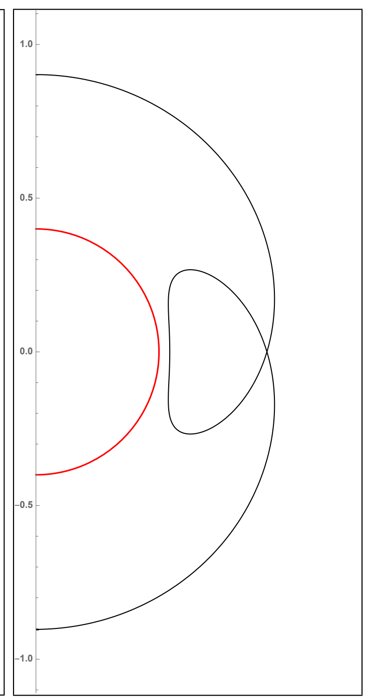

(c) $a = 0.4$

Figure 6.5: The MOTS which exist inside the apparent horizon, and outside the surface $R = a$, for $0.3 \leq a \leq 0.4$. All plots are of $(x, y) = (R\cos\Theta, R\sin\Theta)$.

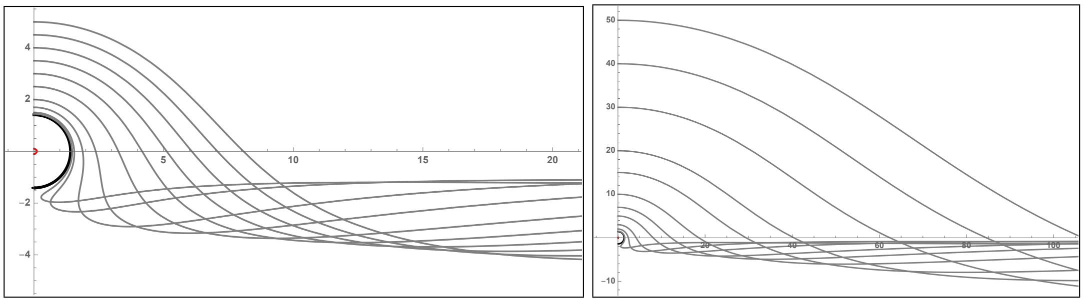

Figure 6.6: The MOTOS which leave the vertical axis for positive $R > R_{AH}$, for $a = 0.1$. Plots $(R\cos\Theta, R\sin\Theta)$.

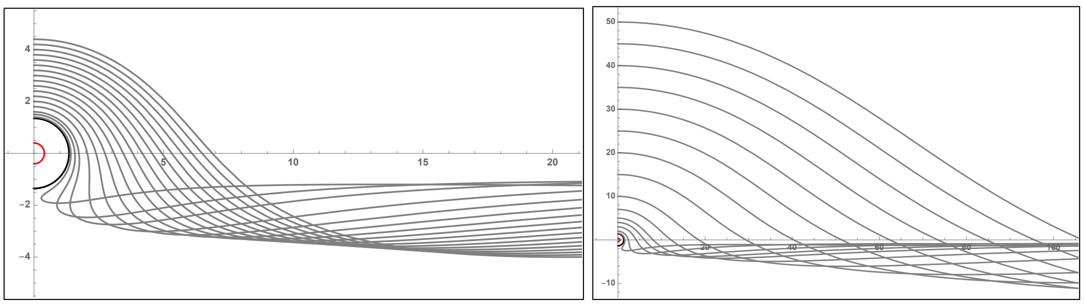

Figure 6.7: The MOTOS which leave the positive vertical axis outside of the apparent horizon, for $a = 0.4$. Plots $(R\cos\Theta, R\sin\Theta)$.

behave analogously to how they do in Schwarzschild; that is, they are of similar shape to the nearest self-intersecting MOTS, with one loop fewer than the self-intersecting MOTS just outside it. Comparison of figure 6.8 to figure 5.8 shows the same sort of downward movement and narrowing of loops occurs, with a cusp in the loop producing a closed MOTS. Note here one can also see the apparent horizon at $R = r_+$ (black outer surface), and can see it decreasing slightly in size as the rotation increases.

Oscillations in MOTOS Near $R = a$

There is, however, an interesting qualitative difference, which exists for the MOTOS that leave the negative vertical axis near to the surface $R = a$: we see a strange sort of oscillation in these MOTOS, which flattens out as they leave the axis farther from the surface.

Figure 6.9 shows these oscillating MOTOS for $a = 0.1$, with the left plot zoomed in sufficiently to show the complicated behaviour, and the right plot zoomed out slightly to indicate that the MOTOS become smooth as they leave the axis farther away from

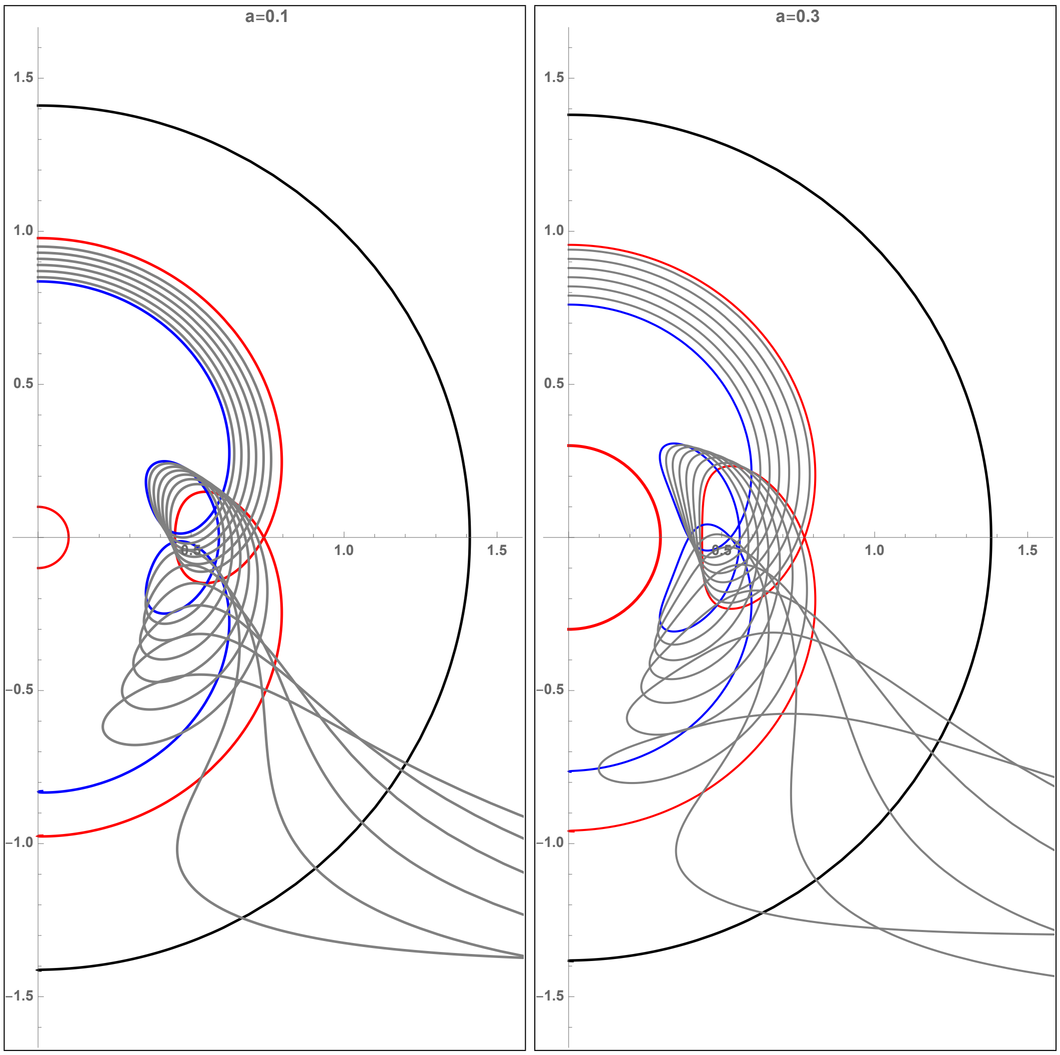

Figure 6.8: These are the analogous plots to 5.8, but for $a = 0.1$ (left) and $a = 0.3$ (right). The thick red inner surface is $R = a$, and the outer black surface is the apparent horizon, $R = r_+$. These plot $(R\cos\Theta, R\sin\Theta)$.

the $R = a$ surface.

Interestingly, this oscillating behaviour becomes less visible as the rotation parameter increases: for $a = 0.3$, it is less of an oscillation and more of double turn-around, and for $a = 0.4$, it becomes more like a single turn in the MOTOS.

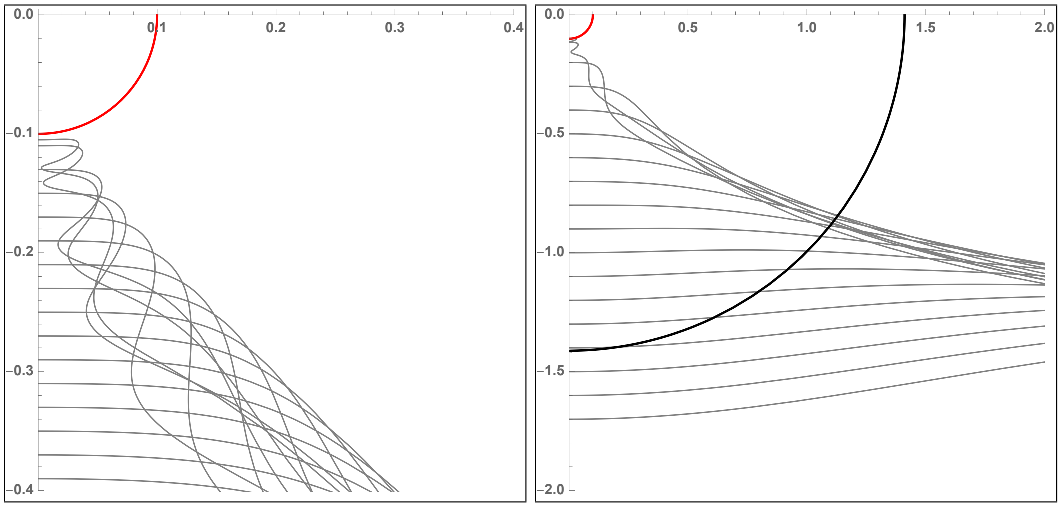

Figure 6.9: Oscillations in the MOTOS which leave the negative vertical axis near the surface $R = a$, for $a = 0.1$. Plots $(x, y) = (R\cos\Theta, R\sin\Theta)$.

As the rotation parameter reduces, the oscillating becomes more dramatic – see figure 6.12 for the oscillations present when the rotation parameter is equal to 0.05. This naturally leads one to ask whether such oscillations are present when $a = 0$, that is, whether there exists a qualitative difference in behaviour of the MOTOS that approach the static spacetime, versus those of the static spacetime itself.

It seems to be the case that if we look increasingly close to the singularity for the ($5D$) Schwarzschild black hole, these oscillations continue to exist—with their period of oscillation (used loosely here) reducing also, thereby causing them to appear more dramatic. However, it is also the case that the amplitude of the oscillations reduces alongside the period, meaning that as $a \to 0$, the amplitude will also go to zero, and the oscillations will flatten out completely for Schwarzschild—which is expected, given that none were seen in the previous chapter. This increase in number of oscillations while, simultaneously, the amplitude of each is decreasing is visible if one compares the left plots on figures 6.9 and 6.12.

Finally, figure 6.13 shows, in the middle and on the right, the MOTOS which leave the vertical axis from $R_0 = 0.0010001$ and $R_0 = 0.001001$, respectively. One

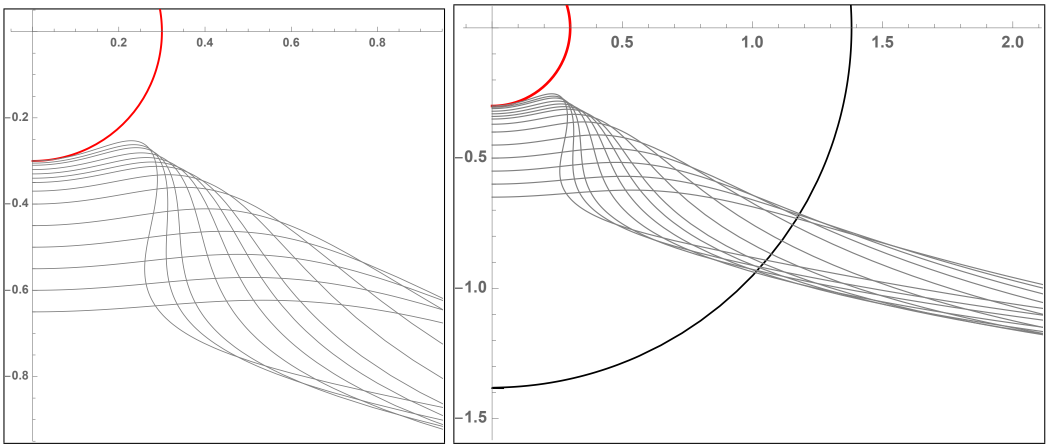

Figure 6.10: Oscillations/turns in MOTOS for $a = 0.3$. Plots $(R\cos\Theta, R\sin\Theta)$.

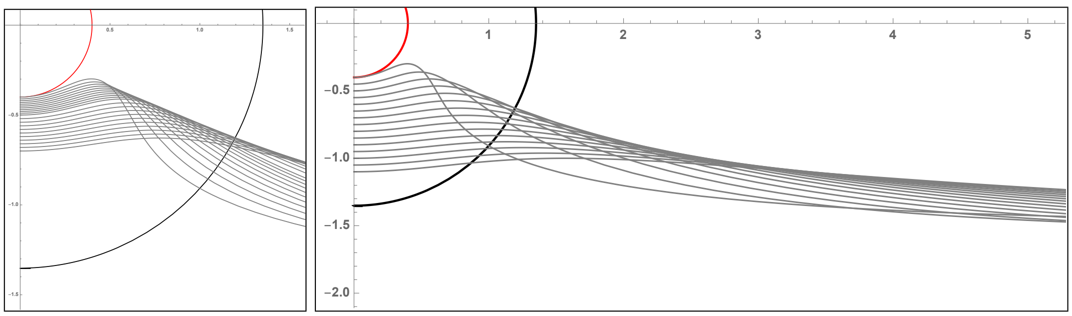

Figure 6.11: Flattening out of the oscillating MOTOS for $a = 0.4$. Plots $(R\cos\Theta, R\sin\Theta)$.

can see how the amplitude and the period of the oscillation reduce as the rotation parameter reduces. In particular, notice that the amplitude nearest to the $R = a$ surface reduces most dramatically. The left-most plot in this figure shows the MOTOS with $R_0 = 0.001$ in Schwarzschild ($a = 0$). Obviously, no oscillations are visible. Following the plots from right to left, the means by which the oscillations limit to the smooth MOTOS is clear.

It is also worth noting that the amplitude and period of the oscillations increase not only with rotation parameter, but also—for a single MOTOS in a spacetime with some given rotation parameter—they will increase as one follows the MOTOS farther away from the $R = a$ surface. This is most obviously visible in figure 6.14, which shows the MOTOS with $R_0 = 0.01001$ for the spacetime with $a = 0.01$ (but of course, it is also clear with careful inspection in all the oscillation figures). The farther the MOTOS is from the $R = a$ surface, the more it pulls away also from the vertical axis,

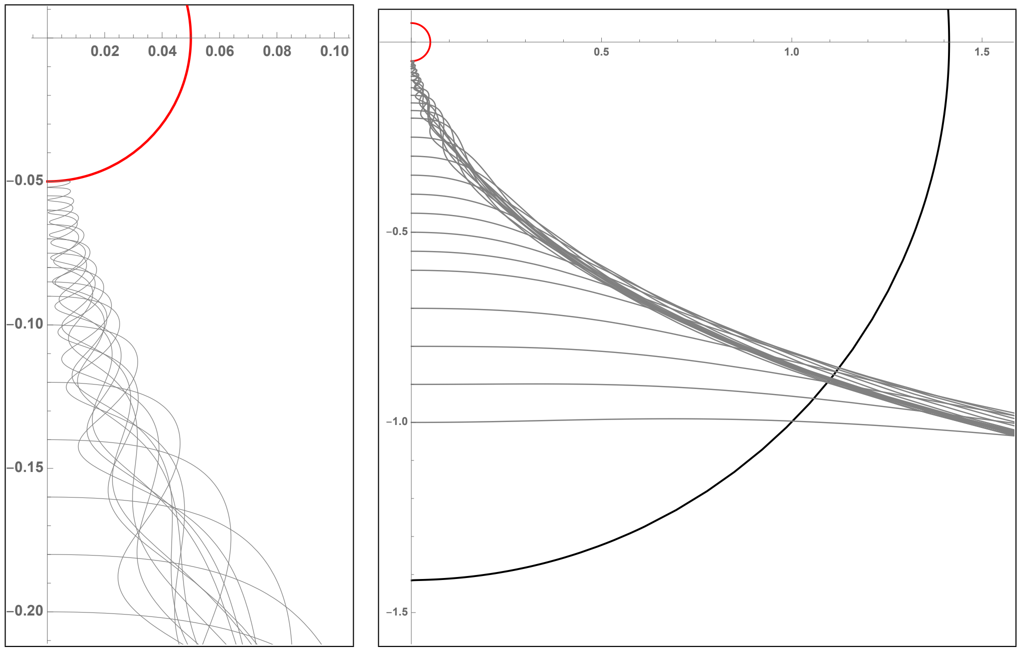

Figure 6.12: Dramatic oscillations for small ($a = 0.05$) rotation parameter. Plots $(R\cos\Theta, R\sin\Theta)$.

so it is difficult to say whether the former or the latter is the relevant factor with which the increase in amplitude/period correlates.

6.4.4 Summary

As expected, the rotating Myers-Perry spacetime is richer in the complexity of MOTS and MOTOS behaviour. While there are strong similarities to the Schwarzschild spacetime in the MOTOS that leave the vertical axis above and outside the apparent horizon (both for small rotation, of course, but also for larger rotation), there are qualitative differences in those which leave the vertical axis inside the apparent horizon, but below $R = a$: oscillations in these MOTOS are seen, which increase in frequency as the rotation parameter of the spacetime is reduced. They limit to the smooth case of the Schwarzschild spacetime through their amplitude simultaneously reducing, increasing confidence that they are not some sort of error in either the numerics or the derivations.

Importantly, we continue to find self-intersecting MOTS in this spacetime, for all values of the rotation parameter up to and including $a = 0.4$. These MOTS are,

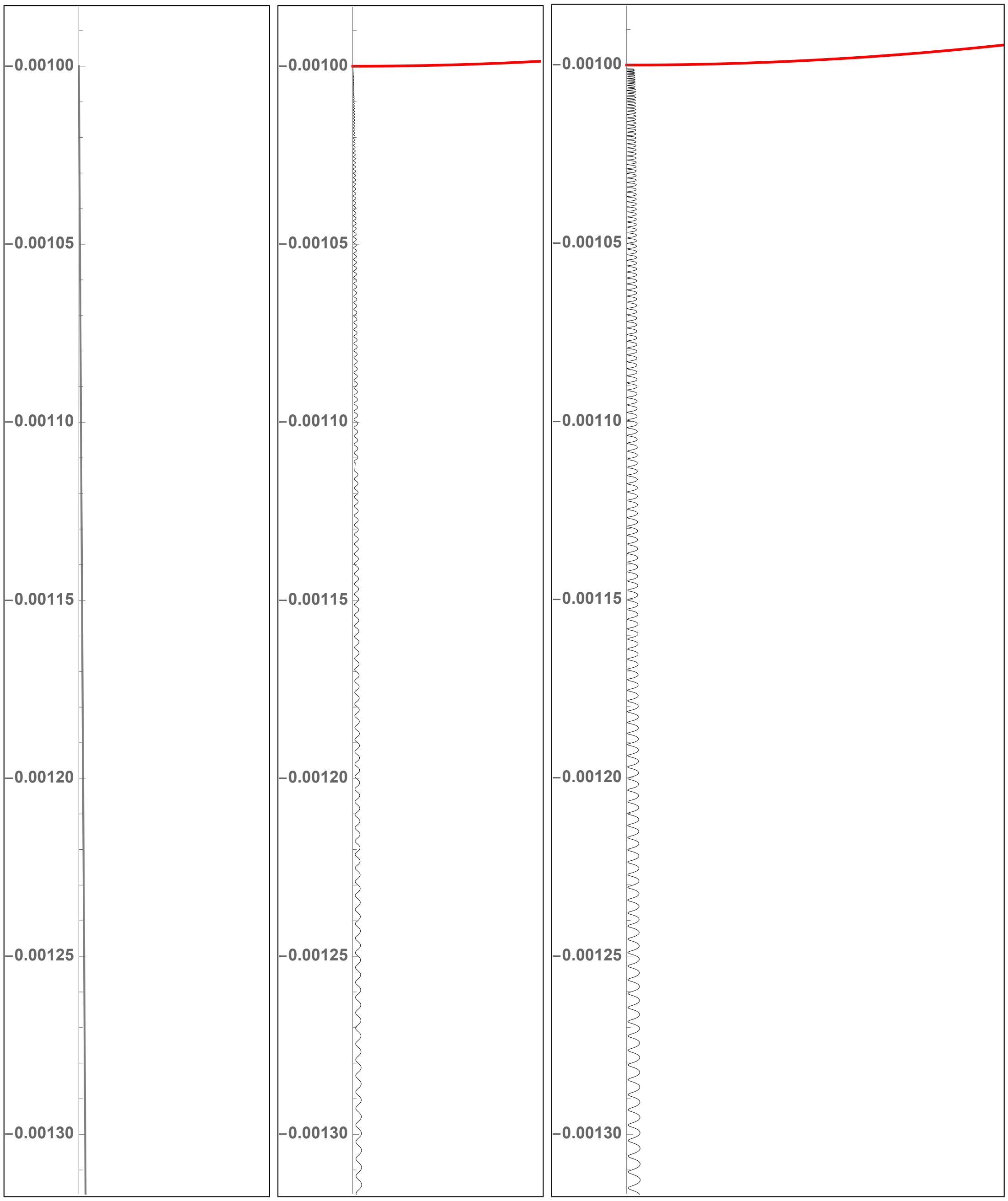

Figure 6.13: The MOTOS which leave the vertical axis from $R_0 = 0.0010001$ (middle), and $R_0 = 0.001001$ (right), for $a = 0.001$. One the left is the MOTOS which has $R_0 = 0.001$, for $a = 0$ (Schwarzschild). The horiztal axis for all three of these plots is on the scale 1×10^{-5}, and they are shown with the same aspect ratios. These all plot $(x, y) = (R\cos\Theta, R\sin\Theta)$.

however, warped around the surface $R = a$, with their warping becoming more dramatic as this surface increases in size. The loops themselves also intersect one another sooner (that is, when there are fewer of them), the faster the rotation is. However, the fact that these self-intersecting MOTS continue to exist in this spacetime—one which differs from the $4D$ Schwarzschild both in dimension *and* in rotation—speaks to the generality of their existence.

It has been briefly mentioned that the coordinates used fail across $R = a$, and so limit the number of MOTS which can be found. While there is (not yet published) work my collaborators have done in spacetimes which have finite numbers of self-intersecting MOTS—where the number is limited by the existence of an inner horizon in the spacetime—this is likely not so relevant here. The inner horizon in these coordinates for Myers-Perry exists outside of the surface $R = a$, where it is farther outside it for larger rotation (it exists at $r_- = \sqrt{\mu - \sqrt{\mu(\mu - 2a^2)}}$, which is $\sqrt{1 - \sqrt{1 - 2a^2}}$ here). However, the MOTS found easily penetrate this horizon, and it does not seem to be the surface which they wrap around when warping. Hence, only $R = a$ was plotted in the figures of this chapter, since it is the surface relevant to the shape of the MOTS.

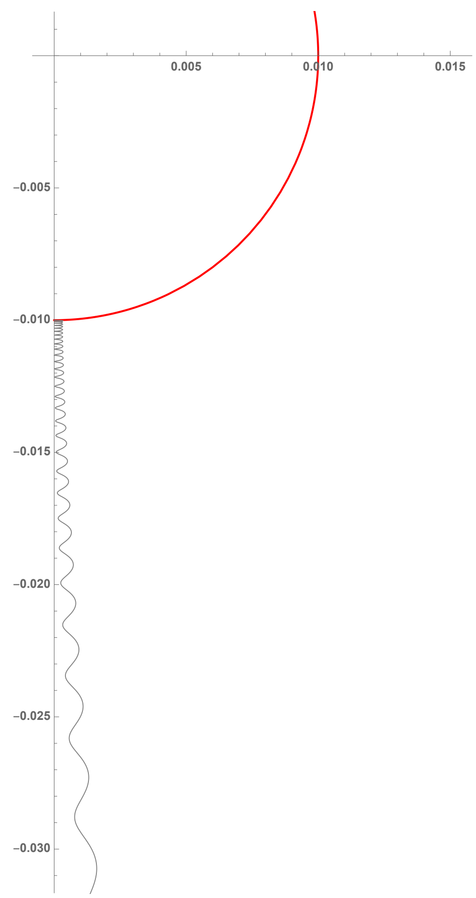

Figure 6.14: Oscillations for $a = 0.01$, $R_0 = 0.01001$. The increase in amplitude/period along the single MOTOS is seen. Plots $(R\cos\Theta, R\sin\Theta)$.

There exists precedent for Painlevé-Gullstrand coordinates failing in certain spacetimes: for instance, they fail in Anti-de Sitter space, as well in the inner region of Reissner-Nordström [17]. In the latter, it is also the case that the surface across which the coordinates fail exists inside the inner horizon. An important next step for this research is finding a coordinate system which penetrates the $R = a$ surface, allowing for us to see whether there exist self-intersecting MOTS inside it. Note that this surface is not a horizon, and the singularity in this spacetime exists at $r = 0$. It will also be worthwhile to look more closely at the large-r limit for Myers-Perry, just as was mentioned for the Schwarzschild case.

Chapter 7

Conclusion

The purpose of this work was to explore the generality of self-intersecting marginally outer trapped surfaces, first seen in binary black hole mergers [30], and subsequently seen again in 4-dimensional Schwarzschild spacetime by my collaborators [11]. We searched for these self-intersecting MOTS in two different 5-dimensional spacetimes, in order to determine whether adding a dimension would affect their existence or shape. We were motivated also by the possibility that the MOTS, and their open analogues MOTOS, might be simpler asymptotically in $5D$ than they were in $4D$, because of results suggesting this from [15].

For $5D$ Schwarzschild, we worked first in Weyl coordinates [1], a five-dimensional generalization of cylindrical coordinates, and then in the usual Schwarzschild coordinates (both with a toroidal foliation of S^2). For Myers-Perry, we worked in a case where all rotation parameters were equal, and the spacetime was asymptotically flat.

We searched for MOTS by means of finding MOTOS, or marginally outer trapped open surfaces, and following a continuous sequence of them until one closes. This method was originated in [11], and worked equally well for finding MOTS in 5-dimensions as it did in four. Our method for locating the MOTOS consisted of defining a general rotationally symmetric hypersurface in a constant timeslice of the spacetime, and from this calculating the outward-oriented null expansion of it. This was then set equal to zero, and in doing so, we were able to put the final equations of motion into a form similar to the geodesic equations. These are called MOTSodesic equations, for obvious reasons, in this thesis and in [12, 32, 31]. These MOTSodesic equations are second order differential equations, were easily numerically solved. The

MOT(O)S were plotted by means of a 'shooting method'; that is, an initial value form which the MOT(O)S would leave the vertical axis was chosen, and MOTS were found by increasing/decreasing this value as necessary until the surface closed.

We found the self-intersecting MOTS are sufficiently general phenomena that they exist in both of the five-dimensional spacetimes studied: $5D$ Schwarzschild and Myers-Perry. Their behaviour in $5D$ Schwarzschild was found to be nearly indistinguishable from $4D$ Schwarzschild—most notably, there were once again an infinite number of the self-intersecting MOTS in the former, as was found in the latter [11].

In $5D$ Myers-Perry, the number of self-intersecting MOTS we were able to find was constrained by the coordinate system used, which failed across the surface $R = a$. The larger the rotation parameter, a, that was chosen, the fewer MOTS existed outside of it (and inside the apparent horizon). For this reason, the fastest rotation studied was $a = 0.5$, and the only MOTS we were able to see in this spacetime was the apparent horizon, and the inner horizon—no self-intersecting MOTS were found. For $a = 0.4$, one self-intersecting MOTS fit between $R = a$ and the apparent horizon, for $a = 0.35$ there were two, etc. $a = 0.1$ was sufficiently slowly rotating that many-looped MOTS were able to be found (where it was not easy to count the number). All self-intersecting MOTS in Myers-Perry hugged the surface $R = a$, and the larger the rotation parameter, the more distorted the loops became in doing so.

For comparison to four dimensions, MOTOS outside of the apparent horizon (above and below it) were also found. In both five-dimensional spacetimes, the MOTOS that left the vertical axis from above the apparent horizon did not differ dramatically from their analogues in four dimensions: the only difference was that the affect of the apparent horizon—causing the MOTOS to wrap around it—was stronger, i.e., it existed out for further values of the radial coordinate.

The MOTOS that left from the negative vertical axis (with upward directed null normal—for downward directed null normal, this would apply to those which leave above the apparent horizon) were different from four dimensions. For $5D$ Schwarzschild, the MOTOS crossed one another and seemed to order themselves oppositely to how they left the horizontal axis; this compared to four dimensional Schwarzschild, where they found that these MOTOS remained the same order for large r. On the scale of the apparent horizon and larger, the MOTOS which left the negative vertical axis in $5D$ Myers-Perry presented a similar sort of behaviour as $5D$

Schwarzschild, with the ordering perhaps reversing.

We had hoped, in five dimensions, the MOTOS might be neatly ordered both above the apparent horizon, and for the negative vertical axis. Instead, we found that they were neither neatly ordered above nor below it (not obviously at least). While the fact that the $5D$ Schwarzschild MOTOS which leave from above the apparent horizon are not neatly ordered supports the claim that $5D$ Schwarzschild is qualitatively very similar in its MOTS and MOTOS to $4D$, the ordering in general seems to be worse in five dimensions. It will therefore be very valuable to take series expansions in the large r limit for both $5D$ spacetimes, to determine whether the MOTOS are in fact less ordered, or whether the reversal that seems to be visible does occur.

Something found here, which had not been found previously, was the existence of oscillations in the MOTOS that leave from the negative vertical axis in Myers-Perry. These oscillations were found to increase in frequency but decrease in amplitude as the rotation parameter reduced, limiting to $5D$ Schwarzschild, where the MOTOS are smooth (because the amplitude of the oscillations goes to zero). This is new and novel behaviour, and requires further study. Preliminary results by my collaborators indicate similar sort of oscillations may be present in the Kerr spacetime, so they are a result of the rotation.

What is the most obvious conclusion to be drawn from this work is that these self-intersecting MOTS exist in a variety of spacetimes, and that adding a dimension to the spacetime does not affect their existence, nor does adding rotation. This supports the claims of their generality.

Valuable next steps to the work contained in this thesis will be to attempt to find coordinates which do not fail across any surfaces inside the apparent horizon of Myers-Perry, and thus penetrate to the singularity. In this way, we may determine whether there exist infinite MOTS in this spacetime, or whether the MOTS found here are, in fact, all that exist. It will also be worthwhile, as mentioned, to take series expansions of the large r limit in both five-dimensional spacetimes, to establish whether there is any clean ordering of the MOTOS as $r \to \infty$. Finally, searching for the oscillating MOTOS in other spacetimes with rotation is required to better understand them.

Bibliography

[1] Aghil Alaee and Hari K. Kunduri. Remarks on mass and angular momenta for U(1)2-invariant initial data. *Journal of Mathematical Physics*, 57(3), 2016.

[2] Lars Andersson, Marc Mars, and Walter Simon. Stability of marginally outer trapped surfaces and applications. *Springer Proceedings in Mathematics and Statistics*, 26:111–138, 2013.

[3] Lars Andersson and Jan Metzger. The area of horizons and the trapped region. *Communications in Mathematical Physics*, 290(3):941–972, 2009.

[4] Peter Anninos, David Bernstein, Steven R Brandt, David Hobill, Edward Seidel, and Larry Smarr. Dynamics of black hole apparent horizons. *Phys. Rev. D*, 50(6):3801–3815, 9 1994.

[5] Peter Anninos, Karen Camarda, Joseph Libson, Joan Massó, Edward Seidel, and Wai-Mo Suen. Finding apparent horizons in dynamic 3D numerical spacetimes. *Phys. Rev. D*, 58(2):24003, 6 1998.

[6] Abhay Ashtekar and Gregory J. Galloway. Some uniqueness results for dynamical horizons. *Advances in Theoretical and Mathematical Physics*, 9(1):1–30, 2005.

[7] Abhay Ashtekar and Badri Krishnan. Isolated and dynamical horizons and their applications. *Living Reviews in Relativity*, 7, 2004.

[8] B. P. Abbott et al. (LIGO Scientific Collaboration and Virgo Collaboration). Observation of Gravitational Waves from a Binary Black Hole Merger. *Physical Review Letters*, 116(6):061102, 2 2016.

[9] Ivan Booth. Black-hole boundaries. *Canadian Journal of Physics*, 83(11):1073–1099, 2005.

[10] Ivan Booth, Lionel Brits, Jose A. Gonzalez, and Chris Van Den Broeck. Marginally trapped tubes and dynamical horizons. *Classical and Quantum Gravity*, 23(2):413–439, 2006.

[11] Ivan Booth, Robie A. Hennigar, and Saikat Mondal. Marginally outer trapped surfaces in the Schwarzschild spacetime: Multiple self-intersections and extreme mass ratio mergers. *Physical Review D*, 102(4):1–20, 2020.

[12] Ivan Booth, Robie A. Hennigar, and Daniel Pook-Kolb. Ultimate fate of apparent horizons during a binary black hole merger I: Locating and understanding axisymmetric marginally outer trapped surfaces. 4 2021.

[13] Ivan Booth and Jonathan Martin. Proximity of black hole horizons: Lessons from Vaidya spacetime. *Physical Review D - Particles, Fields, Gravitation and Cosmology*, 82(12):1–16, 2010.

[14] A. S. Eddington. A comparison of Whitehead's and Einstein's formulæ, 1924.

[15] Roberto Emparan and Marina Martínez. Exact event horizon of a black hole merger. *Classical and Quantum Gravity*, 33(15), 2016.

[16] Roberto Emparan, Marina Martínez, and Miguel Zilhão. Black hole fusion in the extreme mass ratio limit. *Physical Review D*, 97(4), 2018.

[17] Valerio Faraoni and Geneviève Vachon. When Painlevé–Gullstrand coordinates fail. *European Physical Journal C*, 80(8), 2020.

[18] David Finkelstein. Past-Future Asymmetry of the Gravitational Field of a Point Particle. *Physical Review*, 110(4), 1958.

[19] Anshu Gupta, Badri Krishnan, Alex B. Nielsen, and Erik Schnetter. Dynamics of marginally trapped surfaces in a binary black hole merger: Growth and approach to equilibrium. *Physical Review D*, 97(8):1–18, 2018.

[20] S. W. Hawking and G. F. R. Ellis. *The Large Scale Structure of Space-Time*. Cambridge University Press, 5 1973.

[21] Badri Krishnan. Fundamental properties and applications of quasi-local black hole horizons. *Classical and Quantum Gravity*, 25(11), 2008.

[22] Badri Krishnan. Quasi-local black hole horizons. *Springer Handbook of Spacetime*, pages 527–555, 2014.

[23] Hari K. Kunduri, James Lucietti, and Harvey S. Reall. Gravitational perturbations of higher dimensional rotating black holes: Tensor perturbations. *Physical Review D - Particles, Fields, Gravitation and Cosmology*, 74(8):1–29, 2006.

[24] P. Mösta, L. Andersson, J. Metzger, B. Szilágyi, and J. Winicour. The merger of small and large black holes. *Classical and Quantum Gravity*, 32(23):1–17, 2015.

[25] Robert C. Myers. Myers–perry black holes. *Black Holes in Higher Dimensions*, 9781107013:101–133, 2012.

[26] Ramesh Narayan. Black holes in astrophysics. *New Journal of Physics*, 7, 2005.

[27] Roger Penrose. Gravitational collapse and space-time singularities. *Physical Review Letters*, 14(3):57–59, 1965.

[28] Eric Poisson. *A relativist's toolkit : the mathematics of black-hole mechanics.* Cambridge University Press, 2004.

[29] Daniel Pook-Kolb, Ofek Birnholtz, Badri Krishnan, and Erik Schnetter. Existence and stability of marginally trapped surfaces in black-hole spacetimes. *Physical Review D*, 99(6):32–35, 2019.

[30] Daniel Pook-Kolb, Ofek Birnholtz, Badri Krishnan, and Erik Schnetter. Interior of a binary black hole merger. *Physical Review Letters*, 123(17):1–6, 2019.

[31] Daniel Pook-Kolb, Ivan Booth, and Robie A. Hennigar. Ultimate fate of apparent horizons during a binary black hole merger II: Horizons weaving back and forth in time. 4 2021.

[32] Daniel Pook-Kolb, Robie A. Hennigar, and Ivan Booth. A Pair of Pants for the Apparent Horizon. pages 2–7, 4 2021.

[33] Erik Schnetter and Deirdre Shoemaker. Introduction to isolated horizons in numerical relativity. *Physical Review D - Particles, Fields, Gravitation and Cosmology*, 67(2):1–15, 2003.

[34] K Schwarzschild. On the Gravitational Field of a Mass Point According to Einstein's Theory. *Abh. Konigl. Preuss. Akad. Wissenschaften Jahre 1906,92, Berlin,1907*, pages 189–196, 1 1916.

[35] Larry Smarr, Andrej Čadež, Bryce Dewitt, and Kenneth Eppley. Collision of two black holes: Theoretical framework. *Phys. Rev. D*, 14(10):2443–2452, 11 1976.

[36] P. C. Vaidya. The External Field of a Radiating Star in General Relativity. *General Relativity and Gravitation*, 31(1):119–120, 1999.

[37] Robert M. Wald. *General Relativity.* University of Chicago Press, Chicago, 1984.